

University of Alabama in Huntsville

LOUIS

Dissertations

UAH Electronic Theses and Dissertations

2013

Analytical evaluation of the trajectories of hypersonic projectiles launched into space

John David Stutz

Follow this and additional works at: <https://louis.uah.edu/uah-dissertations>

Recommended Citation

Stutz, John David, "Analytical evaluation of the trajectories of hypersonic projectiles launched into space" (2013). *Dissertations*. 29.

<https://louis.uah.edu/uah-dissertations/29>

This Dissertation is brought to you for free and open access by the UAH Electronic Theses and Dissertations at LOUIS. It has been accepted for inclusion in Dissertations by an authorized administrator of LOUIS.

**ANALYTICAL EVALUATION OF THE TRAJECTORIES OF HYPERSONIC
PROJECTILES LAUNCHED INTO SPACE**

by

JOHN DAVID STUTZ

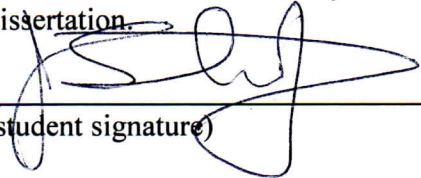
A DISSERTATION

**Submitted in partial fulfillment of the requirements
for the degree of Doctor of Philosophy
in
The Department of Mechanical Engineering
to
The School of Graduate Studies
of
The University of Alabama in Huntsville**

HUNTSVILLE, ALABAMA

2013

In presenting this dissertation in partial fulfillment of the requirements for a doctoral degree from The University of Alabama in Huntsville, I agree that the Library of this University shall make it freely available for inspection. I further agree that permission for extensive copying for scholarly purposes may be granted by my advisor or, in his/her absence, by the Chair of the Department or the Dean of the School of Graduate Studies. It is also understood that due recognition shall be given to me and to The University of Alabama in Huntsville in any scholarly use which may be made of any material in this dissertation.



(student signature)

3/11/13
(date)

DISSERTATION APPROVAL FORM

Submitted by John Stutz in partial fulfillment of the requirements for the degree of Doctor of Philosophy in Mechanical Engineering and accepted on behalf of the Faculty of the School of Graduate Studies by the dissertation committee.

We, the undersigned members of the Graduate Faculty of The University of Alabama in Huntsville, certify that we have advised and/or supervised the candidate on the work described in this dissertation. We further certify that we have reviewed the dissertation manuscript and approve it in partial fulfillment of the requirements for the degree of Doctor of Philosophy in Mechanical Engineering.

John T. Caskey 3/11/13 Committee Chair
(Date)

Jonatuan Rogers Jonatuan Rogers
Date 3/7/2013

W. B. Fisher

Robert Woodruff

D. Keith Halgym Department Chair

Gregory Chalger College Dean

Rhonda Kay Steede 3/19/13 Graduate Dean

ABSTRACT
The School of Graduate Studies
The University of Alabama in Huntsville

Degree Doctor of Philosophy College/Dept. Mechanical Engineering

Name of Candidate John Stutz

Title Analytical Evaluation of the Trajectories of Hypersonic Projectiles Launched into Space

An equation of motion has been derived that may be solved using simple analytic functions which describes the motion of a projectile launched from the surface of the Earth into space accounting for both Newtonian gravity and aerodynamic drag. The equation of motion is based upon the Kepler equation of motion differential and variable transformations with the inclusion of a decaying angular momentum driving function and appropriate simplifying assumptions.

The new equation of motion is first compared to various numerical and analytical trajectory approximations in a non-rotating Earth reference frame. The Modified Kepler solution is then corrected to include Earth rotation and compared to a rotating Earth simulation. Finally, the modified equation of motion is used to predict the apogee and trajectory of projectiles launched into space by the High Altitude Research Project from 1961 to 1967.

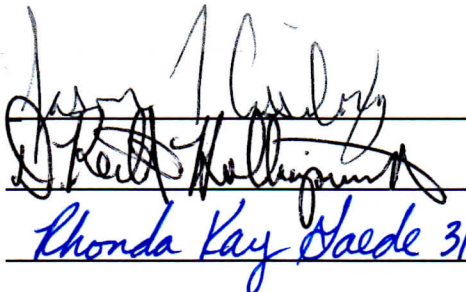
The new equation of motion allows for the rapid evaluation of projectile trajectories and intercept solutions that may be used to calculate firing solutions to enable ground launched projectiles to intercept or rendezvous with targets in low Earth orbit such as ballistic missiles.

Abstract Approval:

Committee Chair

Department Chair

Graduate Dean


John Stutz
John Stutz
Rhonda Kay Gaede 3/19/13

ACKNOWLEDGMENTS

My appreciation is extended to my entire dissertation committee, but most sincerely to Dr. Nathan Slegers for his tireless dedication to ensuring rigor and formality in the presentation of this material and patient guidance in the field of linear theory. Utmost gratitude is also offered to Dr. Jason Cassibry for the courage to accept an unfamiliar graduate student and provide not only keen academic guidance as an advisor but also patient mentoring as a friend. A most heartfelt thanks is extended to Dr. Jeff Keller for his technical support, many hours of listening to me gripe, and generous use of his whiteboard. My eternal devotion and gratitude is extended to my wife Brenda and my children, Abigail, John David, Daniel, and Ava who sacrificed many hours of family time and suffered through many a long-winded discourse on aerodynamics and orbital mechanics with a vague smile.

Finally, I dedicate the work presented in this dissertation as an offering to the Creator of the universe and my Lord God. I have come to appreciate the beauty of the system that I have had the privilege of studying and hope that this small contribution may lead not to more efficient ways for the created to destroy each other, but for us to bring greater peace.

Ecclesiastes 12:12, Proverbs 3:5,6

TABLE OF CONTENTS

	Page
List of Figures	ix
List of Symbols	xii
Chapter	
I. PROJECTILE TRAJECTORIES	1
A. Introduction and Problem Statement	1
B. Space Guns	6
C. Literature Review	8
D. Summary	13
II. ANALYSIS OF SPACE GUN PROJECTILE TRAJECTORIES	14
A. Reference Trajectories	14
B. Aerodynamic Behavior of the Projectiles	21
III. DERIVATION OF THE MODIFIED KEPLER EQUATION	25
A. Kepler Equation	26
B. Derivation of the Angular Momentum Driving Function	28
C. The Modified Kepler Equation	33
IV. COMPARISON OF THE MODIFIED KEPLER EQUATION TO OTHER TRAJECTORY METHODS	37
A. MKS Reference Trajectories	37
B. Baseline Hypersonic Projectile Trajectories	44
C. Verification of Modified Kepler Equation Assumptions for the Baseline Projectile	49
V. CONVERSION OF THE MODIFIED KEPLER SOLUTION FOR A ROTATING EARTH	57
A. Initial Velocity Correction for Earth Rotation	58

B.	Aerodynamic Drag Force Misalignment	56
C.	Error in the ECI Modified Kepler Solution	62
D.	Discussion	66
VI.	EVALUATION OF HARP DATA USING THE CORRECTED MODIFIED KEPLER SOLUTION	69
A.	HARP Projectile Overview	69
B.	HARP Trajectory Data Collected	71
C.	Martlet 2C (Mod 2) Apogee Comparison for the Barbados Gun	76
D.	Martlet 2C (Mod 2) Apogee Comparison for the Yuma Gun	79
E.	Martlet 2C (Mod 2) Trajectory Comparisons	80
VII.	CONCLUSIONS AND FUTURE RESEARCH	87
A.	Use of the Modified Kepler Solution to Intercept Ballistic Missiles	87
B.	Other Sources of Uncertainty	89
C.	Ground Support Fire	90
D.	Closing	91
	APPENDIX A: 3DOF Numerical Simulation of Hypersonic Projectiles	93
	APPENDIX B: 6DOF Numerical Simulation of Hypersonic Projectiles	98
	APPENDIX C: Taylor-Maccoll Code	102
	APPENDIX D: Tabulated Data and Calculations for Barbados 16" HARP Gun Apogee Data Fit	104
	APPENDIX E: Tabulated Data and Calculations for Yuma 16" HARP Gun Apogee Data Fit	105
	REFERENCES	106

LIST OF FIGURES

Figure	Page
1.1 Operational View of Projectile Ballistic Missile Defense.....	2
1.2 Response Times Available to Identify a Ballistic Missile Launch, Calculate a Firing Solution, and Launch an Interceptor Projectile.....	3
1.3 Lorentz Force Utilized to Propel a Railgun Projectile.....	8
2.1 Atmospheric Density from the NASA Standard Atmosphere (1976) with Multi Stage.....	16
2.2 Altitude vs Range for 50 degree Launch Angle.....	18
2.3 Cross Range vs Range for 50 degree Launch Angle.....	19
2.4 Velocity vs Range for 50 degree Launch Angle.....	19
2.5 Angle of Attack vs Range for 50 degree Launch Angle.....	20
2.6 Range vs Time for 50 degree Launch Angle.....	20
2.7 Swerve of Projectile for a 50 degree Launch Angle.....	21
2.8 Mach & Drag Coefficient vs. Range for a 50 degree Launch Angle.....	22
2.9 Altitude vs. Range while in the Lower Atmosphere for a 50 degree Launch Angle.....	23
2.10 Specific Angular Momentum vs. Range for a 50 degree Launch Angle.....	24
3.1 Polar Coordinates for Projectile Trajectory.....	26
3.2 Atmospheric Density from the NASA Standard Atmosphere (1976) with Exponential Curve Fit.....	30
3.3 Angular Range Approximate Relationship with Altitude.....	31
3.4 Open Loop Frequency Response of the Non-Linear and Linearized Modified Kepler Equation to the Driving Function.....	35
4.1 Altitude vs Range for 50 degree Launch Angle.....	38
4.2 Cross Range vs Range for 50 degree Launch Angle.....	38

4.3	Velocity vs Range for 50 degree Launch Angle	40
4.4	Range vs Time for 50 degree Launch Angle	40
4.5	Geometry for Total Error Calculation between Numerical Simulation and Kepler Solution	42
4.6	Total Position Error between the 3DOF Numerical Simulation and Modified Kepler Solution	42
4.7	Computational Effort and Error to Calculate Apogee	44
4.8	Comparisons of Various Projectiles with MKS	45
4.9	Drag Coefficient of a 4 Degree Right Cone	47
4.10	Modified Kepler Trajectories of the Baseline Projectile	48
4.11	Three Term Modified Kepler Solution Total Error	49
4.12	Asymptotic Angular Momentum Error	50
4.13	Three Term Modified Kepler Solution Total Error with Asymptotic Angular	51
4.14	Comparison of Numerical Simulation to Straight Line Approximation	52
4.15	Three Term Modified Kepler Solution Error with the Exponential Density Model used in the Numerical Simulation	53
4.16	Drag Coefficient over Angular Range from Numerical Simulation	54
4.17	Three Term Modified Kepler Solution Total Error with a 20% increase in Initial Velocity	55
4.18	Total Error with 6 m/s Headwind and 6 m/s Crosswind	56
5.1	Initial Velocity Correction due to Earth Rotation	59
5.2	Misalignment of Aerodynamic Drag Force with Corrected Velocity Vector	60
5.3	The Initial Velocity in an Inertial Reference Frame from the Rotating Reference Frame	62
5.4	Total position Error of the ECEF Modified Kepler Solution for the Baseline Projectile fired from 0 Degrees Latitude on a Bearing of 090T	63

5.5	Total position Error of the ECEF Modified Kepler Solution for the Baseline Projectile fired from 0 Degrees Latitude on a Bearing of 000T.....	64
5.6	Total position Error of the ECEF Modified Kepler Solution for the Baseline Projectile fired from 0 Degrees Latitude on a Bearing of 270T.....	64
5.7	Total position Error of the ECEF Modified Kepler Solution for the Baseline Projectile fired from 45 Degrees Latitude on a Bearing of 090T.....	65
5.8	Total position Error of the ECEF Modified Kepler Solution for the Baseline Projectile fired from 45 Degrees Latitude on a Bearing of 000T.....	65
5.9	Total position Error of the ECEF Modified Kepler Solution for the Baseline Projectile fired from 45 Degrees Latitude on a Bearing of 270T.....	66
5.10	Relative Position of the Relative Velocity Vector to the initial Velocity Vector for East Fired Projectiles.....	67
5.11	Relative Position of the Relative Velocity Vector to the initial Velocity Vector for West Fired Projectiles.....	68
6.1	Drawing of the Martlet 2C (Mod 2).....	70
6.2	16 inch Barbados HARP Gun.....	73
6.3	16 inch Barbados HARP Gun (Present Day).....	74
6.4	Barbados Gun Site, Gun Bearing Measured Relative to Airstrip.....	75
6.5	Apogee Error between Corrected Modified Kepler Solution and Measured Apogee Data for Barbados 16” HARP Gun Martlet 2C (Mod 2) Rounds.....	78
6.6	Apogee Error between Corrected Modified Kepler Solution and Measured Apogee Data for Yuma 16” HARP Gun Martlet 2C (Mod 2) Rounds.....	80
6.7	Radar Data and ECEF Modified Kepler Solution for Round 206 from the Barbados Gun.....	81
6.8	Radar Data and ECEF Modified Kepler Solution for Round 188 from the Barbados Gun.....	82
6.9	Radar Data and ECEF Modified Kepler Solution for Round 227 from the Barbados Gun.....	83
6.10	Radar Data and ECEF Modified Kepler Solution for Round 181 from the Barbados Gun.....	84

6.11	Radar Data and ECEF Modified Kepler Solution for Round 221 from the Barbados Gun.....	85
------	---	----

LIST OF SYMBOLS

a	=altitude
a_{tangent}	=acceleration of the projectile tangent to direction of motion
A	=cross sectional area of projectile
c, C	=constants
C_D	=aerodynamic drag coefficient
C_{D0}	=aerodynamic drag coefficient at launch
F_{drag}	=aerodynamic drag force
F_{inline}	=aerodynamic drag force collinear with direction of motion
F_{tangent}	=aerodynamic drag force tangent to direction of motion
G	=universal gravitation constant
k	=atmospheric density decay constant
L	=angular momentum of projectile
L_{∞}	=angular momentum of projectile after escaping sensible atmosphere
L_0	=angular momentum of projectile at launch
L_{apogee}	=angular momentum of projectile at apogee
LA	=latitude
LO	=longitude
m	=mass of projectile
M	=Mass of Earth
Ma	=Mach number of projectile
N	=ratio of drag force to gravitational force
r	=distance of projectile from the center of the Earth
\dot{r}	=first derivative of radial position with respect to time
\ddot{r}	=second derivative of radial position with respect to time
r_0	=initial distance of projectile from the center of the Earth
r_i	=radial projectile from the center of the Earth at simulation time step i
r_{sim}	=distance of projectile from the center of the Earth from numerical simulation
r_{Kepler}	= distance of projectile from the center of the Earth from analytical solution
R^2	= coefficient of determination
t	=time
t_{sim}	=time calculated from numerical simulation
t_{Kepler}	=time calculated from analytical solution
u	=inverse of radial position
V	=absolute velocity of projectile in the inertial reference system
V_{rel}	=absolute velocity of projectile in the relative reference system
V_{tangent}	=velocity component tangent to direction of motion
β	=angular momentum decay factor
γ	=exponential decay of atmospheric density along angular range
ϵ_r	=error between numerical simulation and analytic solution along radial direction
ϵ_{θ}	=error between numerical simulation and analytic solution along angular direction
ϵ_{total}	=total position error between numerical simulation and analytic solution

θ	=angular range along Earth's surface
θ_i	=angular range along Earth's surface at time step i
θ_{apogee}	=angular range at projectile apogee
$\dot{\theta}$	=first derivative of angular range with respect to time
μ	=misalignment angle between direction of travel and aerodynamic drag force
ρ	=atmospheric density
ρ_0	=atmospheric density at launch
τ	=transformed atmospheric density decay constant
ϕ	=elevation of projectile trajectory in the inertial reference system
ϕ_0	=elevation of projectile trajectory at launch
ϕ_{rel}	=elevation of projectile trajectory at launch in the relative reference system
ω	=angular velocity of the Earth rotation

CHAPTER 1

PROJECTILE TRAJECTORIES

The desire to hit a target with a projectile is the driving force behind the science of ballistics (from the Greek βάλλειν “to throw”). The subject of this dissertation is one of the most extreme forms of ballistics: projectiles thrown with such a large initial momentum from the surface of the Earth that they have the potential to leave the atmosphere and travel into space. Although of interest from a purely technical nature, “space guns” that are capable of launching projectiles into space have been a reality since the High Altitude Research Project (HARP) of the 1960s [1,2]. Electromagnetic railguns and light gas guns with even higher muzzle velocities are currently under development. The ability to quickly and accurately predict the motion of hypervelocity projectiles is needed to enable these guns for a variety of missions.

A. Introduction and Problem Statement

There are multiple uses for space guns. For civilian use they can place supplies into space at a low cost or to quickly launch low Earth orbit satellites to replace damaged ones [3,4]. For military uses, a hypervelocity projectile is ideal for long range ground support fire or anti-aircraft fire [5]. The most important use of space guns may be to destroy ballistic missiles in flight [6]. If possible, then this use would be a major step to

making ballistic missiles obsolete.

A gun that is capable of placing a hypersonic projectile into space is an attractive alternative to the current method of using an interceptor missile to shoot down a ballistic missile. An operational view of this concept is given in Figure 1.1. In effect, the gun replaces the missile in placing the maneuvering kill vehicle in position to detect and intercept the ballistic missile or its warhead. Assuming the kill vehicle can be designed to withstand the acceleration of the launch, the cost of placing the kill vehicle on an intercept course should be drastically reduced by the use of a gun while reducing the time to intercept and enabling earlier intercepts.

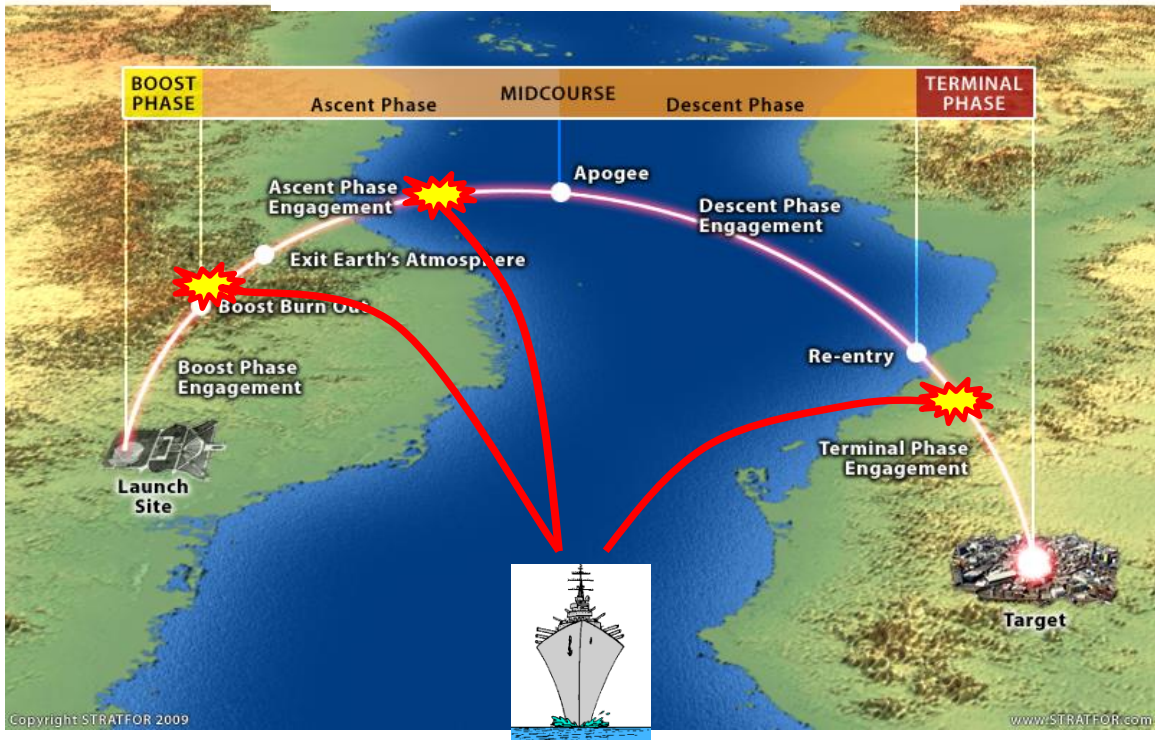


Figure 1.1 Operational View of Projectile Ballistic Missile Defense [7]

(background image used with permission)

The high initial speed of hypersonic projectiles gives them an advantage in intercepting ballistic missiles. A comparison of acceleration curves from numerical simulations for notional short range and long range ballistic missiles as shown in Figure 1.2 indicates the advantage a railgun projectile has at reaching a desired altitude. Assuming a high enough rate of fire or sufficient number of guns, the gun(s) may place multiple projectiles on the most likely trajectories of the ballistic missile while it is still in the boost phase. The uncertainty in the future position of the missile during boost decreases the likelihood of an intercept but the low cost of the projectile compared to the ballistic missile make the waste of a few projectiles minor compared to a similar tactic using ballistic missile interceptors. Note that for the best cases, the time available to calculate intercept solutions is less than a minute.

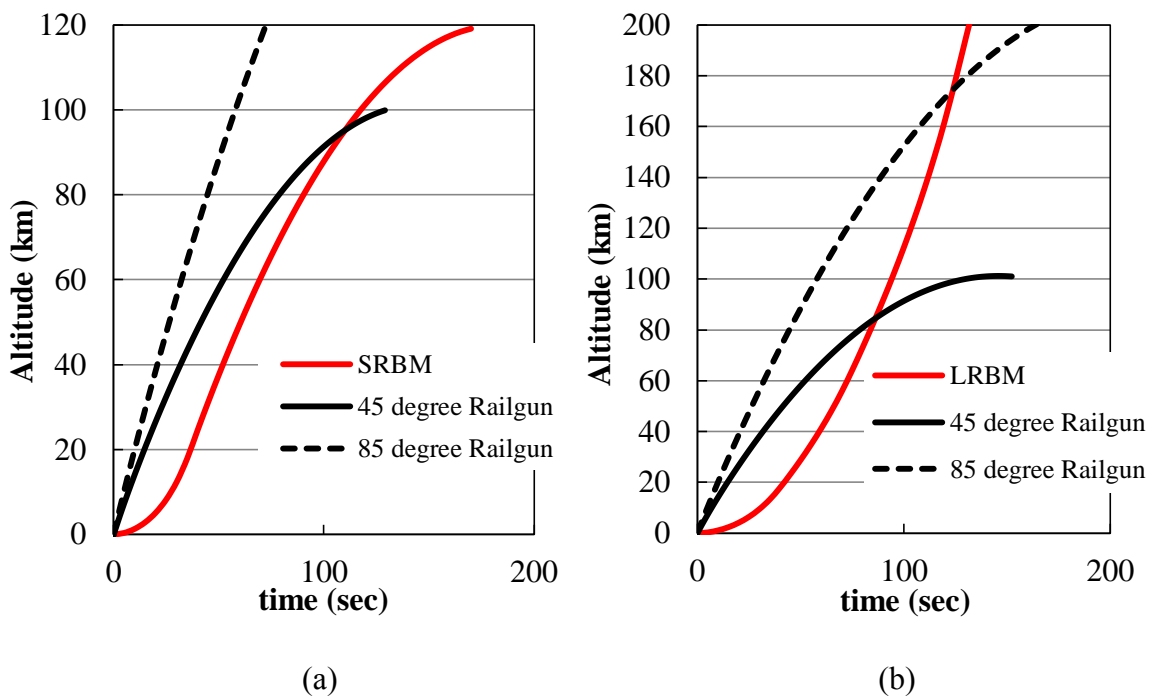


Figure 1.2 Response Times Available to Identify a Ballistic Missile Launch, Calculate a Firing Solution, and Launch an Interceptor Projectile

The sensor on the ballistic missile interceptor must detect an object that is traveling at a high velocity at extremely high altitudes. The detection of a relatively high temperature target during or immediately after boost or a target that is aero-thermally heated during reentry allows for the use of lower cost mid-wave infrared (MWIR) sensors in the place of the more expensive and sensitive long wave infrared (LWIR) sensors needed for long range midcourse defense [8,9,10]. These lower cost sensors justify the expenditure of multiple projectiles fired at missiles with uncertain trajectories during boost.

Finally, the gun may be used to place an extremely inexpensive debris field in the path of a boosting ballistic missile. The ballistic missile would be forced to fly through a field of high speed micro-projectiles that could prove damaging to a ballistic missile under the stress of boosting.

For any of these applications, the solution of the equations of motion between the launch point and the desired point of intercept requires the solution of the two point boundary value problem (TPBVP). Assuming the gun location and the position of the target is either known or can be estimated, the solution of the TPBVP is the correct bearing, elevation, and time of fire for the projectile to pass through the desired point in space at the correct time. The error in the solution of the TPBVP can be taken as an initial estimate of the sensor performance and divert capability or fragmentation pattern needed to ensure intercept.

For a projectile launched for a railgun or other type of space gun that leaves the sensible atmosphere, the projectile will travel through atmospheric zones from those

dominated by atmospheric effects to pure Kepler motion. The standard Kepler solution overshoots the simulated trajectory due to the lack of a drag term and the constant density flat fire theory undershoots due to an assumption of constant density and gravity. The lack of a discernible boundary between the atmospheric zones makes the handoff of solutions between the various theories difficult. A modern projectile linear theory approach that updates between 500 m and 2 km along the trajectory can capture the varying density at the expense of numerous calculations on the order of what would be required for a point mass simulation.

To solve for a single intercept appears to be possible with many if not all of these approaches. However, it is a common approach to overwhelm a ballistic missile defense system by launching multiple missiles at once to overload the capabilities of that system. This raid type scenario will push the limits of numerical or segmented linear theory capability as a large number of intercepts must be evaluated quickly and prioritized for likely success. It is doubtful that these methods of calculating intercepts will be quick enough to calculate raid size intercept solutions during the raid event.

To enable the use of space guns such as railguns to intercept ballistic missiles, rapid evaluation of the projectile trajectory upon detection of a potential target will be among the primary requirements. The TPBVP can be solved using multiple iterative numerical simulation techniques that are well established at the expense of the time required for the computations.

B. Space Guns

The idea of projectiles with sufficient velocity to escape the Earth's atmosphere is not a new concept and can be traced back at least to Jules Vern's science fiction novel *From the Earth to the Moon* published in 1886. In the novel, a gigantic gun is created with the sole purpose of sending a large projectile vehicle to the moon with passengers inside.

The first attempt to build a space gun must be credited to the Nazi war machine of the Second World War. As part of the vengeance weapons program that included the first cruise missile (the V-1) and the first ballistic missile (the V-2), the development of a gun that could theoretically place projectiles into space was initiated [11,12]. The V-3 (Vergeltungswaffe 3) super gun (codenamed the High Pressure Pump) was intended to launch projectile approximately 165 km with a barrel elevation of 45-50 degrees from Mimoyecques in northern France to the heart of London, England. The gun site was never finished due to an extensive bombing campaign by the Allied Forces. A similar gun concept was also utilized to bombard Luxemburg but the guns were mounted at an angle of approximately 34 degrees and fired at a distance of 43 km which most likely resulted in an apogee well below 40 km which does not qualify as truly leaving the atmosphere.

No record of a successful attempt to actually put a projectile into space can be found until the work of Dr. Gerald Bull from 1961-1967 as part of the High Altitude Research Program (HARP) [1,2]. Project HARP was funded by the US Army to place projectiles into the upper atmosphere to study upper level wind patterns using a modified 16 inch battleship gun. The HARP program succeeded in placing a projectile to 180 km.

The HARP experiments were conducted in several locations with the majority of the work occurring on either the island of Barbados with observer sites spread out on the surrounding islands or the Yuma Proving grounds in Yuma, Arizona.

While the HARP data is the only trajectory data that could be found for these types of projectiles, there is evidence of a nuclear weapons test in 1957 as part of “Operation Plumbob” where a several hundred pound manhole cover was captured by a high speed camera being blown off at several dozen kilometers per second that is likely the first, if unintentional, manmade space object [13,14]. Due to a lack of any verifiable data that the cover actually went into space and the sensitive nature of the propulsion, the claim of Sputnik as the first manmade object was never publicly contested.

Of more recent development and the driving force behind this dissertation is the recent advancement in railgun technology supported by the U.S. Navy with muzzle energies exceeding 32 MJ. Railguns produce acceleration of the projectile not through pressure created by the burning of propellant materials but directly from electric current. A large electrical current is passed through the projectile from either side creating a Lorentz force pushing the projectile down the length of the barrel as shown in Figure 1.3.

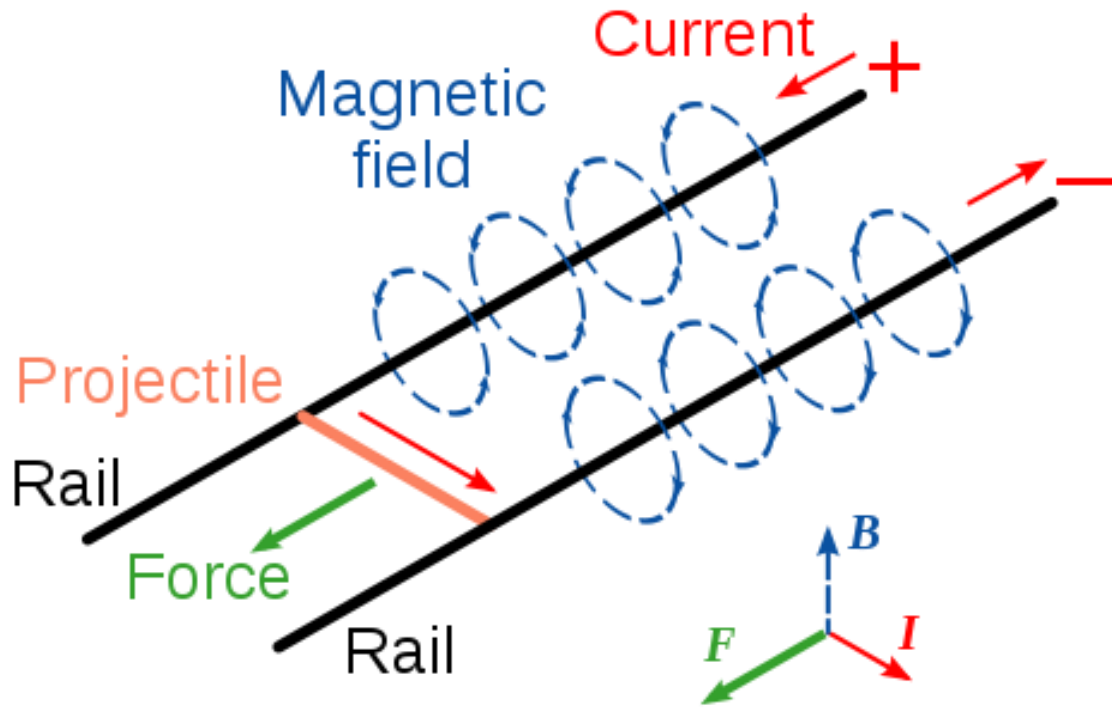


Figure 1.3 Lorentz Force Utilized to Propel a Railgun Projectile [15]

(image used with permission)

Although still in development, the railgun is planned to have a high rate of fire with muzzle velocities over 2 kilometers per second. These properties make the possibility of railgun-launched anti-ballistic missile projectiles an attractive option to create a low-cost, early intercept for ballistic missile defense.

C. Literature Review

The motion of objects due to varying gravity can be traced back to the work of Johannes Kepler in his 1609 text *Astronomia nova* (A New Astronomy) [16]. Kepler was the first to apply geometric shapes to orbits of the planets and to speculate upon a force that keeps the planets moving around the sun. Kepler speculated that this force must decay with distance from the sun. Kepler was also one of the first people that Galileo

Galilei sent his observations of the moons around Jupiter in 1610 to verify the possibility of the orbits [17]. In honor of Johannes Kepler, the equation of motion that results from his genius and insight will be referred to in this dissertation as the standard Kepler equation and its solution as the standard Kepler solution.

Sir Isaac Newton formalized Kepler's observations in his text *Philosophiæ Naturalis Principia Mathematica* (Mathematical Principles of Natural Philosophy) in 1687 [18]. Newton postulated his famous three laws of motion that became the statement of the conservation of momentum and proposed the inverse squared model of universal gravitation. Newton was also the first to propose the famous two body problem to calculate simple orbits.

The projectile motion around the Earth most closely resembles the classic two body problem when the gravitational force between the Earth and the projectile are the only gravitational forces taken into account. The solution of the two body problem is somewhat formalized and can be found in detail in most orbital mechanics texts (see for example Ref. [19,20]). The classical derivation and solution to the two body problem will be shown in Chapter 2 as it forms the foundation of the current research.

The use of projectiles has been considered for exo-atmospheric intercepts. *Gevelhoff, H., and Manz, B.* detailed a methodology of calculating firing solutions for using a gun mounted on one space platform to intercept a satellite or ballistic missile by direct solution of the standard Kepler equation [21]. Their method assumes the lack of any atmospheric drag and is not directly applicable to the ground launched projectile problem.

The solution of the Kepler TPBVP was also used by *Ahn, J., and Roh, W.* to

estimate the impact point of missiles or rockets in real time as they boost by ignoring aerodynamic drag [22]. As the missile or rocket is boosting, the instantaneous position and velocity vector can be used to estimate the impact point in the case of a motor failure. This would be useful for the recovery of hardware in the event of a catastrophic failure over water where a search area may be required quickly.

Orbital mechanics, including the two body problem, are commonly used to calculate the position of satellites in low Earth orbit (LEO). The atmospheric density at LEO altitudes is negligible and often ignored. The minor atmospheric drag can modify the orbits of satellites slightly over time and has therefore been studied extensively [23-36]. The general approach is to assume constant angular momentum and treat the drag as a very small nonlinear perturbation to the standard drag free standard Kepler solution and calculate the perturbation using a Taylor series expansion of the drag term.

The nonlinear equations of motion that describe the motion of the projectile can be modeled using a numerical simulation of the projectile and what little information on railgun projectile trajectories in literature is calculated using this method [37]. In the lack of large amounts of experimental data on space gun projectiles, this approach is also taken in this thesis to provide a standard with which to compare analytical solutions.

There have been previous efforts to analytically solve for trajectories that include atmospheric drag. *Shi, Y, et al.* have utilized a perturbation technique to estimate skip trajectories for the return of the Apollo capsule from lunar missions.[38,39,40] Their approach divides the skip trajectory into an initial descent phase into the atmosphere, ascent phase out to the atmosphere, a Kepler phase outside the atmosphere, and final descent phase to the surface. In each stage within the atmosphere, the trajectory is

calculated assuming either gravity or drag is predominant with the other treated as a perturbation. The analytic models allowed for the calculation of landing position of the Apollo capsule with the limited computational power available in the 1960s during reentry. These analytic trajectories did not extend into the lower atmosphere where the rate of change of the atmospheric density has a significant impact on the trajectory as is expected to affect ground launched projectiles.

There is ongoing work in the field of applied mathematics to capture the shape of trajectories of projectiles with the nonlinear drag terms [41,42]. All examples that can be found assume constant gravity and constant atmospheric density. The decay of atmospheric density as the projectile reaches higher altitudes is a driving force in the shape of trajectory for projectiles launched from the ground and the solutions being developed would not be expected to extrapolate well to the problem of interest.

The study of endo-atmospheric projectile trajectories has also been extensively studied. Traditional projectile linear theory makes the historical assumptions such as projectile symmetry, small pitch and yaw angles, small aerodynamic angles of attack, a large roll rate compared to the pitch and yaw rates, and velocity along the axis of revolution as the total velocity [43]. In addition, the Magnus force is also ignored but the Magnus moment is included. These assumptions are sufficient to decouple the equations of motions for an analytic solution but the requirement for a small pitch angle makes this approach impractical for anything other than flat trajectories and is often referred to as the flat-fire solution.

A new method was proposed as a variation of standard linear theory that allows high launch angles that violate the flat fire assumption [44]. The method still assumes a

small pitch variation and is appropriate for high quadrant elevations of high speed projectiles over short distances that have approximately straight line trajectories. Both standard and high elevation linear theory exhibit poor impact point prediction for long-range shots with high gun elevations characteristic of indirect fire munitions. The trajectory of space guns is expected to have significant curvature similar to indirect fire munitions. Neither standard linear or high quadrant linear theory would be expected to predict the trajectory accurately.

Modified Linear Theory relaxes the small pitch angle assumption while maintaining the other linear theory assumptions [45]. This allows for all other states to appear in a linear fashion while the pitch angle is operated on by trigonometric functions. Thus pitch angle is assumed constant when appearing with other independent variables but integrated with the trapezoid method when appearing in a trigonometric function. This method can be used to model the trajectory of space gun projectiles for a non-rotating Earth but the need to update the trajectory for aerodynamic and atmospheric properties along the trajectory requires a large number of calculations on the order of a simple numerical simulation for the long trajectories expected.

While modified linear theory addresses large pitch angles, it fails when the angle of attack is larger such as in low speed trajectories. MLT was corrected in [46] by further assuming that the vertical velocity and pitch rate may be significant and the roll rate is small and that the total velocity can be calculated as if the projectile was a point mass.

All of the linear theories contain part of the solution needed for the analysis of space gun trajectories but only MLT is adequate for capturing the high elevation, large pitch angle change, and large angle of attack. The MLT is unfortunately unable to

account for the rotating Earth effects and is rather computationally expensive. A new Modified Kepler method that is proposed also assumes a small angle of attack in the atmosphere and a decaying density model so that the trajectory can be modeled in only three degrees of freedom that trades off the accuracy slightly for a significant improvement in efficiency of the method.

D. Summary

The development of the US Navy Railgun creates the potential of anti-ballistic missile projectiles. The first step to enable this usage is the quick evaluation of potential firing solutions to determine if the ballistic missile will be in range of the gun at some point in its trajectory and what firing solutions would be needed to enable a potential intercept.

The Modified Kepler equation enables an estimated solution of the trajectory of a projectile launched into space from the surface of the Earth. The analytical form of the solution will enable the rapid calculation of firing solutions that are needed to enable use of space guns to destroy ballistic missiles in flight.

CHAPTER 2

ANALYSIS OF SPACE GUN PROJECTILE TRAJECTORIES

The motion of a rigid body projectile can be described in six dimensions, three translation (x,y,z) and three rotation (φ,θ,ψ). Six Degrees of Freedom (6DOF) numerical simulations of the six coupled equations of motion and Modified Linear Theory (MLT) are capable of describing this motion accurately at the expense of numerous computations. A point mass assumption simplifies the motion down to Three Degrees of Freedom (3DOF) by assuming that the forces on the projectile are independent of the attitude of the projectile relative to the oncoming air. This is the same as saying the projectile is inherently aerodynamically stable and will always turn into the oncoming airflow. 3DOF numerical simulations are considerably more efficient than 6DOF schema but are still computationally expensive for iterative solutions of two point boundary value problems (TPBVP) such as firing solutions. The Kepler transformation is a classic trajectory solution that simplifies the trajectory down to one degree of freedom which is analytically solvable but does not account for atmospheric drag. The proposed Modified Kepler equation developed in this thesis provides a simple analytic one degree of freedom solution that allows for multiple iterations for the TPBVP firing solution in real time as the gun swings into place.

A. Reference Trajectories

The rotation of the Earth complicates the study of ballistics. It is often common

in artillery to include Coriolis and centrifugal corrections based upon the latitude of the launch point and the bearing fired to correct for the rotating reference frame of the Earth. This effect becomes more pronounced as the projectile velocities and range increase. To prevent these complications and allow for comparison with Modified Linear Theory which does not correct for rotation, a non-rotating Earth model is initially used for analysis and will be corrected later.

An Earth Centered Earth Fixed (ECEF) Cartesian reference frame was selected for numerical simulation and MLT solutions to prevent the Coriolis and centrifugal effects from complicating the Modified Kepler comparisons for initial study. The ECEF model assumes the origin is at the center of a perfect sphere with a radius of 6378 km. The sphere is non-rotating and has a mass of 5.972×10^{24} kg. It is therefore unimportant where the launch point is located or what bearing it is launched.

A model of atmospheric density as a function of altitude was needed for the numerical simulations and MLT. A multi-segment curve fit to the NASA Standard Atmosphere (1976) was chosen [47]. The model provides density for altitudes up to 100 km. The comparison of the multi stage model to the tabulated standard atmosphere is shown in Figure 2.1.

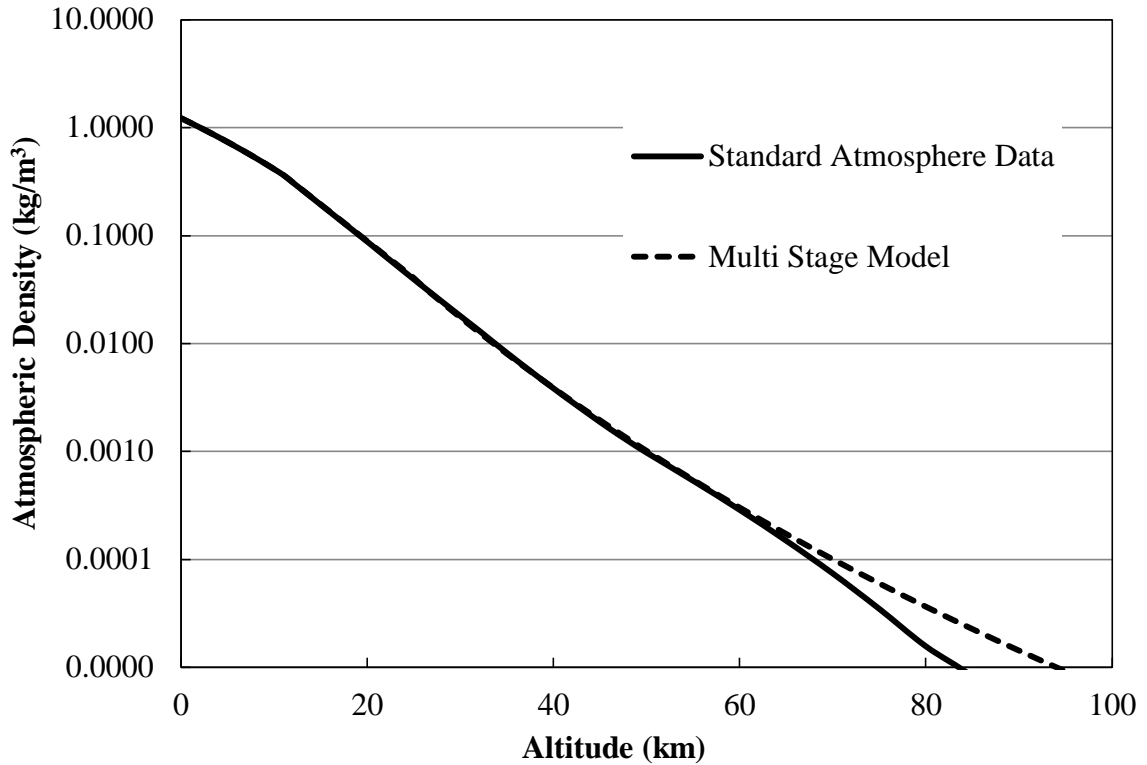


Figure 2.1 Atmospheric Density from the NASA Standard Atmosphere (1976) [47]
with Multi Stage Model

The multi stage model used is:

for altitudes (a) over 10.769 km the density (ρ) is given by,

$$\rho = 0.37454745e^{-0.00015682(a-10769)} \frac{\text{altitude(in meters)}}{\text{speed of sound} = 295.92987 \frac{\text{m}}{\text{s}}}, \quad (2.1)$$

for altitudes less than 10.769 km,

$$\rho = 1.22581(1 - 0.00002257a)^{4.256} \frac{\text{altitude(in meters)}}{\text{speed of sound} = 14.9390\sqrt{518 - 0.01170a}}. \quad (2.2)$$

Two projectiles were used in the initial study. Both projectiles used in this comparison are representative direct fire fin-stabilized projectile with six fins. The first projectile (designated HP for heavy projectile) is 39.5 mm in diameter with projectile

mass, mass center measured along the stationline, roll inertia, and pitch inertia are 15.66 kg, 0.507 m, 0.00853 kg-m², and 6.20934 kg-m² respectively. The second projectile (designated LP for light projectile) is 26.8 mm in diameter with projectile mass, mass center measured along the stationline, roll inertia, and pitch inertia are 5.029 kg, 0.347 m, 0.00033 kg-m², and 0.24021 kg-m² respectively and identical to HP in aerodynamic coefficients. The projectile initial conditions for both projectiles in a standard 6DOF reference frame are as follows: $x = 0.0$ m, $y = 0.0$ m, $z = 0.0$ m, $\phi = 0.0$ deg, $\theta = 50.0$ deg, $\psi = 0.0$ deg, $u = 2022$ m/s, $v = 0.0$ m/s, $w = 0.0$ m/s, $p = 10.0$ rad/s, $q = 0.0$ rad/s, and $r = 0.0$ rad/s. The projectiles are traveling through standard atmosphere with a 5 m/s cross wind. This results in a 32 MJ launch for the HP which is the current state of the art for railgun technology and a 10 MJ launch for the LP.

The trajectory was calculated by a standard 4th order Runge Kutta 6DOF simulation, a custom written 2nd order 3DOF simulation (included in Appendix A) [48], and Modified Linear Theory as described by *Costello* [45]. The various methods are compared in the standard trajectory views in Figures 2.2-2.7. To see the limited influence of aerodynamic forces on the trajectory, the ratio of the drag force to the gravitational force (N) is shown on the trajectory Figure 2.2.

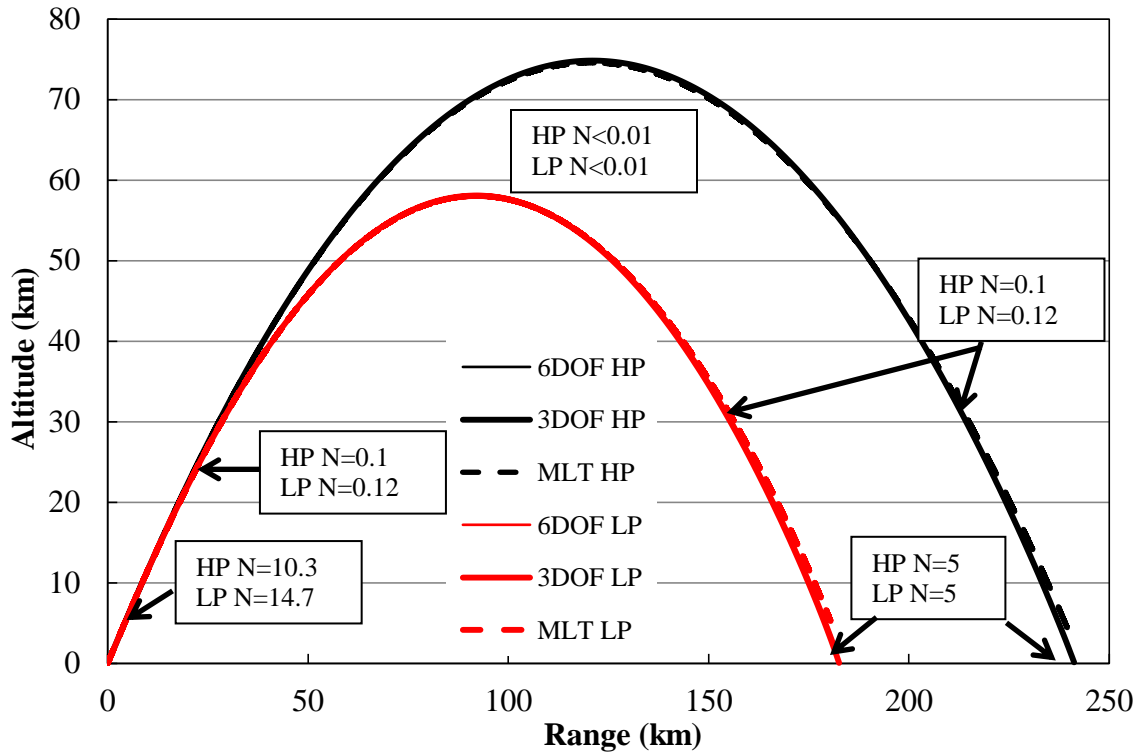


Figure 2.2 Altitude vs Range for 50 degree Launch Angle

(N=drag force/gravitational force)

The drag force starts out as the dominant force but quickly becomes less than 10% of the gravitational force. Above an altitude of 40 km, the aerodynamic force is less than 1% of the gravitational force. Thus the gravitational force is the dominant force in the shape of the projectile over the vast majority of the trajectory.

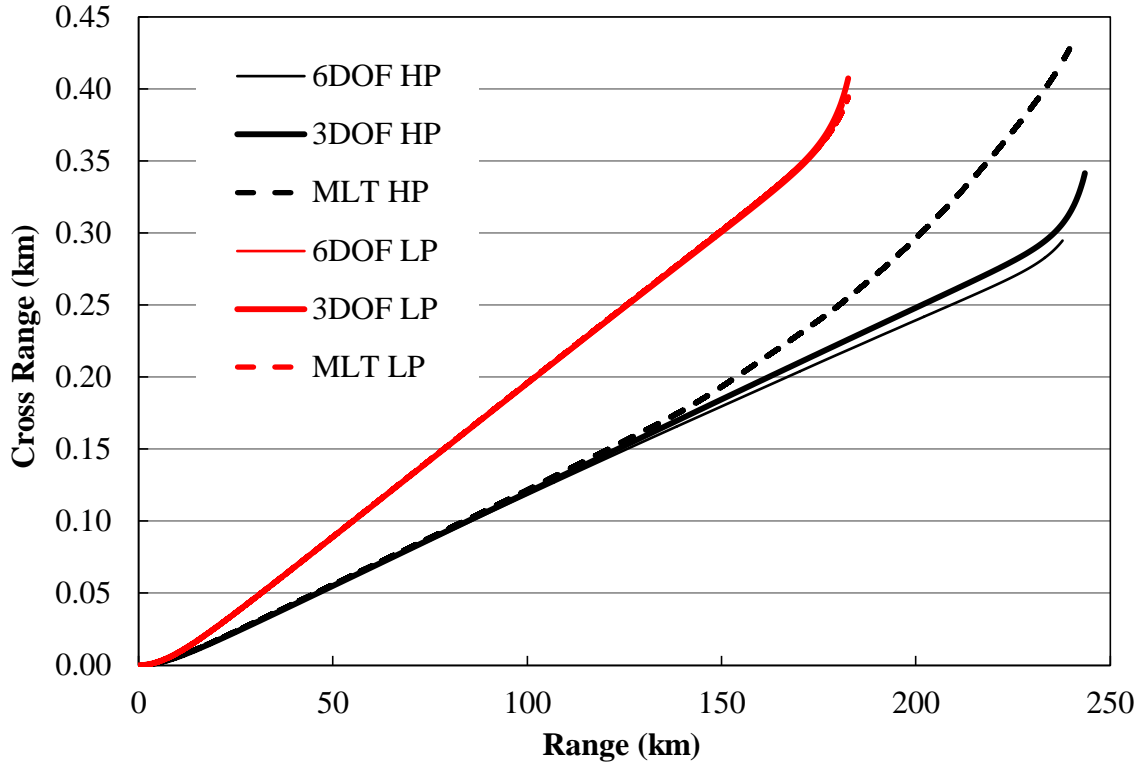


Figure 2.3 Cross Range vs Range for 50 degree Launch Angle

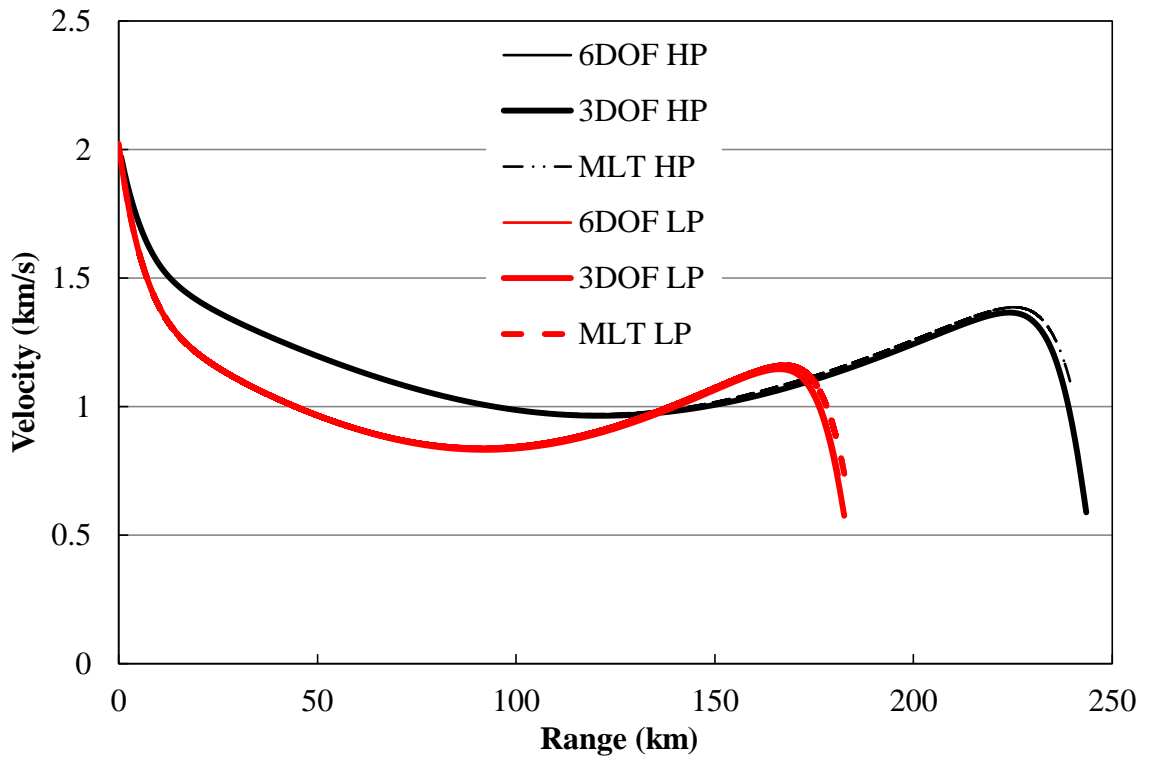


Figure 2.4 Velocity vs Range for 50 degree Launch Angle

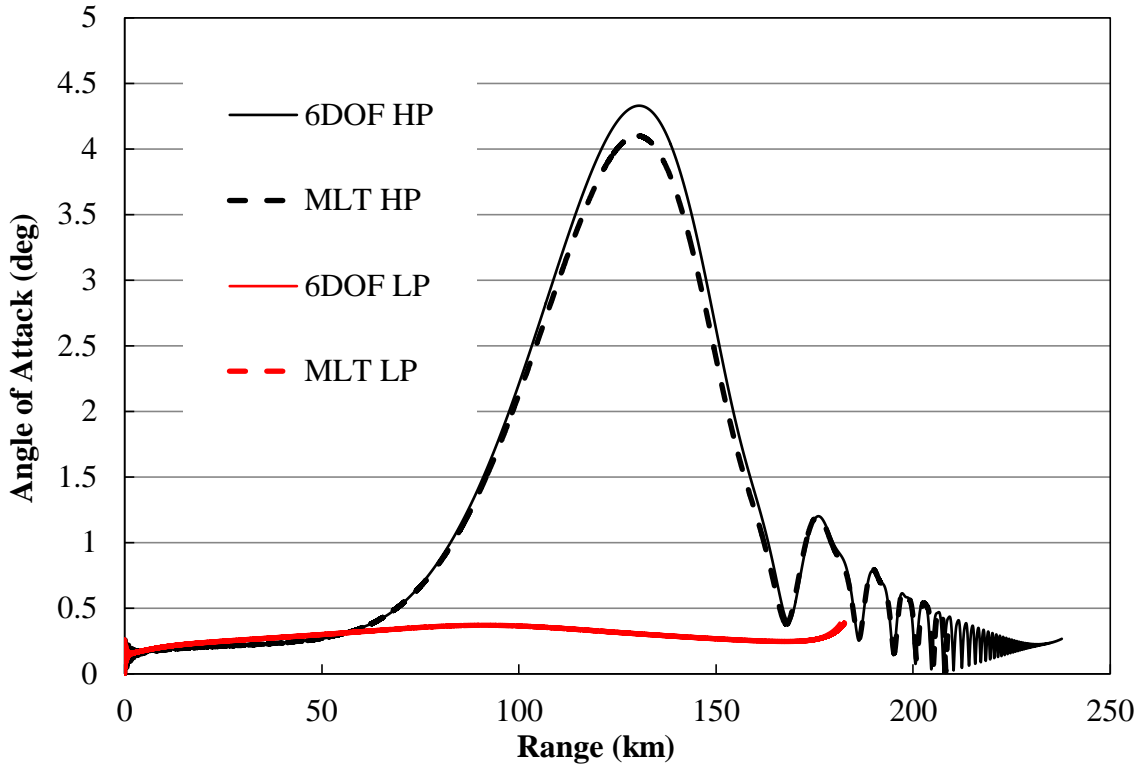


Figure 2.5 Angle of Attack vs Range for 50 degree Launch Angle

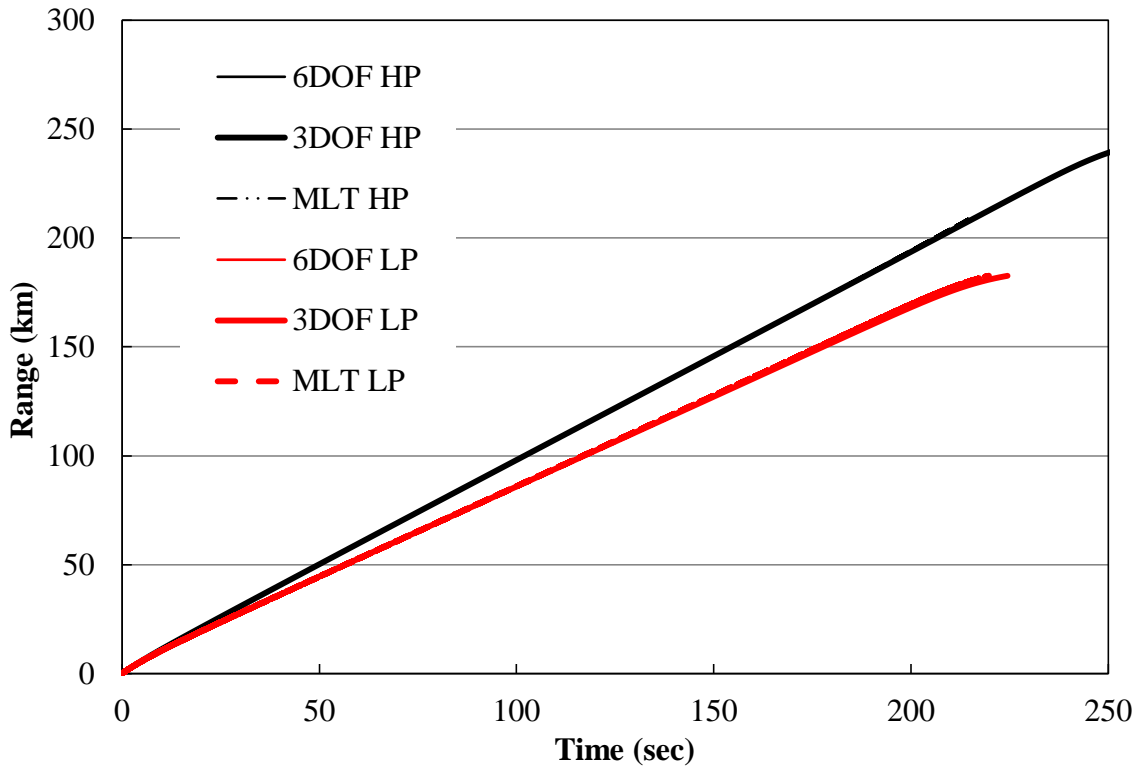


Figure 2.6 Range vs Time for 50 degree Launch Angle

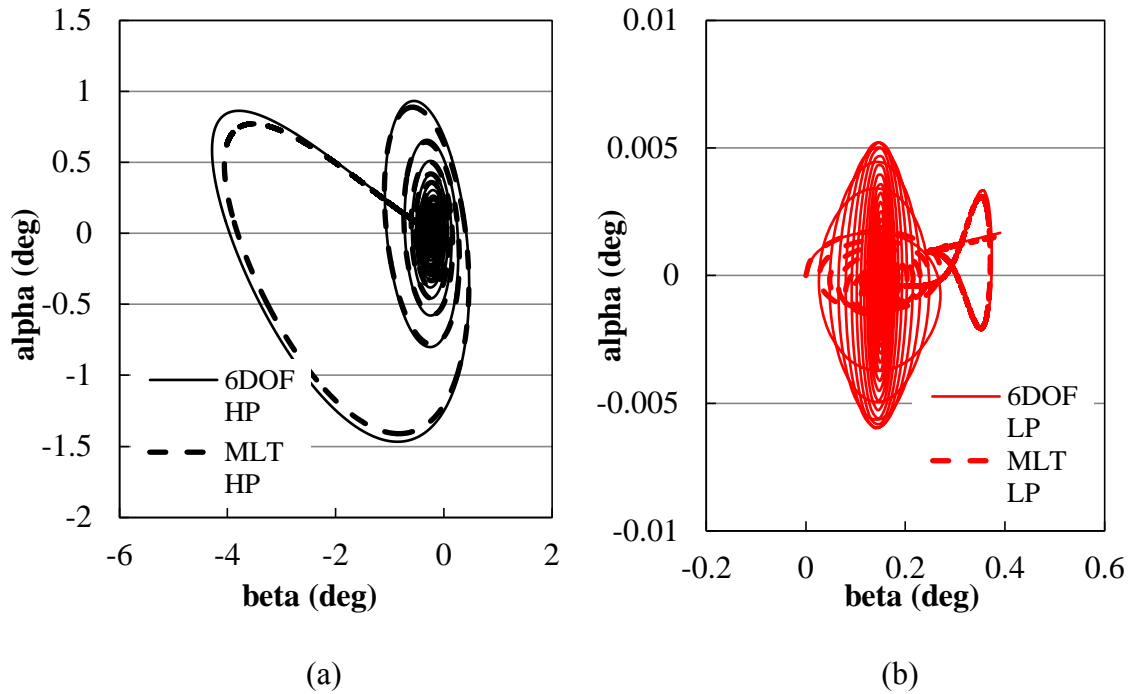


Figure 2.7 Swerve of Projectile for a 50 degree Launch Angle

B. Aerodynamic Behavior of the Projectiles

As can be seen, MLT predict the projectile motion accurately relative to the numerical simulation. As the projectile is aerodynamically stable and maintains a small angle of attack while within the atmosphere, the 3DOF simulation captures the trajectory accurately despite a large angle of attack while outside the atmosphere. Thus a point mass approach is valid for the evaluation of the trajectory as long as the aerodynamically stable assumption is maintained.

The trajectory of the projectile will cause it to travel through the layers of the atmosphere and result in a widely varying aerodynamic environment. As can be seen in Figure 2.8, the projectile starts with at a high Mach number that drops off slightly slower than the velocity decreases due to the drop in temperature as the projectile gains altitude.

This results in a very slow change in the overall drag coefficient, especially for the heavier projectile that slows down much less in the lower atmosphere.

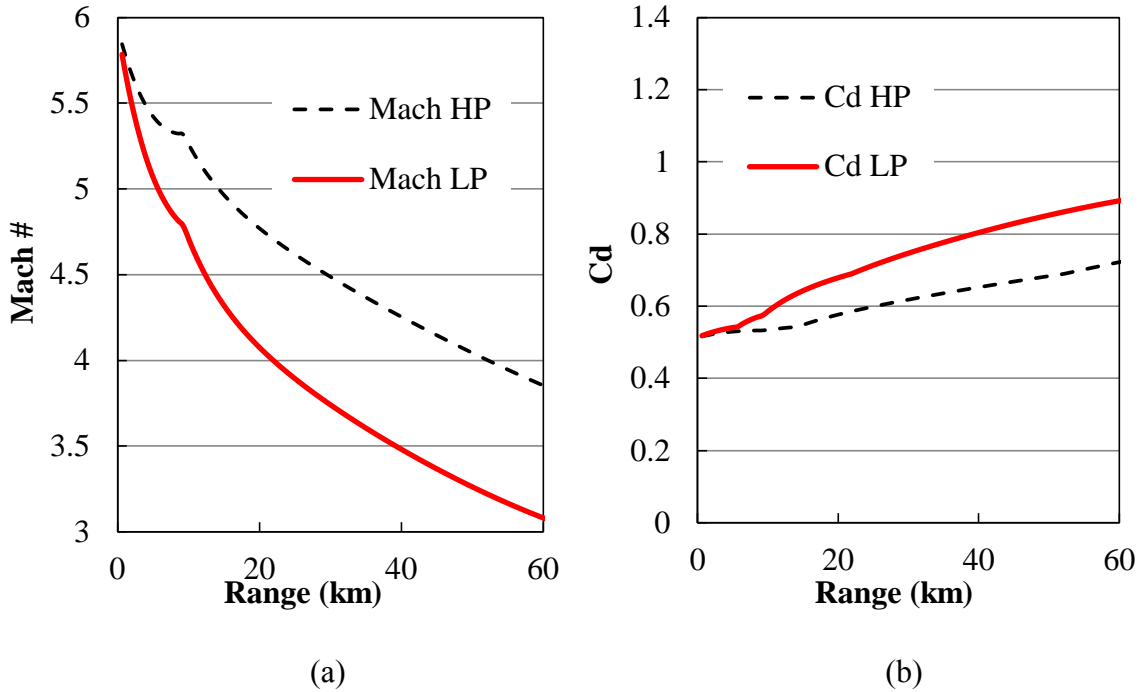


Figure 2.8 Mach & Drag Coefficient vs Range for 50 degree Launch Angle

The projectile has such a large momentum at launch that the drag force and gravity have a minor effect on the curvature of the trajectory while in the lower atmosphere as seen in Figure 2.9. The heavier projectile is less affected by traveling through the lower atmosphere and therefore shows less curvature than the lighter projectile. This approximately straight trajectory while in the lower atmosphere will allow for a simplifying assumption in the later derivation of the new Modified Kepler solution.

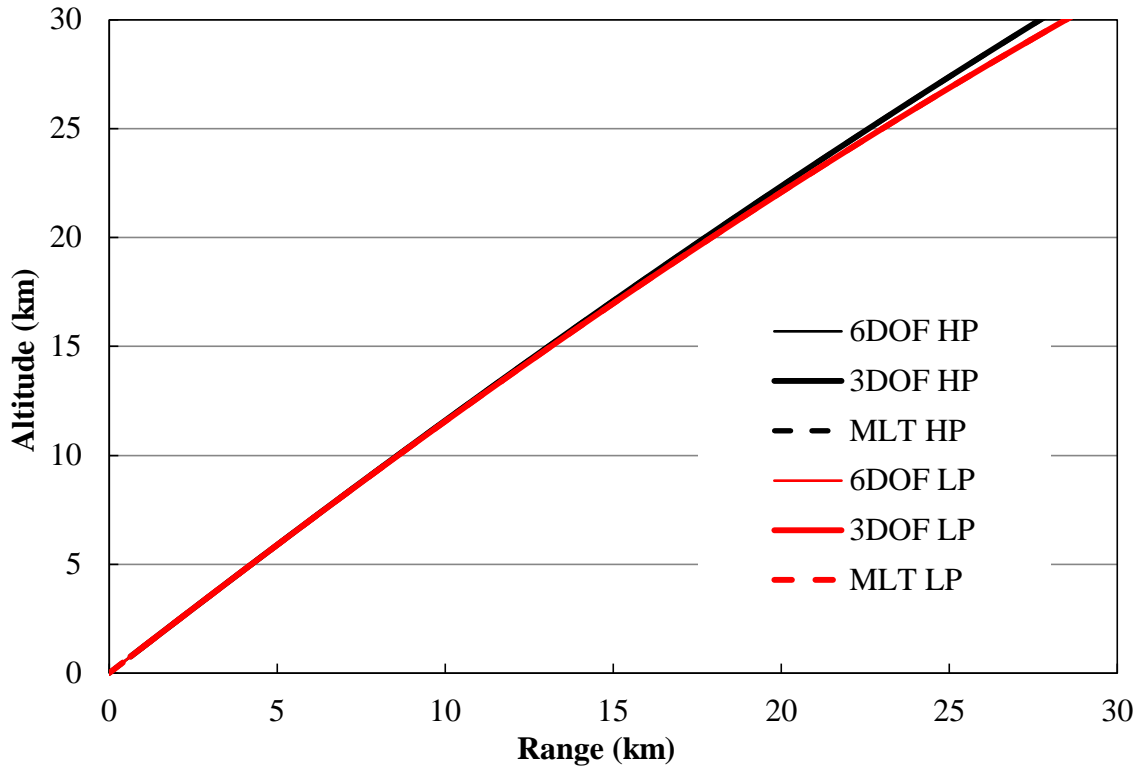


Figure 2.9 Altitude vs. Range while in the Lower Atmosphere for a 50 degree Launch Angle

Finally, it is interesting to look at the angular momentum of the projectiles with respect to the center of the Earth. The specific angular momentum (angular momentum per unit mass) of the projectiles is shown in Figure 2.10. The angular momentum decays while in the lower atmosphere at a rate that is dependent upon the mass and drag properties of the projectile to an asymptotic value as the projectile leaves the lower atmosphere. The angular momentum is then approximately constant while traveling through the upper atmosphere and decays again upon reentry into the lower atmosphere once again.

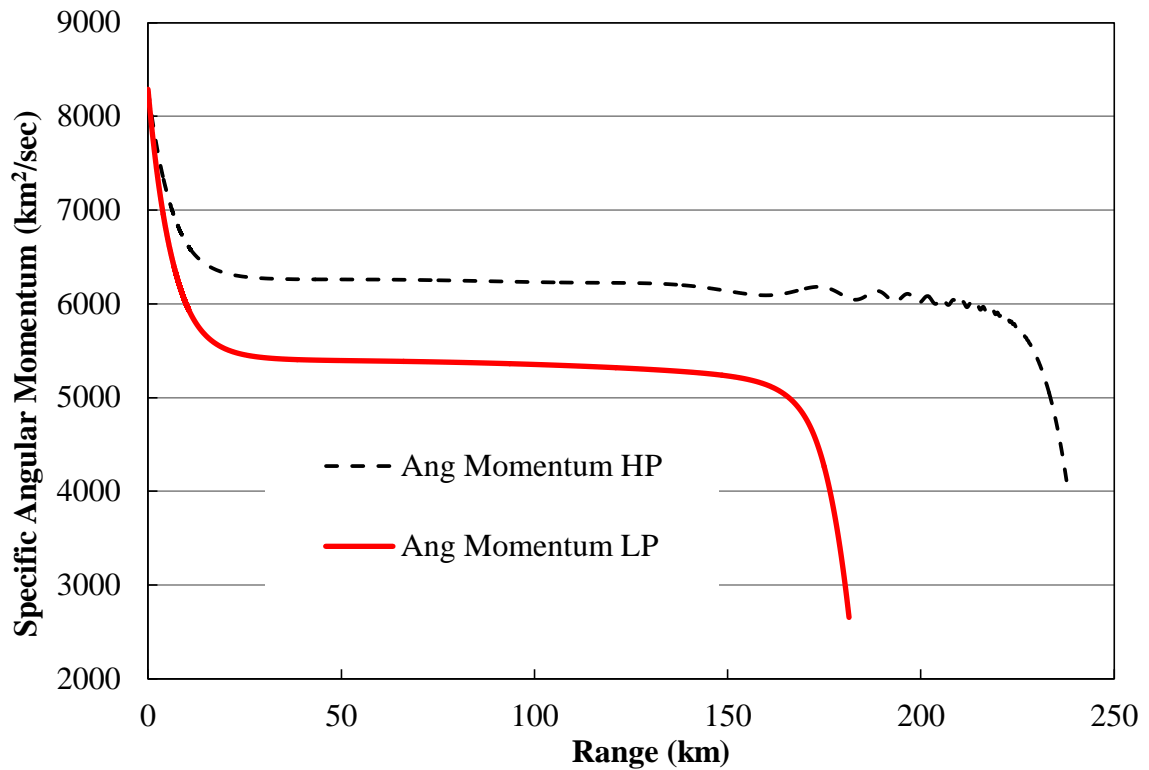


Figure 2.10 Specific Angular Momentum vs. Range for a 50 degree Launch Angle

The behavior of the angular momentum provides a hint at the Modified Kepler solution method. The standard Kepler solution assumes the conservation of angular momentum as is seen after the projectile leaves the lower atmosphere. If a method can be found to estimate the decay of the angular momentum while in the lower atmosphere and predict the asymptotic angular momentum, the trajectory of the projectile can be estimated by modifying the standard Kepler solution.

CHAPTER 3

DERIVATION OF THE MODIFIED KEPLER EQUATION

The Kepler equation allows for the analytic solution of the motion of a particle due to non-uniform gravity classically called the two body problem. In the absence of atmospheric drag, projectile motion can be described by the Kepler equation. This model is appropriate for a projectile at sufficiently high altitudes where drag contributes a negligible amount to the motion. The standard Kepler solution is reasonably valid above 30 km and can be assumed exact at altitudes above 100 km.

The approach taken in this project was to modify the Kepler equation so that it captures the effects of aerodynamic drag while maintaining the simplicity of the standard Kepler equation. To that end, the Modified Kepler solution utilizes the same differential and variable transformations that make the Kepler equation elegant while applying the minimum simplifying assumptions to keep the Modified Kepler equation solvable with simple analytic functions.

Both the standard Kepler equation and the Modified Kepler equations will be derived in a non-rotating Earth model (Earth Centered Earth Fixed) in this chapter for simplicity. The adjustment of the Modified Kepler equation for use on a rotating Earth model (Earth Centered Inertial) will be presented in Chapter 4.

A. Kepler Equation

In standard Kepler motion, all motion is contained in a plane that can be described by polar coordinates $(r(t), \theta(t))$. The radial equation of motion is then modified by a differential transformation based upon the definition of angular momentum so that radial position is dependent upon angular position $r(\theta)$. The resulting single ordinary differential equation effectively describes the motion (trajectory) of the particle with the loss of the time dependence of the motion. Beginning with the conservation of momentum in polar coordinates:

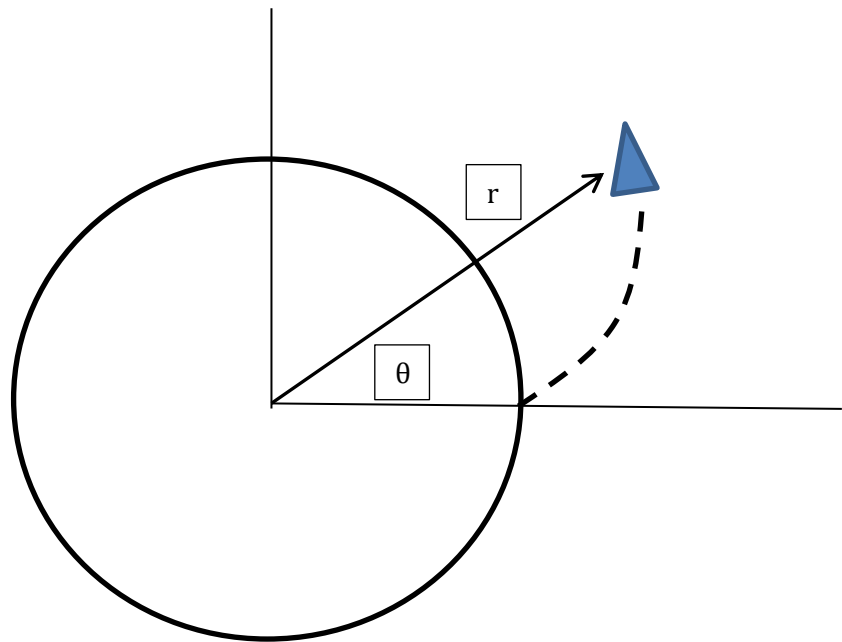


Figure 3.1 Polar Coordinates for Projectile Trajectory

$$m\ddot{\theta}r + m2\dot{r}\dot{\theta} = 0, \quad m\ddot{r} - mr\dot{\theta}^2 = -\frac{mMG}{r^2}, \quad (3.1)$$

where m is the mass of the projectile, M is the mass of the Earth, and G is the universal gravitation constant. Using the definition of angular momentum:

$$L = m\dot{\theta}r^2, \quad (3.2)$$

the differentials with respect to time are transformed into differentials with respect to angular range:

$$\dot{\theta} = \frac{d\theta}{dt} = \frac{L}{mr^2}, \quad (3.3)$$

$$\frac{d}{dt} = \frac{d\theta}{dt} \frac{d}{d\theta} = \frac{L}{mr^2} \frac{d}{d\theta}, \quad (3.4)$$

$$\frac{d^2}{dt^2} = \frac{L}{mr^2} \frac{d}{d\theta} \left(\frac{L}{mr^2} \frac{d}{d\theta} \right). \quad (3.5)$$

The differential transformations are applied to the radial equation of motion (3.1):

$$m \frac{L}{mr^2} \frac{d}{d\theta} \left(\frac{L}{mr^2} \frac{dr}{d\theta} \right) - mr \left(\frac{L}{mr^2} \right)^2 = \frac{-mMG}{r^2}. \quad (3.6)$$

The equation of motion can be further simplified by the variable transformation $u = \frac{1}{r}$:

$$\frac{dr}{d\theta} = \frac{d\frac{1}{u}}{d\theta} = -\frac{1}{u^2} \frac{du}{d\theta}. \quad (3.7)$$

For constant angular momentum, the equation of motion is simplified to the standard

Kepler equation:

$$\frac{d^2u}{d\theta^2} + u = \frac{m^2MG}{L^2}. \quad (3.8)$$

If the angular momentum is assumed to vary with angular range, equation (3.6) requires the embedded differential in the first term to be expanded by the product rule. Performing this expansion and simplifying with the same variable transformation gives the Modified Kepler equation of motion:

$$\frac{d^2u}{d\theta^2} + \frac{1}{L} \frac{dL}{d\theta} \frac{du}{d\theta} + u = \frac{m^2MG}{L^2}. \quad (3.9)$$

It will be shown that the Modified Kepler equation of motion is capable of predicting the trajectory of a projectile with the following assumptions:

1. The projectile is aerodynamically stable within the atmosphere and can be treated as a point mass despite a large angle of attack in the upper atmosphere.
2. The atmospheric density can be modeled as a decaying exponential function with altitude.
3. The angular momentum of the projectile decays within the lower atmosphere as if it was traveling in a straight line.
4. The projectile is traveling with sufficient initial velocity that the Mach number and thus drag coefficient are approximately constant.
5. The change in radial position of the bullet relative to the center of the Earth is insignificant relative to the influence of the aerodynamic forces in calculating the angular momentum.
6. The non-linear term in the Modified Kepler equation of motion $\left(\frac{1}{L} \frac{dL}{d\theta} \frac{du}{d\theta}\right)$ may be neglected with minimal loss of system response to the angular momentum driving function.

B. Derivation of Angular Momentum Driving Function

The behavior of the angular momentum within the sensible atmosphere is needed to evaluate 3.9. Beginning with the conservation of angular momentum about the center of the non-rotating Earth assuming the classic aerodynamic drag relation:

$$\frac{dL}{dt} = -\frac{1}{2} \rho C_D A V^2 r \cos \phi, \quad (3.10)$$

where ρ is the atmospheric density, C_D is the axial drag coefficient, A is the projected cross-sectional area in the direction of travel, V is the absolute velocity relative to the atmosphere, and ϕ is the launch elevation. The density is obviously not a constant value for a projectile that travels into space so a mathematical model of the atmosphere is needed. An exponential model was chosen to model the data of the form (Assumption 2):

$$\rho = \rho_0 e^{-ka}. \quad (3.11)$$

The initial density (ρ_0) is taken as the density at the Earth's surface from the Standard Atmosphere (1.225 kg/m^3). The decay constant (k) was found by optimizing the coefficient of determination between the exponential model and the NASA Standard Atmosphere data. An optimized coefficient of determination ($R^2=0.994$) was found with a constant of 0.117 km^{-1} . The exponential model fit of the data is shown in Figure 3.2. The exponential model does not capture the density above 15 km well but the majority of the angular momentum decay occurs in the lower atmosphere where the exponential model is reasonably accurate.

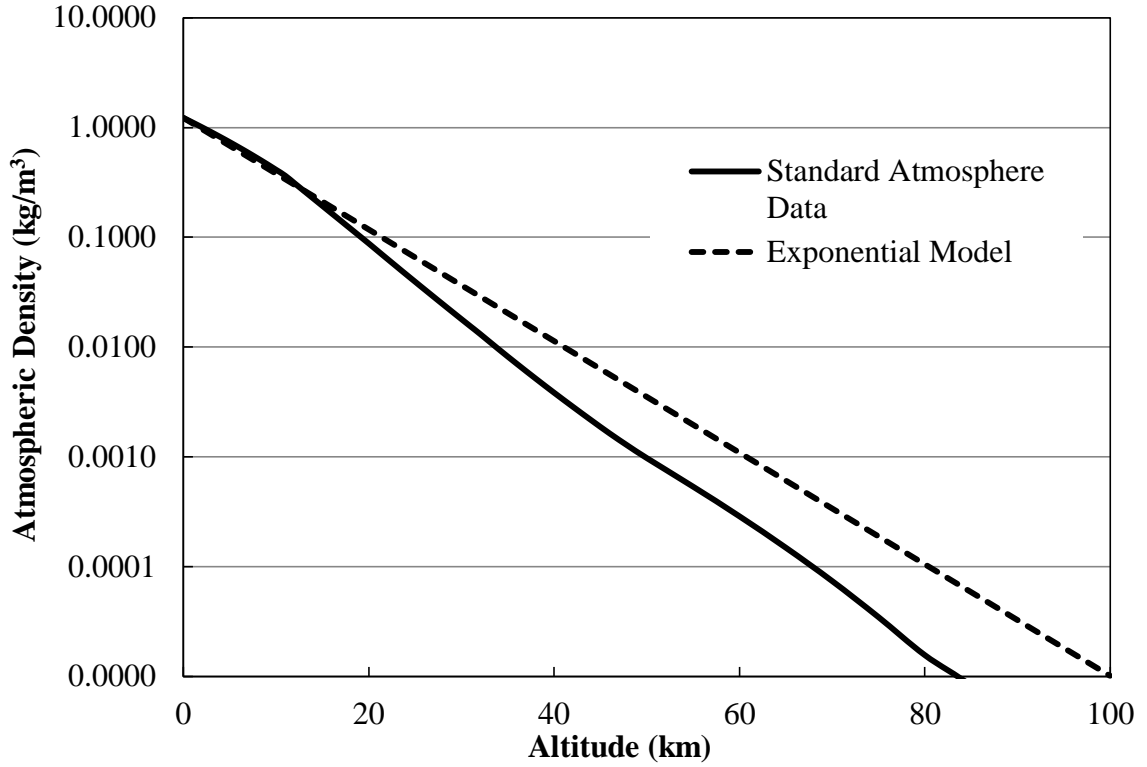


Figure 3.2 Atmospheric Density from the NASA Standard Atmosphere (1976) [47]
with Exponential Model

The rate of change of the angular momentum in terms of the decaying atmospheric density is:

$$\frac{dL}{dt} = -\frac{1}{2}C_D AV^2 r \rho_0 e^{-ka} \cos(\phi). \quad (3.12)$$

The velocity term in equation (3.12) can be removed using the definition of angular momentum:

$$\begin{aligned} \frac{dL}{dt} &= -\frac{1}{2}C_D AV^2 r \rho_0 e^{-ka} \cos(\phi) \frac{L^2}{(mVr \cos \phi)^2} \\ &= -\frac{C_D AL^2 \rho_0}{2m^2 r \cos(\phi)} e^{-ka}. \end{aligned} \quad (3.13)$$

Converting (3.13) to a differential with respect to angular range using the differential transformation (3.4, 3.5):

$$\frac{dL}{dt} = \frac{dL}{d\theta} \frac{L}{mr^2} = -\frac{C_D A \rho_0}{2m^2 r \cos(\phi)} L^2 e^{-ka}, \quad (3.14)$$

$$\frac{dL}{d\theta} = -\frac{C_D A \rho_0}{2m \cos(\phi)} r L e^{-ka}. \quad (3.15)$$

The altitude in equation (3.15) must be converted into an angular range to enable a solution to the equation. For a projectile with sufficient initial velocity to leave the atmosphere, the initial trajectory inside the atmosphere is assumed to be approximately straight (Assumption 3). The altitude can be converted to angular range using this approximation shown in Figure 3.3:

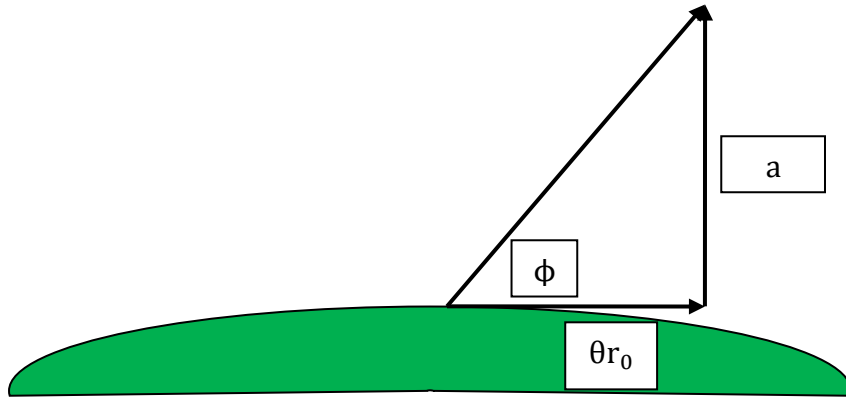


Figure 3.3 Angular Range Approximate Relationship with Altitude

$$a \approx \theta r_0 \tan(\phi), \quad (3.16)$$

$$\frac{dL}{d\theta} = -\frac{C_D A \rho_0}{2m \cos(\phi)} r L e^{-kr_0 \tan(\phi)\theta}. \quad (3.17)$$

The assumption that angular momentum decays as if the projectile travels in a straight line effectively decouples the angular momentum equation from the equation of motion. This is analogous to the assumption that linear momentum decays as if the projectile

travels in a straight line in linear or modified linear theory.

The driving function can be found by the solution of equation (3.17) which can be solved using a separation of variables approach if the radial position and drag coefficient can be assumed to be approximately constant. For the trajectory in the atmosphere to be approximately straight as assumed in equation (3.16), the projectile must be moving rapidly through the air. If the projectile is moving at high enough speeds, the projectile should exhibit close to Mach number independence and result in an approximately constant drag coefficient (Assumption 4). As will be shown later, the drag coefficient changes less than 5% while below 20 km. The radius in equation (3.17) changes less than 1% from its initial value (6378 km) while the projectile is below 20 km where the majority of angular momentum is dissipated (Assumption 5). If both the drag coefficient and radial position is treated as constant for the decay of angular momentum the driving function can be defined as:

$$\frac{dL}{L} = -\frac{C_{D0}A\rho_0}{2m\cos(\phi)}r_0e^{-kr_0\tan(\phi)\theta}d\theta, \quad (3.18)$$

$$\ln|L| = \frac{C_{D0}A\rho_0}{2kmsin(\phi)}e^{-kr_0\tan(\phi)\theta} + C. \quad (3.19)$$

Taking the exponential of equation (3.19) exposes the driving function for angular momentum as a double exponential:

$$L = Ce^{\beta\gamma}, \quad (3.20)$$

with

$$\gamma = e^{-ktan(\phi)r_0\theta}, \quad (3.21)$$

and

$$\beta = \frac{C_{D0}\rho_0A}{2kmsin(\phi)}. \quad (3.22)$$

Evaluating the angular momentum at initial conditions gives the value of the constant:

at

$$\theta = 0,$$

$$\gamma = 1 \text{ and } L = L_0,$$

therefore:

$$L_0 = Ce^\beta,$$

$$C = L_0e^{-\beta},$$

$$L = L_0e^{\beta(\gamma-1)} = L_\infty e^{\beta\gamma}. \quad (3.23)$$

The double exponential makes solution of the Modified Kepler equation difficult so a power series expansion of the double exponential is used:

$$e^{\beta\gamma} = \sum_{n=0}^{\infty} \frac{(\beta e^{-k \tan(\phi) r_0 \theta})^n}{n!}. \quad (3.24)$$

This method of expanding the base exponential of the double exponential driving function is similar to a Taylor series expansion of perturbation force terms used to modify standard Kepler theory for atmospheric drag on satellites. A significant difference is that the value of the atmospheric drag must be very small compared to the gravitational force for perturbation theory whereas the atmospheric drag based angular momentum decay can be significantly larger than gravitational force in the power series expansion method used.

C. Modified Kepler Equation

The Modified Kepler equation (3.9) can be written in terms of the driving function and angular momentum:

$$\frac{d^2u}{d\theta^2} - \tau\beta e^{-\tau\theta} \frac{du}{d\theta} + u = \frac{m^2MG}{L_\infty^2} \sum_{n=0}^{\infty} \frac{(-2\beta e^{-\tau\theta})^n}{n!}, \quad (3.25)$$

where,

$$\frac{1}{L} \frac{dL}{d\theta} = \frac{1}{L_\infty e^{\beta\gamma}} L_\infty e^{\beta\gamma} \beta e^{-\tau\theta} (-\tau) = -\tau\beta e^{-\tau\theta}, \quad (3.26)$$

and

$$\tau = kr_0 \tan \phi. \quad (3.27)$$

For a power series solution approach, the nonlinear term $(\tau\beta e^{-\tau\theta} \frac{du}{d\theta})$ becomes a convolution between the power series expansion of the exponential decay function and the power series expansion of the first derivative of u which makes the direct solution of (3.25) difficult. The equation may be further simplified by the transformation:

$$\tan(\phi) = \frac{\frac{dr}{dt}}{\frac{d\theta}{dt}} = -\frac{du}{d\theta} \frac{1}{u}. \quad (3.28)$$

Equation (3.25) now may be simplified to:

$$\frac{d^2u}{d\theta^2} + u(1 + \tau\beta \tan(\phi) e^{-\tau\theta}) = \frac{m^2MG}{L_\infty^2} \sum_{n=0}^{\infty} \frac{(-2\beta e^{-\tau\theta})^n}{n!}. \quad (3.29)$$

Equation (3.29) is obviously difficult to solve as presented. The natural frequency of the system starts from a relatively large value much greater than one and decays to one as the projectile leaves the atmosphere. For example, for the HP 50 degree trajectory used in this thesis, the initial natural frequency of the system is 27 rad/rad that decays to 1 rad/rad. If the natural frequency of the system is fixed at the asymptotic value of 1 rad/rad, the result is that high frequency components of the driving function are attenuated slightly more than originally predicted as shown in Figure 3.4. The contribution of the high frequency components of the driving function is small enough that the non-linear system may be modeled with the linear estimation with minor errors.

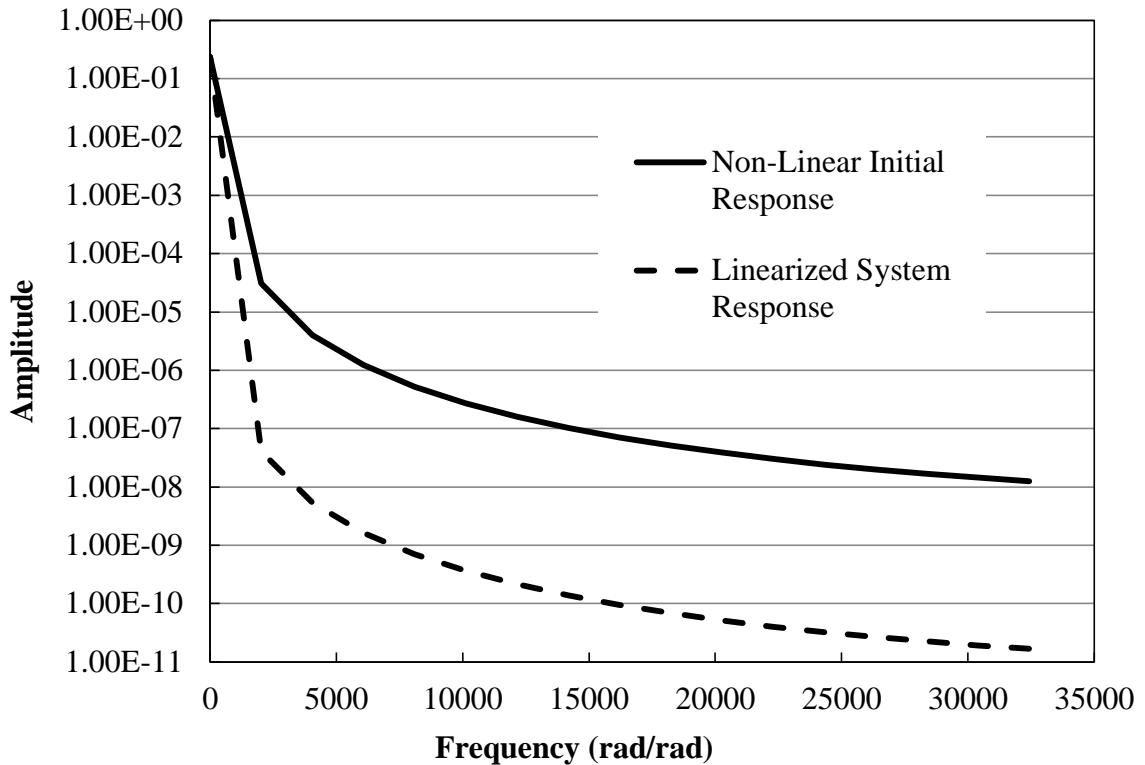


Figure 3.4 Open Loop Frequency Response of the Non-Linear and Linearized Modified Kepler Equation to the Driving Function

There is a resonance not shown at the natural frequency of the un-damped system. The frequency is very low compared to the driving functions and the driving functions decay so quickly that the resonance apparently does not have time to initiate significant error.

Setting the natural frequency of the system to 1 rad/rad (Assumption 6), the Modified Kepler equation for a projectile launched with enough initial velocity that the drag coefficient can be assumed as constant is given by:

$$\frac{d^2u}{d\theta^2} + u = \frac{m^2MG}{L_\infty^2} \sum_{n=0}^{\infty} \frac{(-2\beta e^{-\tau\theta})^n}{n!}. \quad (3.30)$$

The solution of equation (3.30) is straight forward using common analytical functions if the infinite series converges. The Modified Kepler ballistic coefficient for a projectile that is capable of travel into space is much less than 1 which ensures that the power series expansion of the double exponential converges and can be truncated. The larger the ballistic coefficient, the more terms are needed to accurately capture the motion of the projectile.

The time of flight of the projectile (t) given by the integration of the angular momentum definition given by equation (3.2):

$$\int dt = \int \frac{d\theta r^2}{L}, \quad (3.31)$$

$$t = \int \frac{d\theta}{u^2 L_\infty e^{\beta Y}}. \quad (3.32)$$

The integral was evaluated via a simple numerical integration to calculate the time of flight for each angular range position.

The shape of the trajectory is completely analytic but the time of flight to a point on the trajectory is not. For a firing solution, the analytic solution may be iterated for various initial conditions using a non-linear solver very quickly and the final analytic solution used to numerically integrate the time to fire the projectile. This provides for a very rapid calculation of an approximate firing solution.

CHAPTER 4

COMPARISON OF THE MODIFIED KEPLER EQUATION TO OTHER TRAJECTORY METHODS

The Modified Kepler equation provides a very simple method of calculating trajectories of projectiles launched into space but the simplifying assumptions introduce errors. In this chapter we will compare the Modified Kepler solution (MKS) in a non-rotating ECEF reference frame to various other methods of calculating trajectories of space projectiles and compare the results.

A. MKS Reference Trajectory

The same reference trajectory used for the HP was used to compare to the MKS. The various methods are compared in Figures 4.1-4.6.

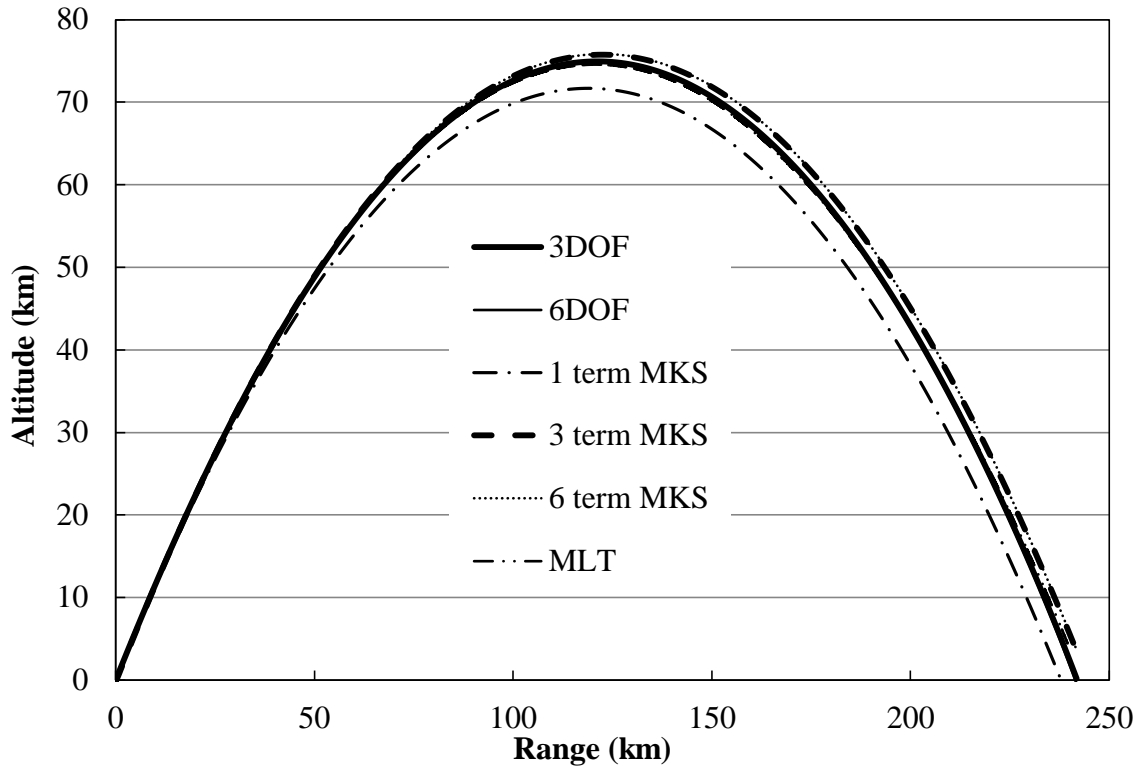


Figure 4.1 Altitude vs Range for 50 degree Launch Angle

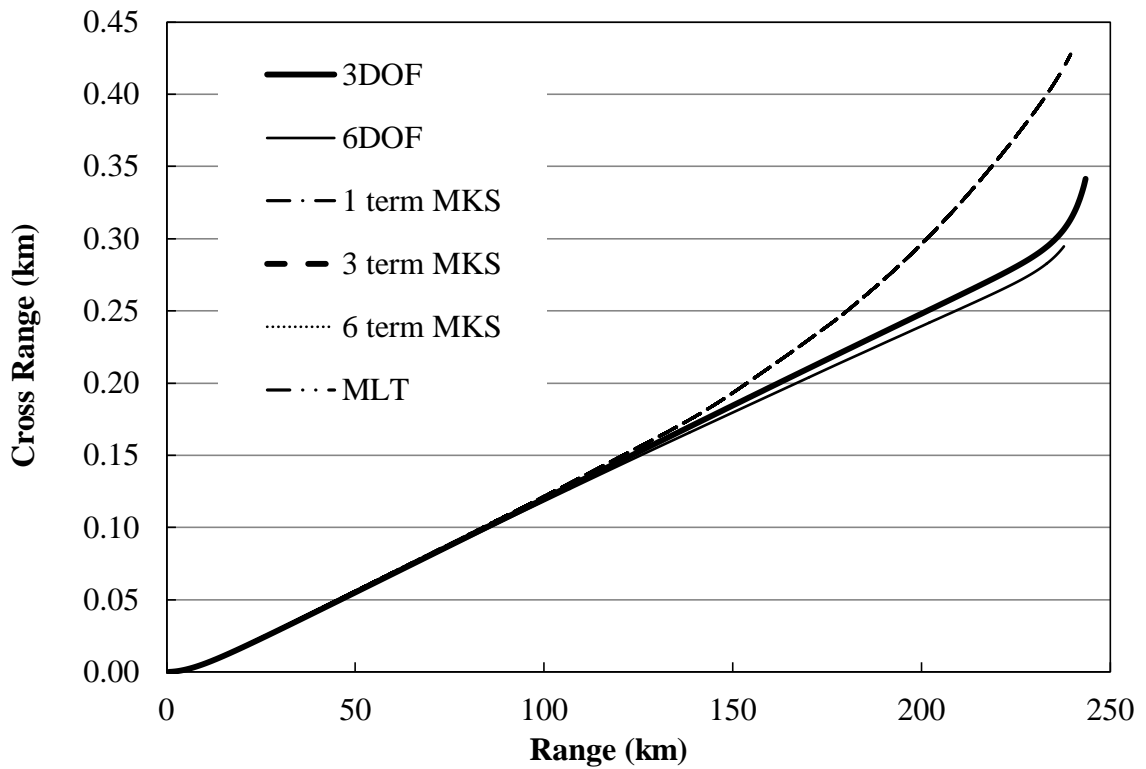


Figure 4.2 Cross Range vs Range for 50 degree Launch Angle

The absolute velocity is readily available from the numerical simulations but must be derived from the Modified Kepler Solution. Starting with the definition of total velocity in polar coordinates:

$$V = \sqrt{\left(\frac{d\theta}{dt}r\right)^2 + \left(\frac{dr}{dt}\right)^2}. \quad (4.1)$$

The differentials with respect to time are converted to angular range by the angular momentum relationship and the radial variable transformation is again used:

$$V = \sqrt{\left(\frac{L}{m}u\right)^2 + \left(\frac{du}{d\theta}\frac{L}{m}\right)^2}, \quad (4.2)$$

with

$$L = L_{\infty}e^{\beta\gamma}. \quad (4.3)$$

The absolute velocities of the various methods are shown in Figure 4.3. Note the sharp decrease in velocity that indicates reentry into the atmosphere in the MLT and numerical simulations. The MKS does not account for this reentry and therefore diverges at reentry.

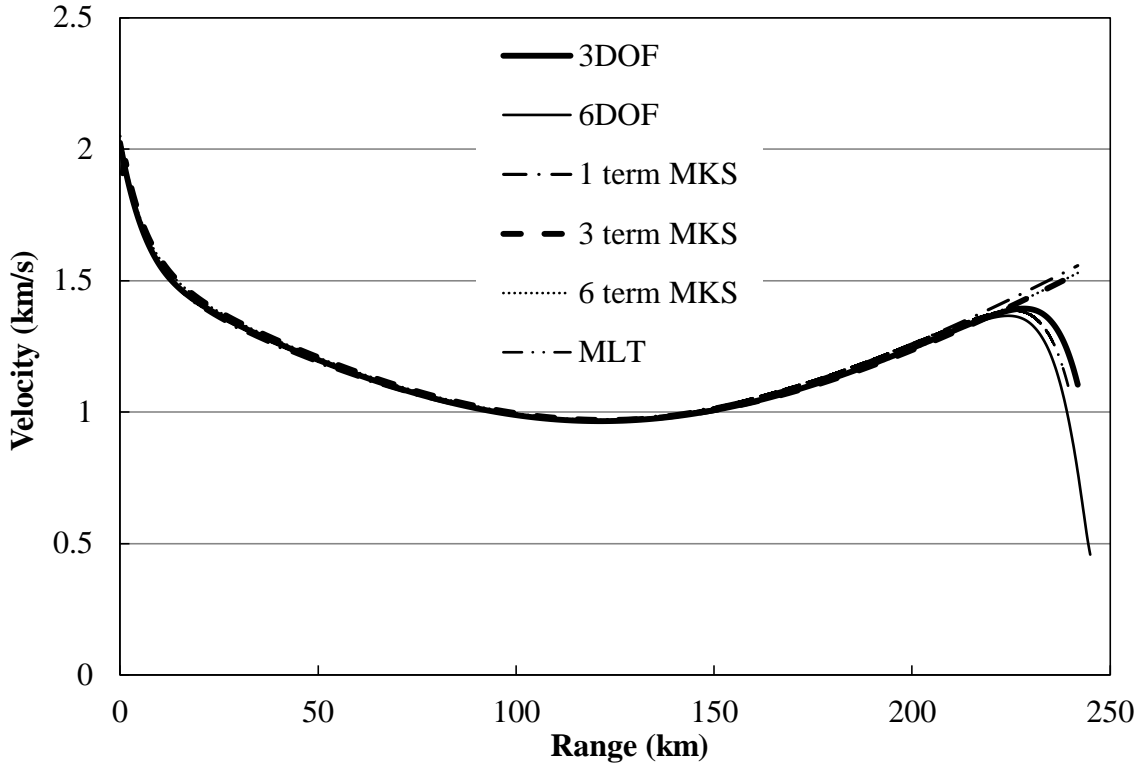


Figure 4.3 Velocity vs Range for 50 degree Launch Angle

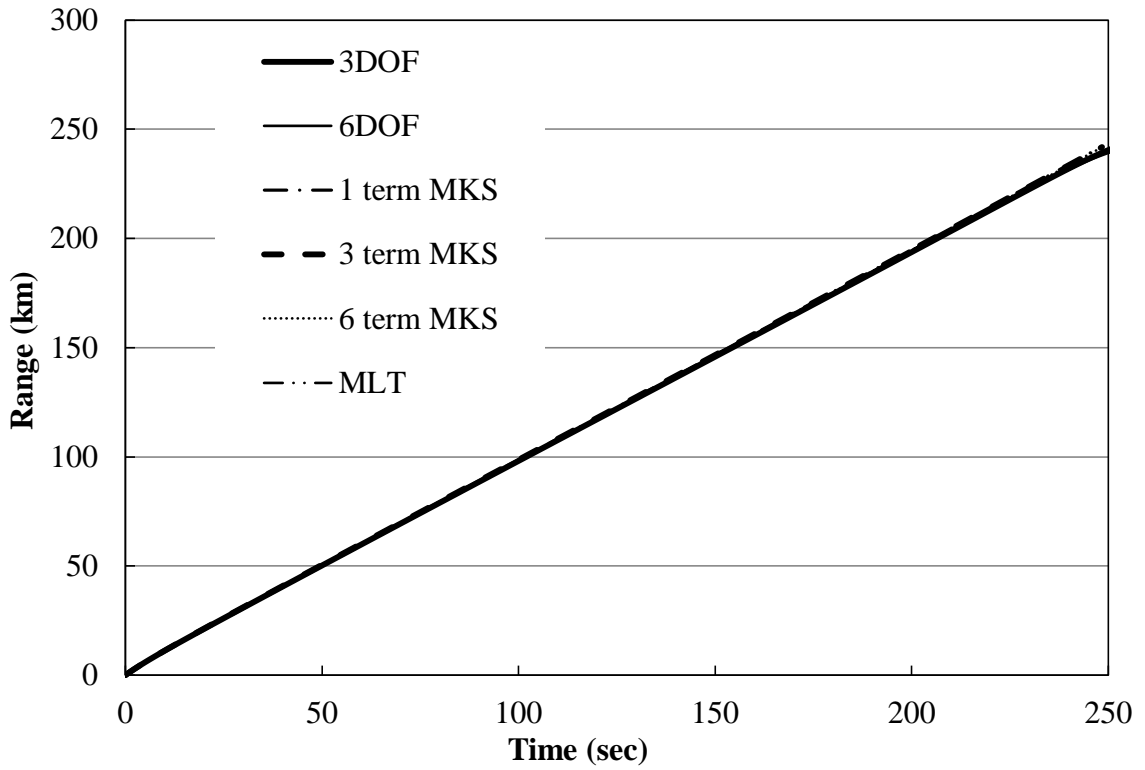


Figure 4.4 Range vs Time for 50 degree Launch Angle

The extreme range of the trajectory makes the error between the trajectories hard to observe. For direct comparison of the 3DOF and 6DOF numerical simulations in which time is the independent variable with Kepler type solutions in which angular range is the independent variable, a method of calculating the instantaneous error at any time step is needed. The total error is the absolute distance between the predicted position of the projectile from the numerical simulation and the predicted position from the Kepler solution for each simulation time step. The radial and time error terms are combined by the relationships:

$$\epsilon_r = r_{\text{sim}} - r_{\text{Kepler}}, \quad (4.4)$$

$$\epsilon_\theta = (t_{\text{Kepler}} - t_{\text{sim}})|V|, \quad (4.5)$$

$$\Phi = \tan^{-1} \left(-r \frac{du}{d\theta} \right) = \tan^{-1} \left[r \left(\frac{1}{r_i} - m^2 \frac{MG}{L^2} \right) \sin(\theta) - r \frac{\tan(\phi_i)}{r_i} \cos(\theta) \right], \quad (4.6)$$

$$\epsilon_{\text{total}} = \sqrt{((\epsilon_r + \epsilon_\theta \cos \phi)^2 + (\epsilon_\theta \sin \phi)^2)}. \quad (4.7)$$

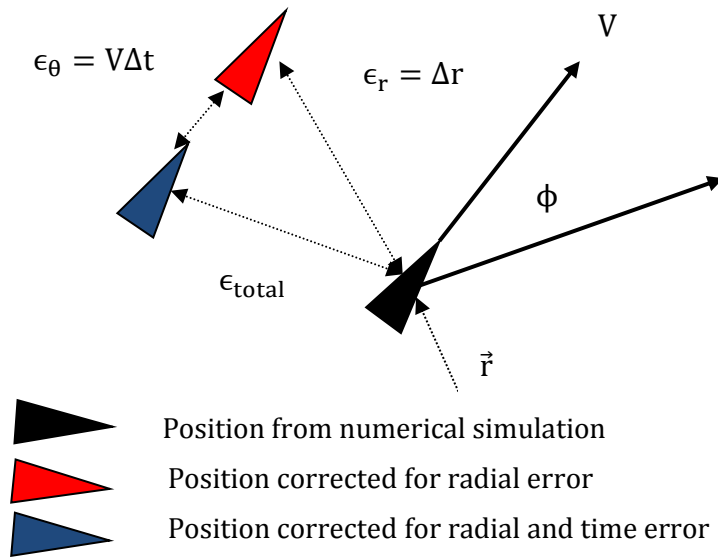


Figure 4.5 Geometry for Total Error Calculation between Numerical Simulation and Modified Kepler Solution

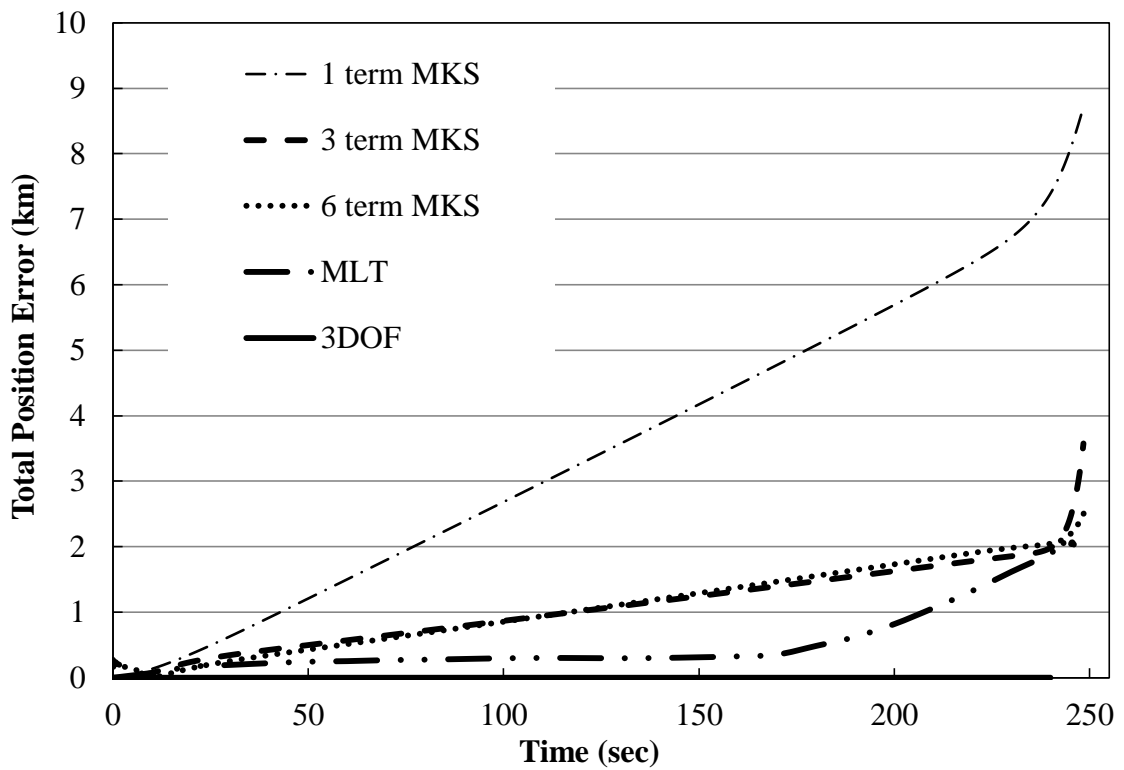


Figure 4.6 Total Position Error between the 3DOF Numerical Simulation and Modified Kepler Solution

The assumption that a point mass approach can accurately predict the trajectory (Assumption 1) is justified by the lack of error between the 3DOF and 6DOF simulations despite a rather significant angle of attack of over 4 degrees at apogee. The atmosphere is just too thin at these high altitudes and the trajectory can be modeled as a point mass trajectory. As long as the projectile is aerodynamically stable, the projectile can be modeled as a point mass with the appropriate drag characteristics.

The influence of wind is also not included in the Modified Kepler solution but as can be seen by the cross range motion (Figure 4.2), the influence of wind is small compared to the error of the Modified Kepler assumptions.

It appears that the three term Modified Kepler solution is capable of capturing the trajectory relatively well and that increasing the number of terms does not significantly increase the accuracy of the solution. This trend was consistent for all projectiles used in this paper. A comparison of accuracy with the computational effort in floating point operations (FLOPS) to calculate the solution is shown in Figure 4.7. As can be seen, the Modified Kepler solution is within 2 km (2.7% of apogee) with four orders of magnitude decrease in computations over a 6DOF and three orders of magnitude decrease over Modified Linear Theory and 3DOF simulations. The only experimental data that is available for projectiles launched into space, given in Chapter 6, show a spread of data much larger than the error in the Modified Kepler Solution suggesting that the Modified Kepler Solution is sufficient for most practical applications within limitations.

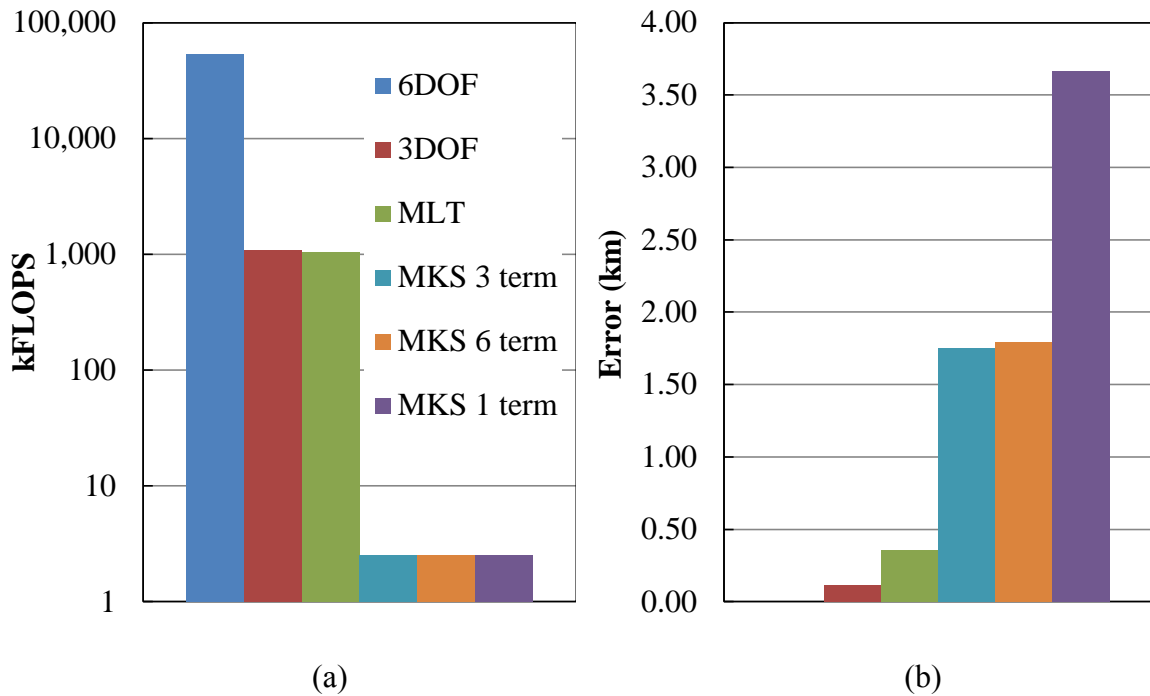


Figure 4.7 Computational Effort and Error to Calculate Apogee

B. Baseline Hypersonic Projectile Trajectories

The direct fire finned projectile used in the previous section is designed for lower atmosphere use. The finned and roll stabilization used to increased accuracy result in a relatively high drag coefficient relative to the weight of the projectile. This can be seen by the high β value. The lower the drag to weight, the closer the assumptions used to derive the Modified Kepler Solution are maintained.

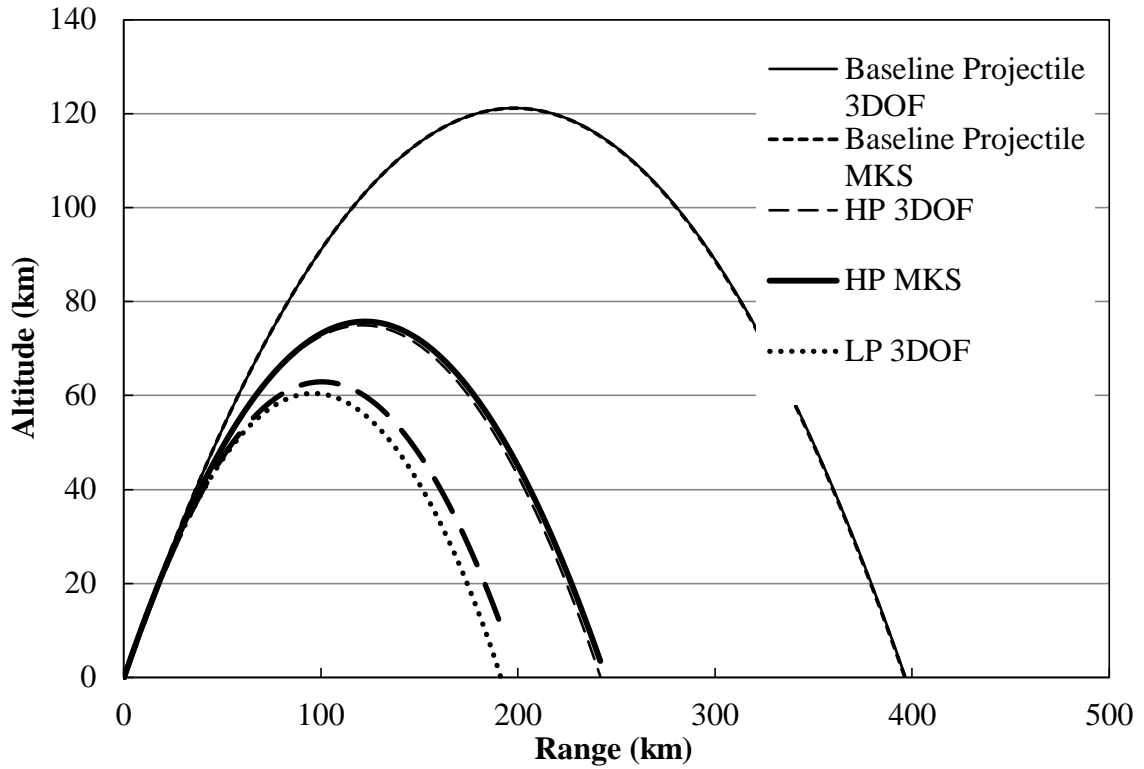


Figure 4.8 Comparisons of Various Projectiles with MKS

Projectile	Drag/Weight at Launch	Altitude where Drag=Weight	MKS Beta
LP	13.665	57.14 km	0.39
HP	10.256	56.98 km	0.28
Baseline Projectile	4.200	40.5 km	0.1

Table 4.1 Comparison of Various Projectiles with MKS

Figure 4.8 shows a comparison of three projectiles trajectories and their corresponding Modified Kepler trajectory estimates with no wind. The baseline projectile is a skirted cone design that has been proposed for use with the Navy Railgun

system.

The small MKS beta value minimizes the errors in the assumptions used to derive the Modified Kepler Solution. The Modified Kepler Solution would not appear to be a useful approach for very light high drag projectile. Based upon the results of the various projectiles used in this study, a beta value of less than 0.25 is required for a reasonably accurate Modified Kepler Solution. The baseline projectile meets this requirement for a large range of barrel elevations and will therefore be used for closer look at the MKS.

The baseline projectile was modeled as a right cone with a half angle of 4 degrees. The baseline projectile has a mass of 11.6 kg with a base cross section area of 0.008 m². The projectile was given an initial velocity of 2.157 km/sec for an initial kinetic energy of 26.985 MJ. The center of mass of the projectile was also assumed to far enough in front of the center of pressure and collinear so that the projectile is inherently aerodynamically stable and maintains a zero angle of attack while in the atmosphere.

It was assumed and later confirmed from the simulation that the projectile would remain in the high supersonic/hypersonic flight regime through the atmosphere. A Taylor-Maccoll solution of the supersonic flow over a right cone was selected to calculate the drag coefficient. The solution approach recommended in *Anderson's* text on aerothermodynamics was implemented to calculate the drag coefficient for a 4 degree half angle cone [49]. The code to implement the Taylor-Maccoll solution is included in Appendix B.

The Taylor-Maccoll solution only provides the surface pressure on the face of the cone. The pressure on the back face of the cone must be assumed. For the projectile study, a back pressure of 75% of the free stream pressure was chosen to match the cone

projectile approximation with the prototype Navy projectile. An exponential decay was used to model the drag coefficient in the numerical simulation:

$$C_D = 0.077e^{-0.38Ma} + 0.014, \quad (4.8)$$

with $R^2 = 0.999$. The drag coefficients and curve fit are given in Figure 4.9.

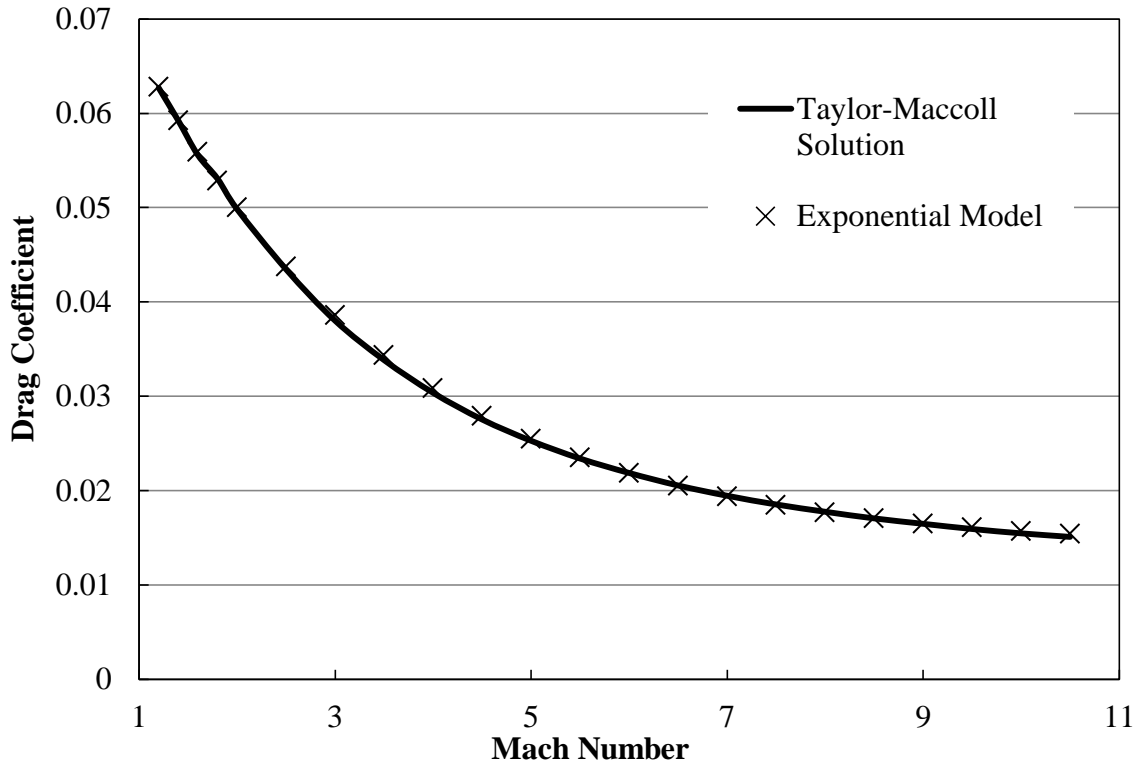


Figure 4.9 Drag Coefficient of Baseline Projectile

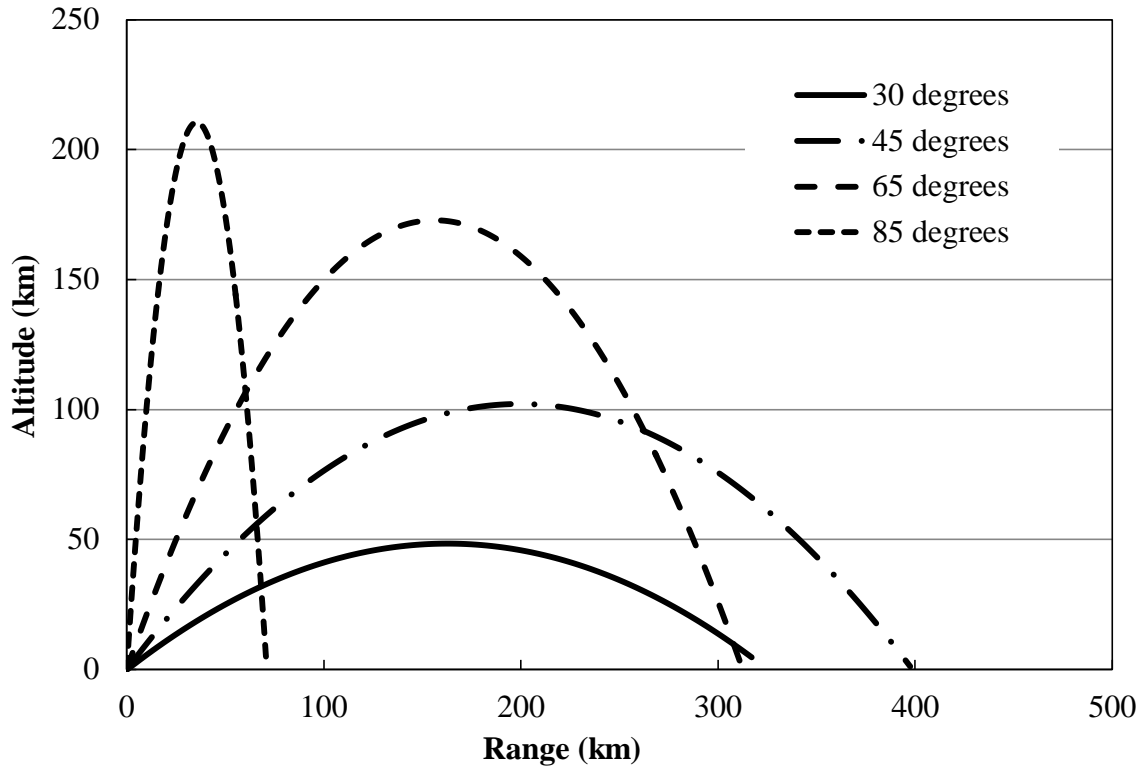


Figure 4.10 Modified Kepler Trajectories of the Baseline Projectile

The three term Modified Kepler solution is compared to the 3DOF numerical simulation for the elevations of fire in Figure 4.11. The error at the lower elevations (30 degrees) can primarily be attributed to the straight line assumption in the Modified Kepler equation derivation. The longer that the projectile stays in the dense lower atmosphere, the less accurate the straight line approximation of angular momentum decay will be. The errors also show an error at launch. From inspection of the Modified Kepler solution, the initial position at launch will be the surface of the Earth and the total position error therefore zero. An error of almost 200 meters at launch is an indication of the numerical error that is created by the truncation of the infinite series in the driving function. This error quickly corrects itself as the angular range value increases.

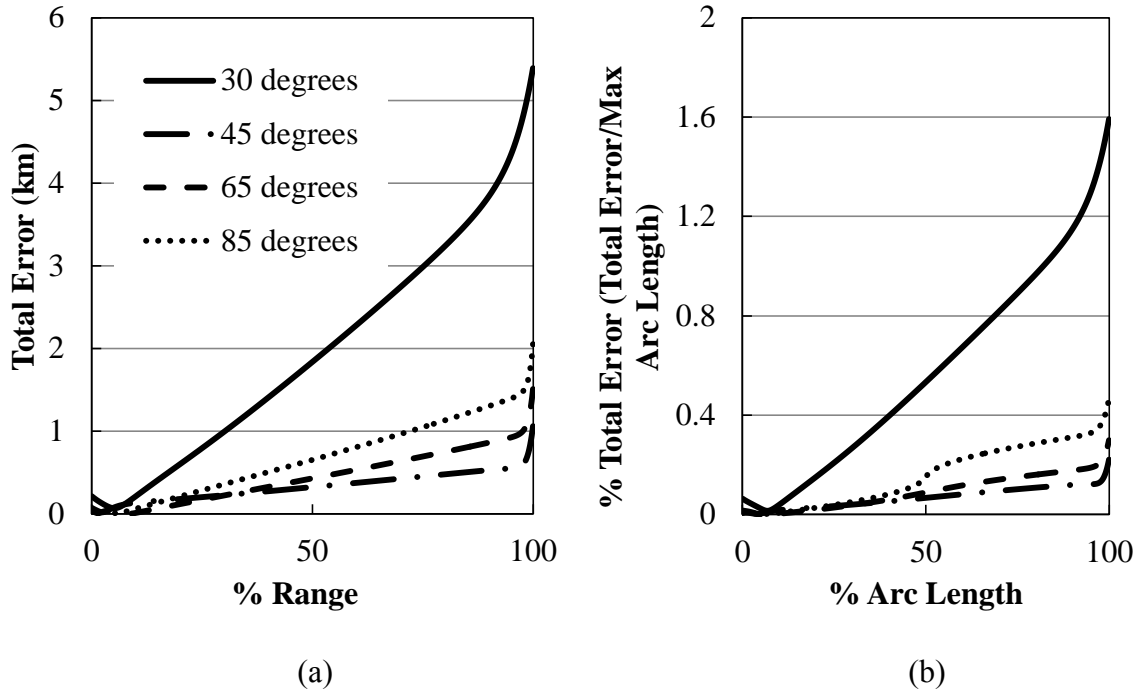


Figure 4.11 Three Term Modified Kepler Solution Total Error

The error at the highest elevation (85 degrees) is greater than the lower elevations and is also unexpected. Based upon the Modified Kepler solution, the highest accuracy should come from a straight line shot up out of the atmosphere. The highest lofted trajectory creates a very small angular range change for a change in altitude resulting in an error in the integration of the time of flight. This time of flight error results in a higher total position error.

C. Verification of Modified Kepler Equation Assumptions for the Baseline Projectile

The divergence of the Modified Kepler solution after the projectile leaves the sensible atmosphere is an indication that the Modified Kepler solution does not capture the asymptotic angular momentum accurately. The error between the predicted asymptotic specific angular momentum and the measured angular momentum at apogee

from the numerical simulation is shown in Figure 4.12.

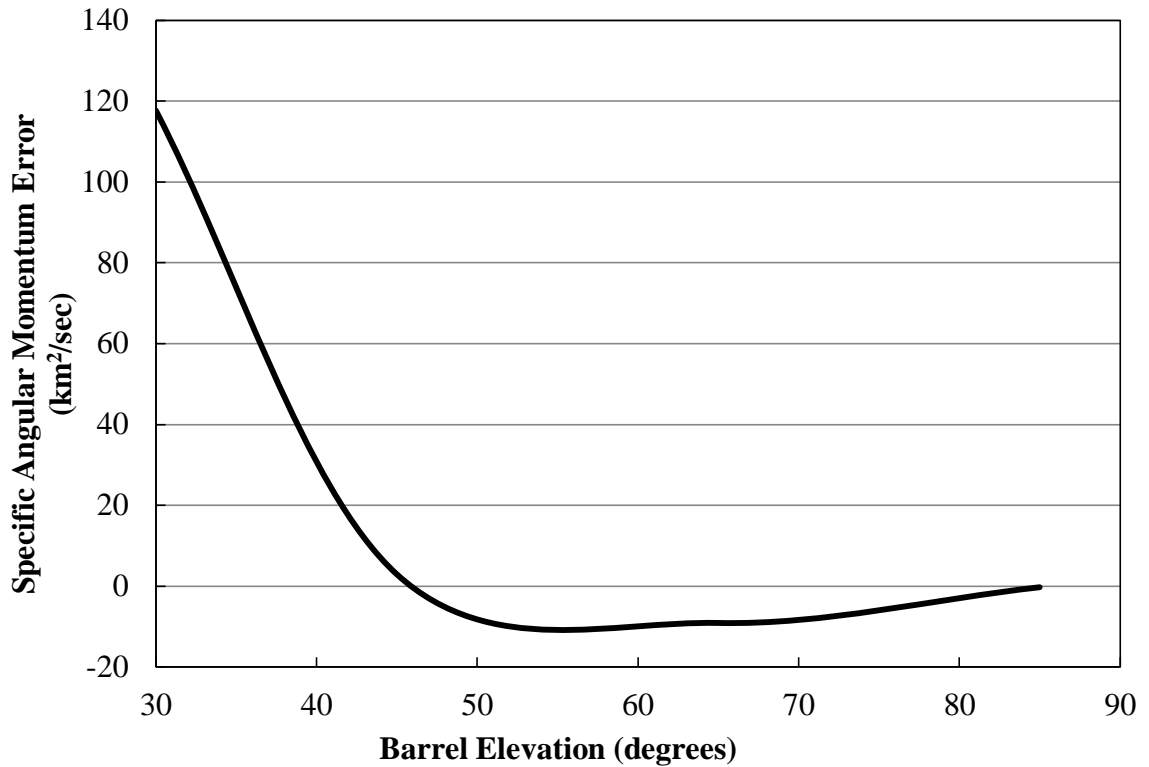


Figure 4.12 Asymptotic Angular Momentum Error

To evaluate the impact of this error, the three term Modified Kepler solution was again compared to the numerical simulation with the asymptotic angular momentum predicted by the Modified Kepler solution replaced with the asymptotic angular momentum of the numerical simulation at apogee in Figure 4.13:

$$L_{\infty} = L_{\text{apogee}} \quad (4.9)$$

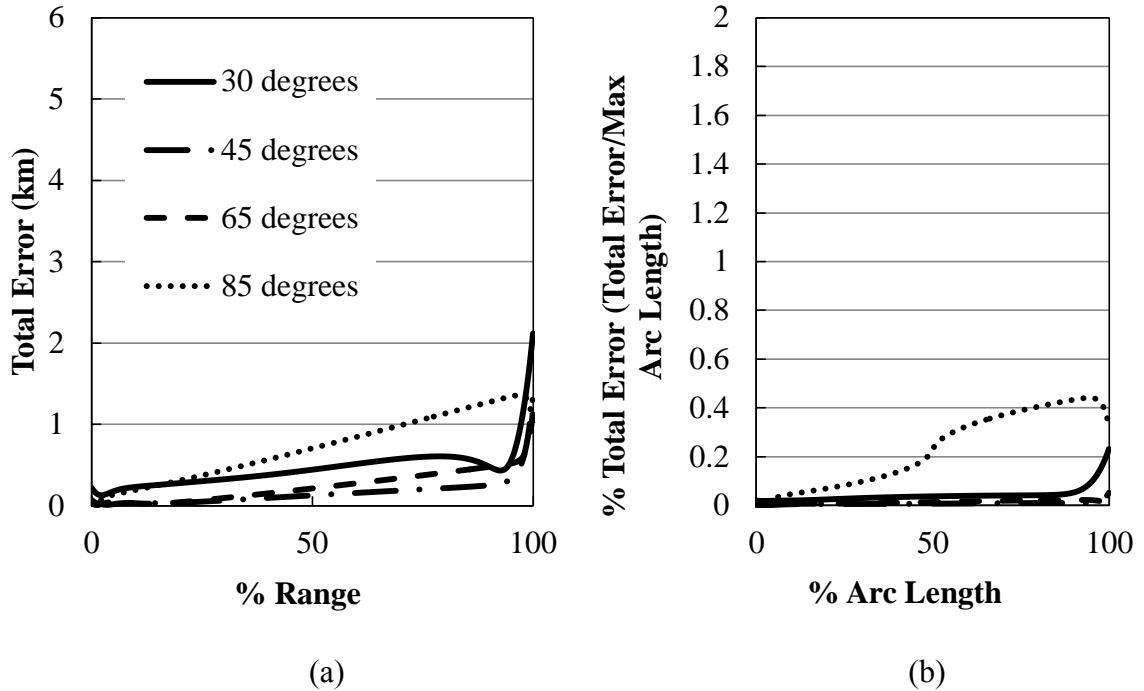


Figure 4.13 Three Term Modified Kepler Solution Total Error with Asymptotic Angular Momentum Correction

Figure 3.16 shows that with the corrected asymptotic angular momentum, the linearized Modified Kepler equation is capable of predicting the motion of the baseline projectile over a large range of barrel elevations and supports the linearization assumption (Assumption 6). This method may be useful to create empirical corrections to increase the accuracy of the Modified Kepler solution as needed.

The error in the capture of the angular momentum at apogee is primarily due to the error in the straight line assumption. This can be verified by comparing the numerical simulation results to a straight line trajectory as shown in Figure 4.14. As would be expected, the lower the barrel elevation, the greater the error in the straight line assumption and thus the angular momentum prediction and the trajectory error.

Assumption 3 is therefore valid for elevated trajectories only and would not be accurate

for flat fire approaches or low speed trajectories that curve significantly while in the lower atmosphere.

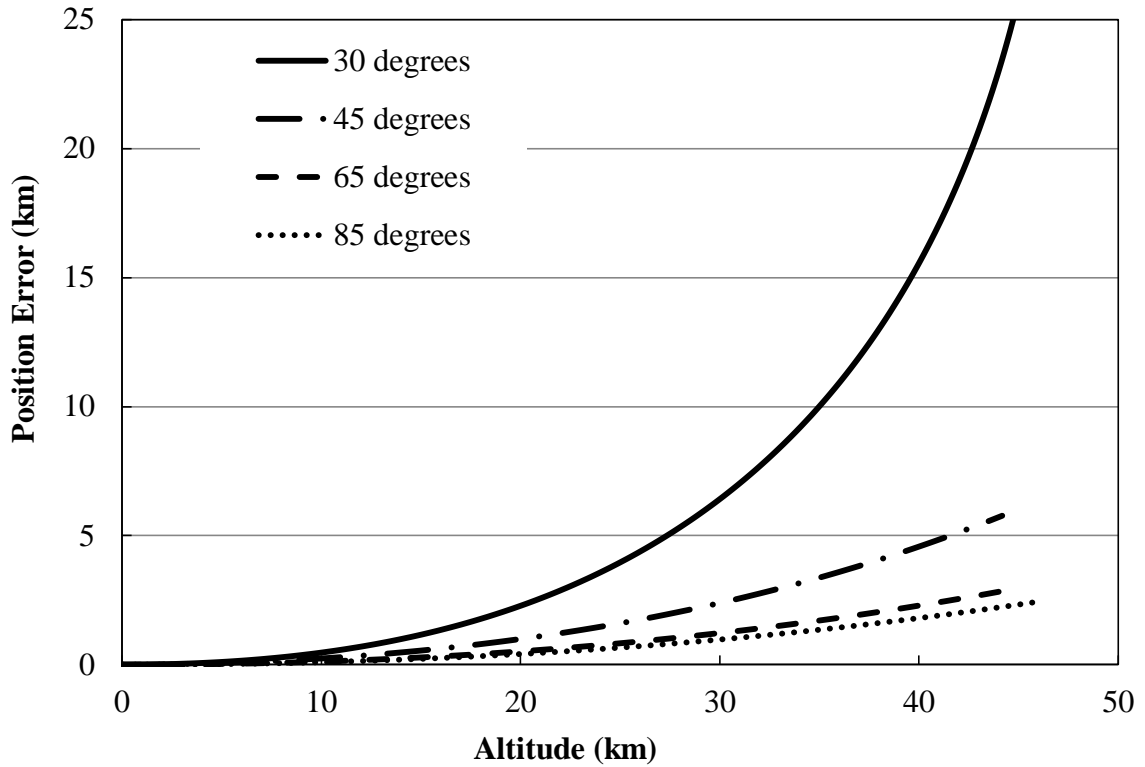


Figure 4.14 Comparison of Numerical Simulation to Straight Line Approximation

The choice of the exponential decay model for atmospheric density used in the Modified Kepler equation and the two stage atmospheric density model used in the numerical simulation is the source of the mismatch between the predicted asymptotic angular momentum and the simulation results. If the exponential decay model is used in the numerical simulation, the three term Modified Kepler solution provides a slightly better result than when the three stage model is used as shown in Figure 4.15.

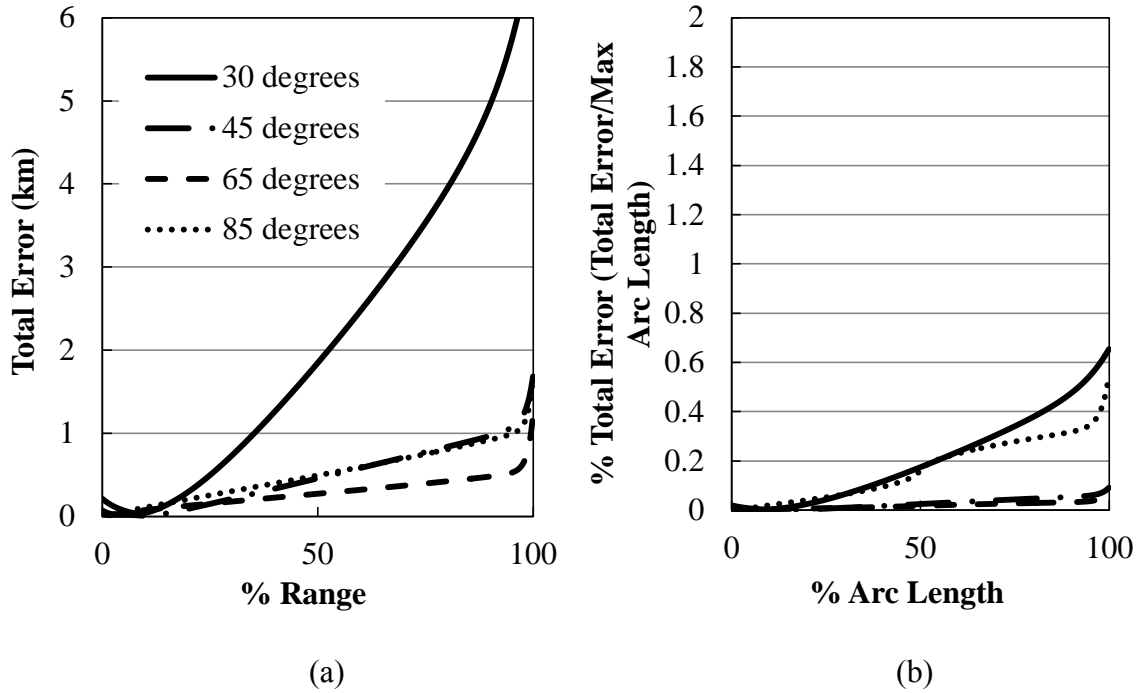


Figure 4.15 Three Term Modified Kepler Solution Error with the Exponential Density Model used in the Numerical Simulation

The drag coefficient is assumed to be constant in the derivation of the Modified Kepler solution. The assumption of Mach number independence and the variation of the drag coefficient can be taken from the numerical simulation to verify the impact of the assumption. Figure 4.16 shows the variation in drag coefficient for the various barrel elevations up to an altitude of 45 km. Although the drag coefficient does creep up at higher altitudes, the value drag coefficient changes less than 5% below 20 km where almost all of the angular momentum dissipation will occur (Assumption 4).

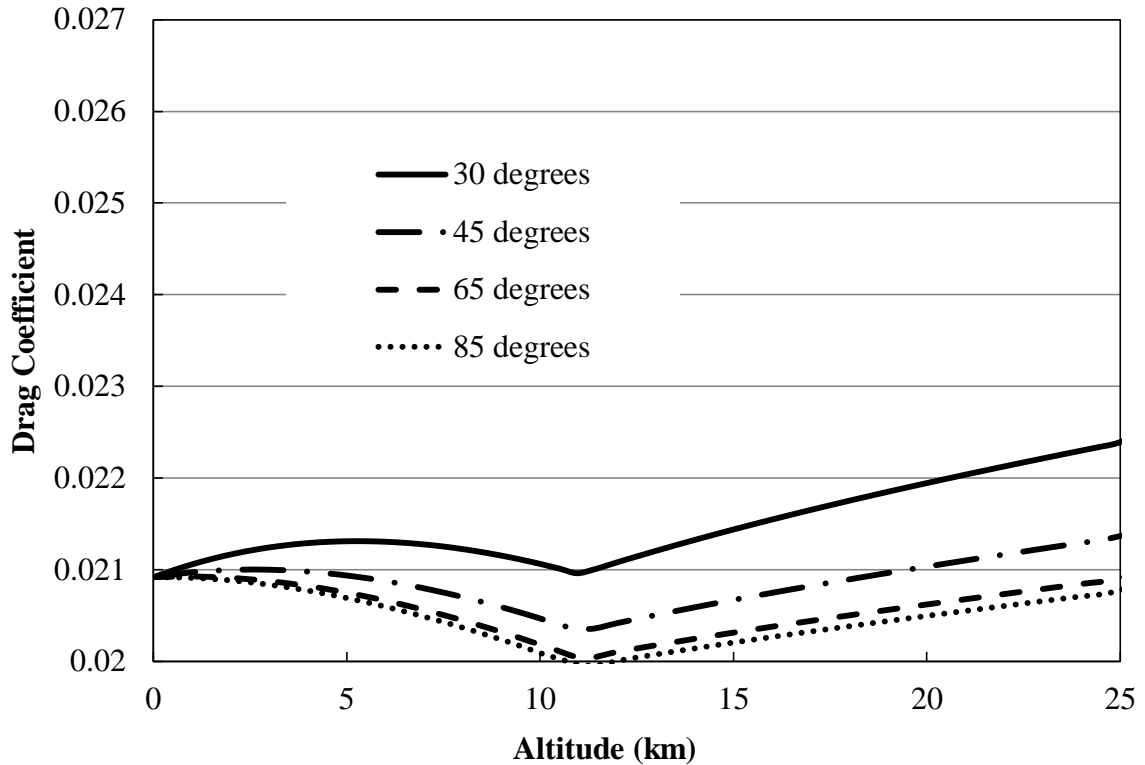


Figure 4.16 Drag Coefficient vs. Altitude from Numerical Simulation

The errors associated with the Modified Kepler solution are tightly connected to the initial launch speed. If the speed is increased, the straight line (Assumption 3) and Mach number independence (Assumption 4) should become increasingly more valid. Figure 4.17 shows the total error for a three term Modified Kepler solution with an initial velocity of 2.59 km/sec, a 20% increase over baseline. The errors for the higher elevations do not improve but there is a dramatic improvement in the lower elevations as would be expected. The faster projectile has a much straighter trajectory in the lower atmosphere and is closer to the assumptions in the derivation of the driving function.

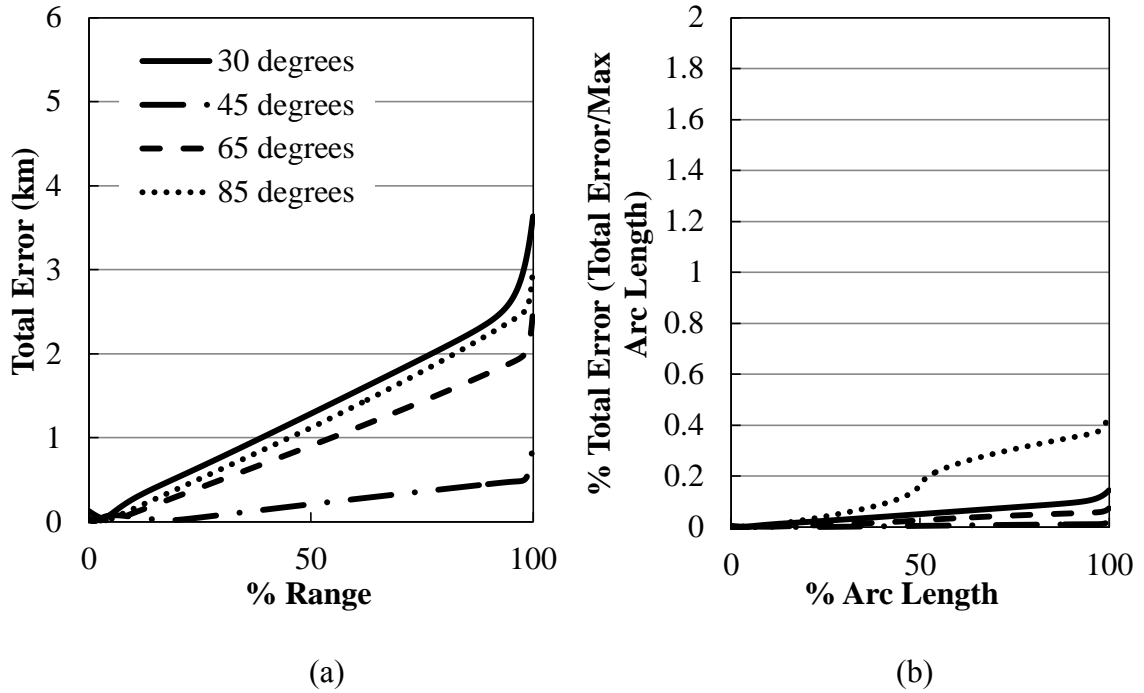


Figure 4.17 Three Term Modified Kepler Solution Total Error with a 20% Increase in Initial Velocity

Finally, the effects of wind are estimated by comparing the three term Modified Kepler solution to a 3DOF with a 6 m/s headwind and a 6 m/s cross wind. As shown in Figure 4.18, the influence of moderate winds is minor.

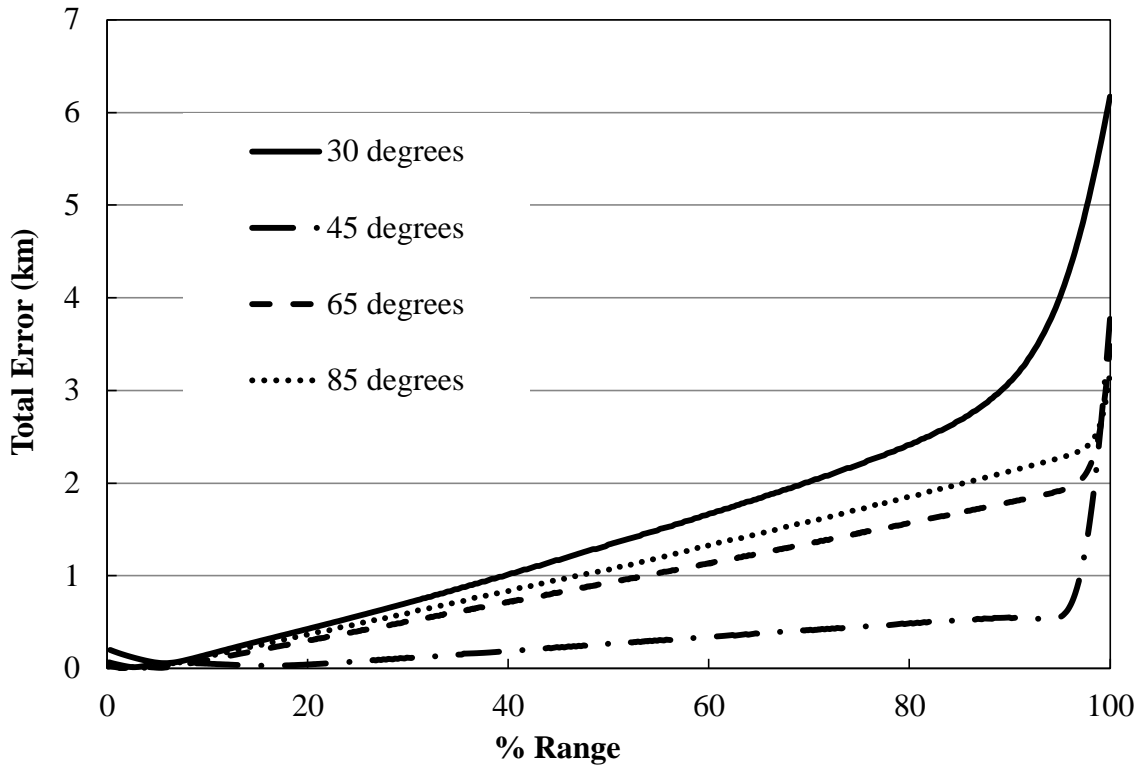


Figure 4.18 Total Error with 6 m/s Headwind and 6 m/s Crosswind

CHAPTER 5

CONVERSION OF THE MODIFIED KEPLER SOLUTION FOR A ROTATING EARTH

To be useful as a practical fire control system, the Modified Kepler solution must be corrected for use on a rotating Earth. The motion of a projectile fired from a rotation Earth can be numerically simulated to any level of accuracy desired at the expense of computational time but the ability to analytically solve for a trajectory in a rotation Earth reference frame is severely limited. Standard Kepler solutions can be easily modified to account for the variation in initial conditions due to a rotation Earth but do not include atmospheric drag. All linear theory models assume a non-rotating reference frame so that the absolute velocity is the same as the relative velocity to the air. A simplified method of correcting for the misalignment between the absolute velocity vector and the relative velocity vector is presented that allows for solution of the Modified Kepler solution on a rotation Earth system. Now that the Modified Kepler solution has been compared to the existing analytical solutions and standard numerical simulations for a non-rotation Earth, the corrected MLT must be compared to custom simulations that include Earth rotation. Unfortunately, this is not as simple as correcting the initial velocity vector to include the rotation correction. The projectile passes through the atmosphere at an angle and speed relative to the ground while the motion with respect to an inertial reference frame must be

corrected for the Earth rotation. In addition, there is an additional correction that must be made for the angular difference between the velocity vector in the inertial reference frame and the aerodynamic drag force vector.

As mentioned in Chapter 1, there has been data collected for projectiles launched into space as part of the High Altitude Research Program (HARP) in the 1960s. To be able to compare the data collected from the HARP program to a Modified Kepler solution, the Modified Kepler solution must take into account the rotation of the Earth.

A. Initial Velocity Correction for Earth Rotation

A true inertial reference frame does not exist on Earth due to the constant rotation and motion of the Earth in the universe. A very accurate approximate reference frame can be found by assuming the Earth Centered Inertial (ECI) reference frame. In the rotating ECI model, the same ideal spherical Earth with a radius of 6378 km is used but assumed to rotate 360 degrees in 24 hours about the z axis (True North axis).

As it is most common and useful to describe the firing solution of the gun (elevation, bearing, muzzle velocity) relative to the surface of the Earth, the velocity of the Earth's surface at the launch point must be added to the initial velocity vector relative to the Earth's surface using vector addition as shown in Figure 5.1.

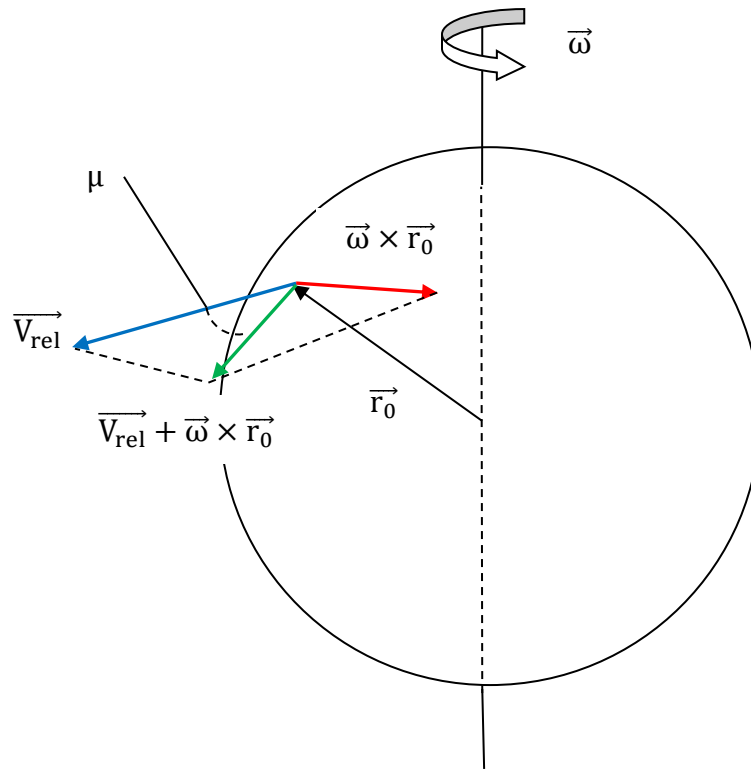


Figure 5.1 Initial Velocity Correction due to Earth Rotation

B. Aerodynamic Drag Force Misalignment

The correction of the initial velocity for Earth rotation creates a misalignment of the aerodynamic drag force, which is in line with the relative velocity vector, from the axis of the corrected velocity vector as shown in Figure 5.2.

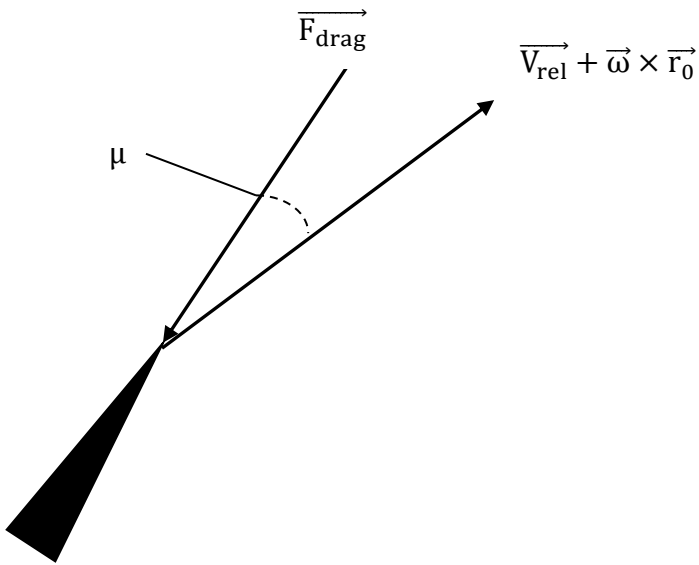


Figure 5.2 Misalignment of Aerodynamic Drag Force with Corrected Velocity Vector

The result of the misalignment is that only the component of the drag force that is in line with the corrected velocity vector acts to decrease velocity and thus angular momentum. The tangential component of the drag force acts to change the bearing and elevation of fire. The Modified Kepler equation was derived with the decay of the angular momentum occurring along the trajectory. Any forces that do not act in line with the actual trajectory of the projectile, other than gravity, are not captured and must be accounted for separately. The drag force may be decomposed into a force along the trajectory and a tangential component. The in line force is easily modified as the cosine of the misalignment angle:

$$F_{inline} = \frac{1}{2} C_D A V_{rel}^2 \rho_0 e^{-ka} \cos \mu. \quad (5.1)$$

Angular momentum must be calculated by the velocity in the inertial reference

frame. To calculate the decay of the angular momentum, the ratio of the relative velocity to the absolute velocity is assumed to be constant as they both decay at the same rate:

$$F_{\text{inline}} = \frac{1}{2} C_D A V^2 \rho_0 e^{-ka} \left(\frac{V_{\text{rel}}}{V} \right)^2 \cos \mu, \quad (5.2)$$

with

$$\left(\frac{V_{\text{rel}}}{V} \right)^2 = \left(\frac{V - \omega \times r}{V} \right)^2 = 1 - \frac{2V_x \omega r}{V^2} \cos(\text{LA}) + \frac{(\omega r)^2}{V^2} \cos^2(\text{LA}). \quad (5.3)$$

The ECI Modified Kepler solution is derived the exact same way as the ECEF Modified Kepler solution given in Chapter 3 using this correction.

The initial conditions may be modified for the addition of the tangential portion of the misaligned drag force as a simple approximation that accounts for the tangent component of the force without changing the Modified Kepler derivation. The tangential component is given by:

$$F_{\text{tangent}} = \frac{1}{2} C_D A V_{\text{rel}}^2 \rho_0 e^{-ka} \sin \mu. \quad (5.4)$$

The force may be converted to acceleration by dividing through by the projectile mass:

$$a_{\text{tangent}} = \frac{1}{2m} C_D A V_{\text{rel}}^2 \rho_0 e^{-ka} \sin \mu. \quad (5.5)$$

Once again applying the straight line trajectory approximation, the misalignment angle becomes a constant. Integrating the acceleration over time gives the resulting velocity developed by the tangential force:

$$V_{\text{tangent}} = \int_0^{\infty} \frac{1}{2m} C_D A V_{\text{rel}}^2 \rho_0 \sin \mu e^{-ka} dt. \quad (5.6)$$

The altitude in equation (5.6) may be converted to a function of time by the assumption:

$$a \approx V_{\text{rel}} \sin(\phi_{\text{rel}}) t. \quad (5.7)$$

The tangential velocity correction is therefore,

$$V_{\text{tangent}} = \frac{C_D A \rho_0 \sin \mu}{2mk \sin(\phi_{\text{rel}})} V_{\text{rel}}. \quad (5.8)$$

The tangent velocity resulting from the aerodynamic force misalignment can now be used to correct for the initial velocity in the same manner as the as the Earth rotation correction. The corrected initial velocity in the ECI reference frame will be the vector addition of all three velocities as shown in Figure 5.3. The direction of the tangential velocity is in the plane created by the relative velocity and the velocity corrected for Earth rotation and tangent to the corrected velocity.

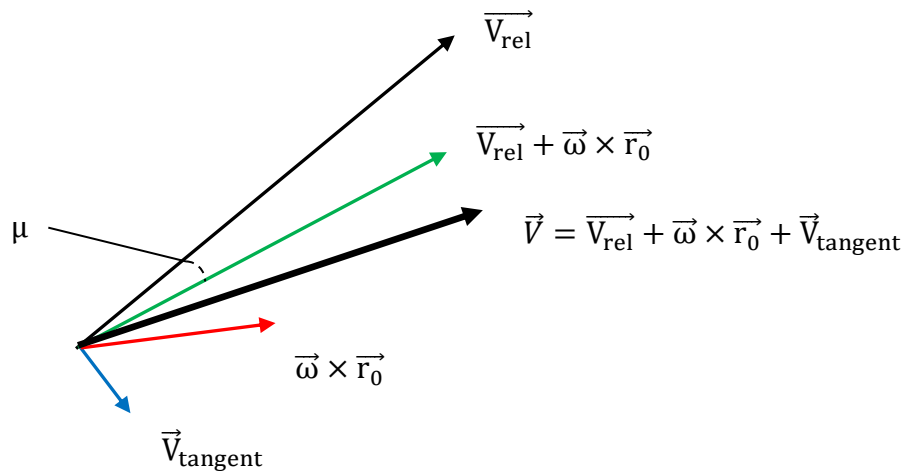


Figure 5.3 Calculation of the Initial Velocity in an Inertial Reference Frame

C. Error in the ECI Modified Kepler Solution

To verify the ECEF Modified Kepler solution, the same baseline projectile as used in Chapter 4 was used in the 3DOF numerical simulation with the Earth rotation enabled. The ECI Modified Kepler solution was verified for a gun located at the equator and latitude 45 degrees firing at 30, 45, 65, and 85 degrees of barrel elevation with bearings of 000T, 090T, and 270T. Note that the angular range (θ) is relative to the launch position in the inertial reference frame and not relative to the position on the

surface of the Earth that is moving.

The total position error concept described in Chapter 4 was again used. The position of the projectile from the ECI Modified Kepler solution was converted to Cartesian coordinates by a simple coordinate transformation. For a given simulation time step, the position error is defined as vector subtraction of the position vector from the ECI Modified Kepler solution from the position vector given by the numerical simulation. The time error is the time calculated for the ECI Modified Kepler solution minus the current model time. The time error is multiplied times the instantaneous velocity of the projectile to create a position error along the trajectory. The total position error is the vector addition of the position error and the error along the trajectory. The total position errors for the various test cases of the ECI Modified Kepler solution are given in Figures 5.4-5.9.

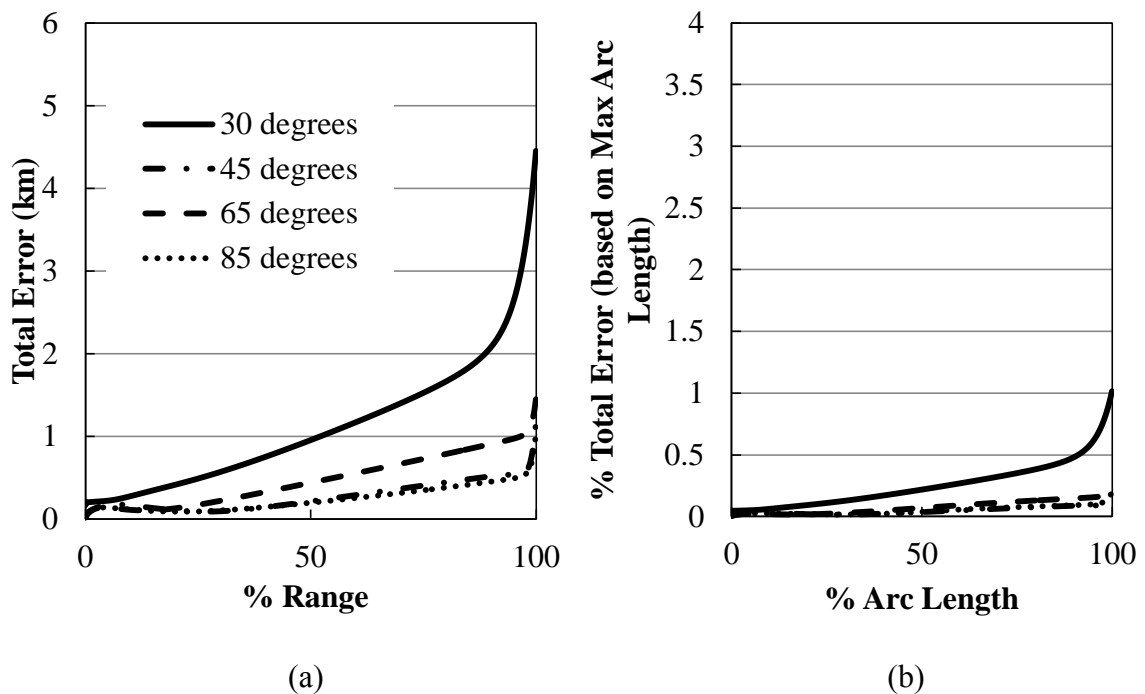


Figure 5.4 Total Position Error of the ECI Modified Kepler Solution for the Baseline Projectile fired from 0 degrees Latitude on a Bearing of 090T

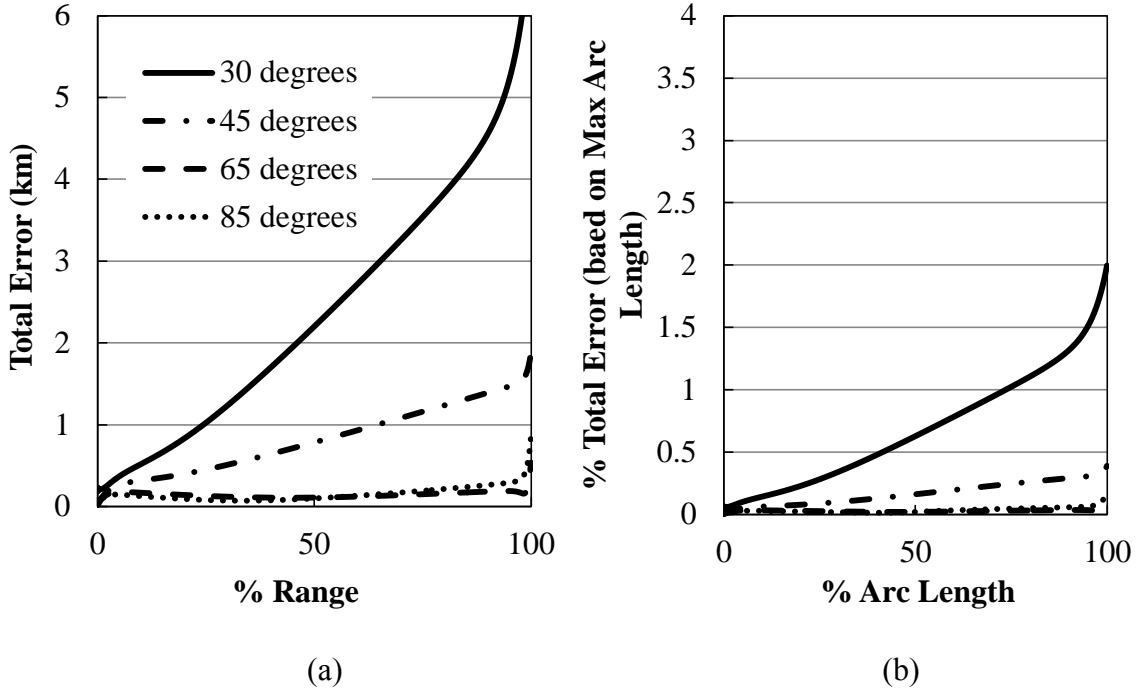


Figure 5.5 Total Position Error of the ECI Modified Kepler Solution for the Baseline Projectile fired from 0 degrees Latitude on a Bearing of 000T

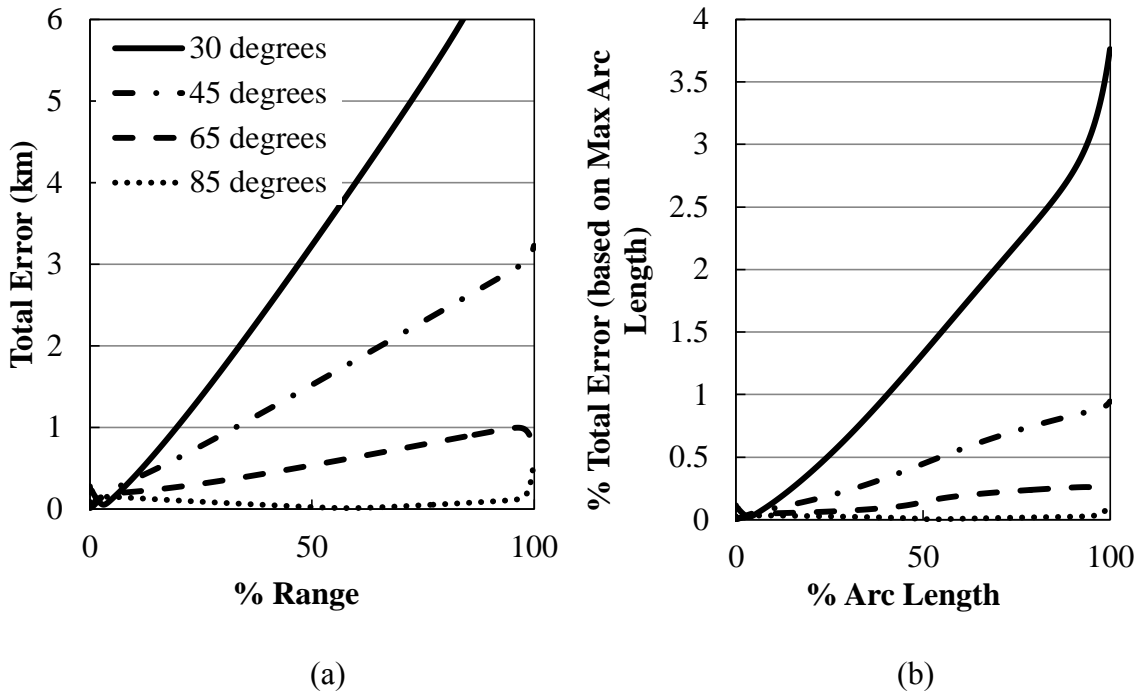


Figure 5.6 Total Position Error of the ECI Modified Kepler Solution for the Baseline Projectile fired from 0 degrees Latitude on a Bearing of 270T

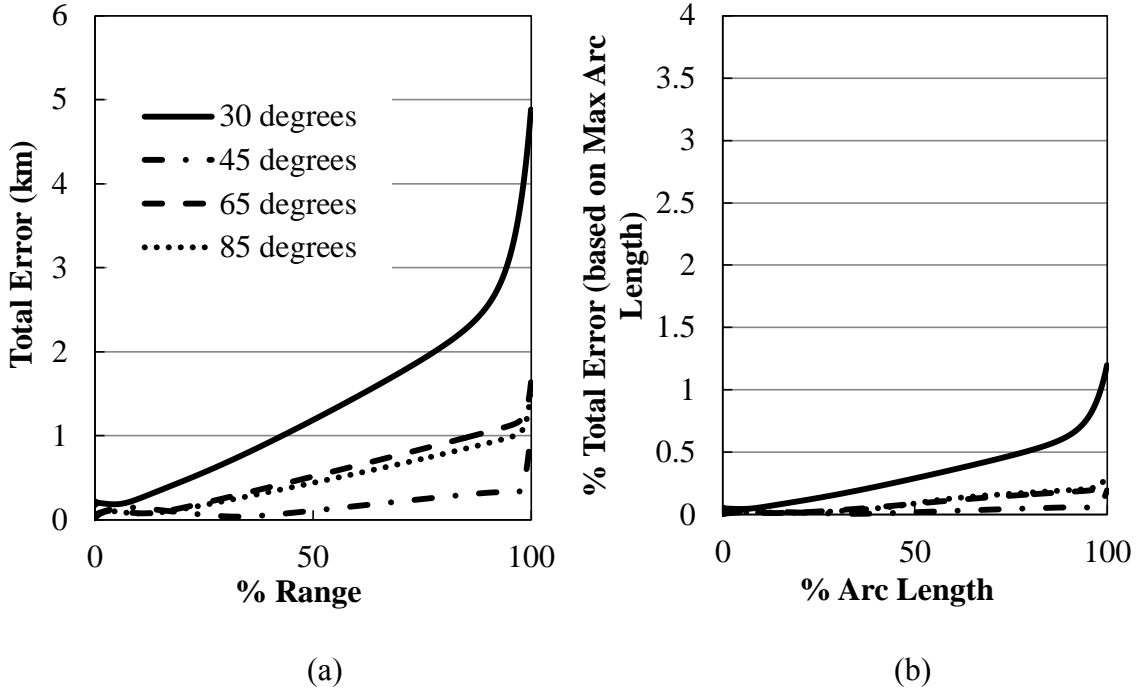


Figure 5.7 Total Position Error of the ECI Modified Kepler Solution for the Baseline Projectile fired from 45 degrees Latitude on a Bearing of 090T

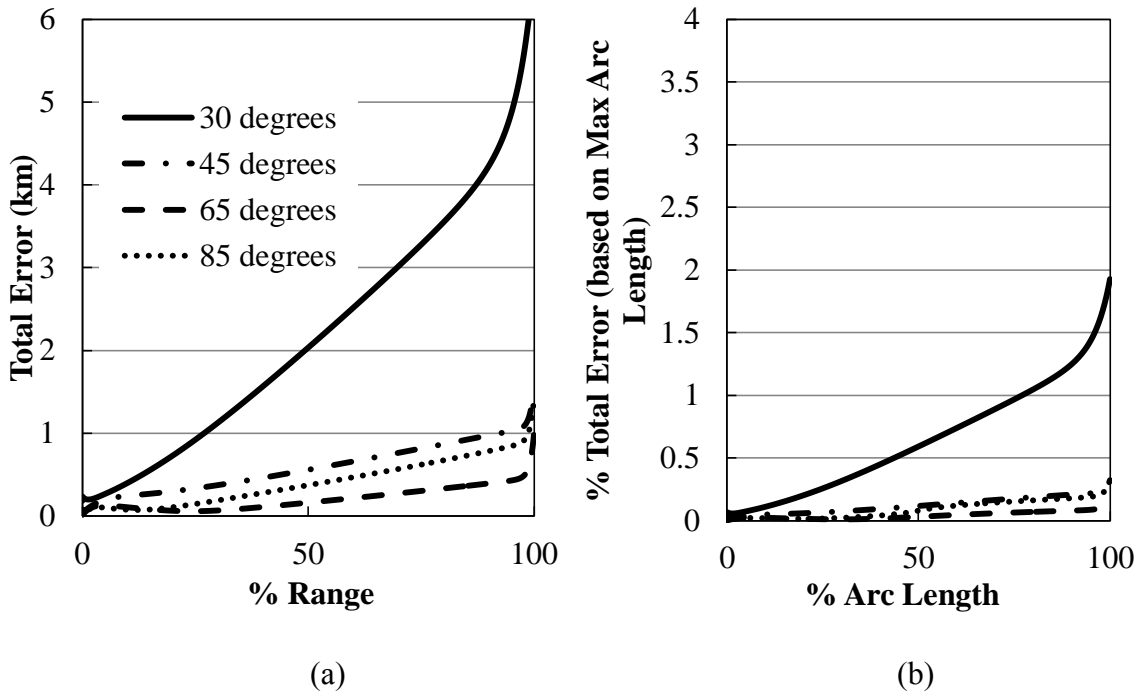


Figure 5.8 Total Position Error of the ECI Modified Kepler Solution for the Baseline Projectile fired from 45 degrees Latitude on a Bearing of 000T

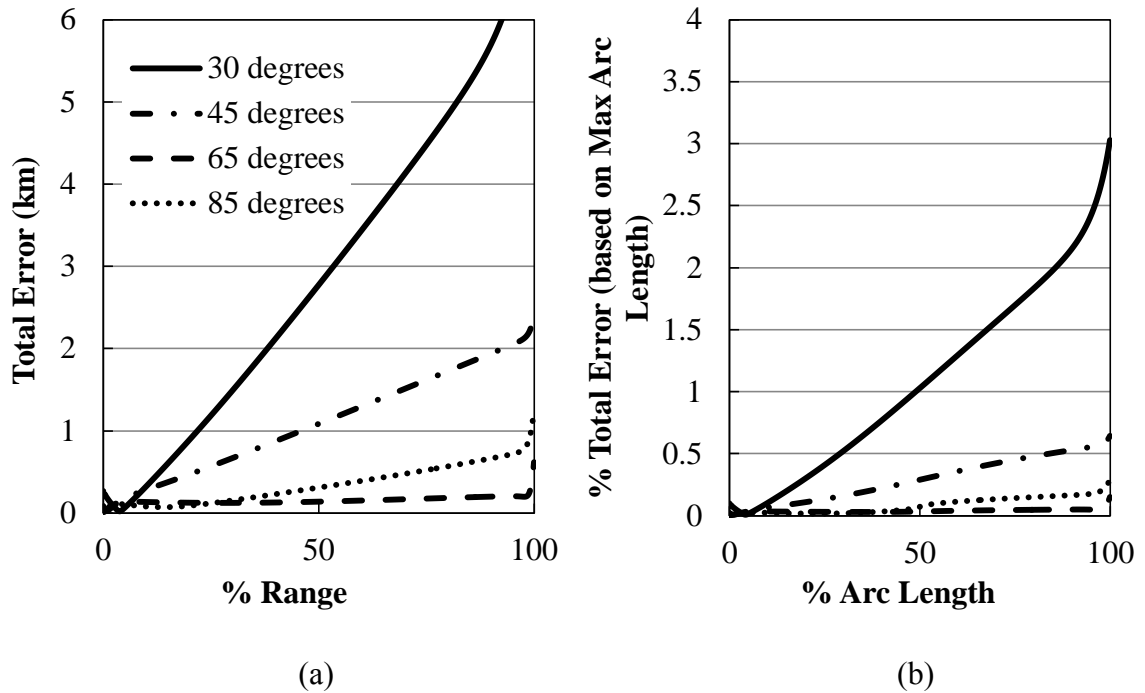


Figure 5.9 Total Position Error of the ECI Modified Kepler Solution for the Baseline Projectile fired from 45 degrees Latitude on a Bearing of 270T

D. Discussion

The ECI Modified Kepler solution appears to have an error bias associated with the bearing of fire. The error in trajectories fired due East and North are significantly lower than for those fired due West.

As seen in the ECI Modified Kepler solution, the error grows for lower elevations. For the higher elevations, the worst total position error of 1.5 km at apogee is found at a bearing of 270T and an elevation of 45 degrees when fired from the equator.

For projectile fired due East, the correction for Earth rotation causes the initial velocity vector to be lower than the relative velocity vector as shown in Figure 5.9. The misalignment angle between the drag force and the velocity vector becomes smaller over time making the cosine of that angle approach 1. Thus the solution converges toward the

true trajectory.

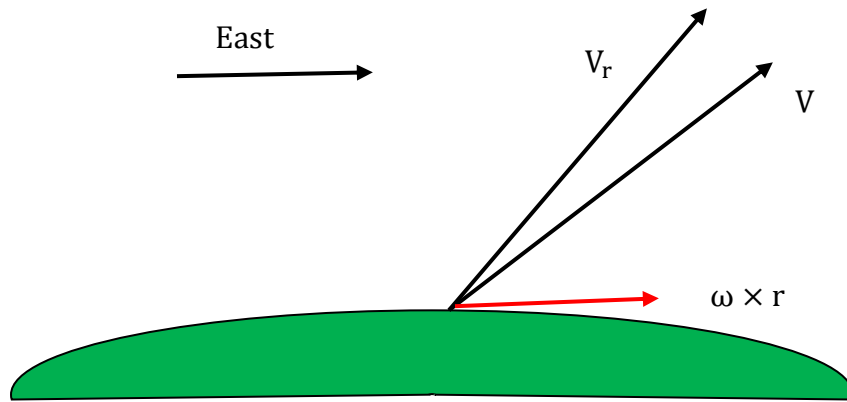


Figure 5.10 Relative Position of Relative Velocity Vector to Initial Velocity Vector for East Fired Projectiles

For projectile launched in a West direction as shown in Figure 5.10, the relative velocity vector is below the corrected velocity vector causing the curve in the trajectory in the atmosphere to increase the misalignment angle and cause the solution to diverge from the true trajectory. The lower the trajectory and closer to the equator for West fired projectiles, the greater the error caused by the straight line trajectory assumption.

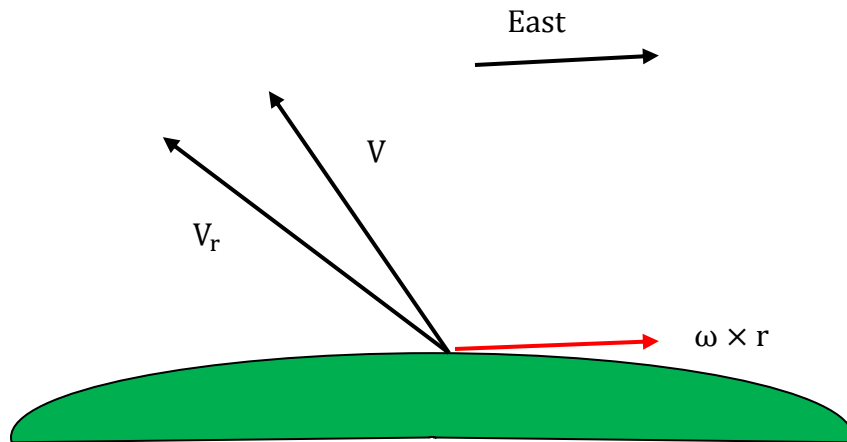


Figure 5.11 Relative Position of Relative Velocity Vector to Initial Velocity Vector for West Fired Projectiles

The ECI Modified Kepler solution appears to be a reasonably accurate estimate of the trajectory of hypersonic projectiles similar to those described by the baseline projectile. For most of the trajectories, the total position error is less than 1 km for ranges out to 400 km and apogees over 200 km. If used to design a projectile divert system, the largest error of 1.5 km at apogee can be used as an estimate for the divert capability that the projectile might need to intercept a ballistic missile.

Of particular interest is the total error for East fired projectiles that are fired at very high elevations. The ECI Modified Kepler solution appears to capture these trajectories with well under 0.5 km of accuracy. This is important to know as the only data available that has been collected from projectiles fired at an elevation of 85 degrees in an Eastward direction under the HARP program as discussed in the next chapter.

CHAPTER 6

EVALUATION OF HARP DATA USING THE CORRECTED MODIFIED KEPLER SOLUTION

The High Altitude Research Program (HARP) was the first successful attempt to put projectiles into space and the only verifiable one in public record. The program used various guns and projectiles but the data that is most relevant to validating the Modified Kepler equation was collected from firing a highly modified 16 inch battleship gun from the island nation of Barbados in the southern Caribbean and a similar gun mounted at the Yuma Test Range in Arizona.

A. HARP Projectile Overview

The HARP program utilized various projectiles as part of the research program but one type of projectile in particular had enough data collected to enable a study of the trajectory using the Modified Kepler equation. The projectile chosen for this study was named the Martlet 2C (Mod 2). The martlet is a small bird and mascot of McGill University, the Alma Mater of the program director Dr. Gerald Bull. The technical drawing of the Martlet 2C (Mod 2) is given in Figure 6.1.

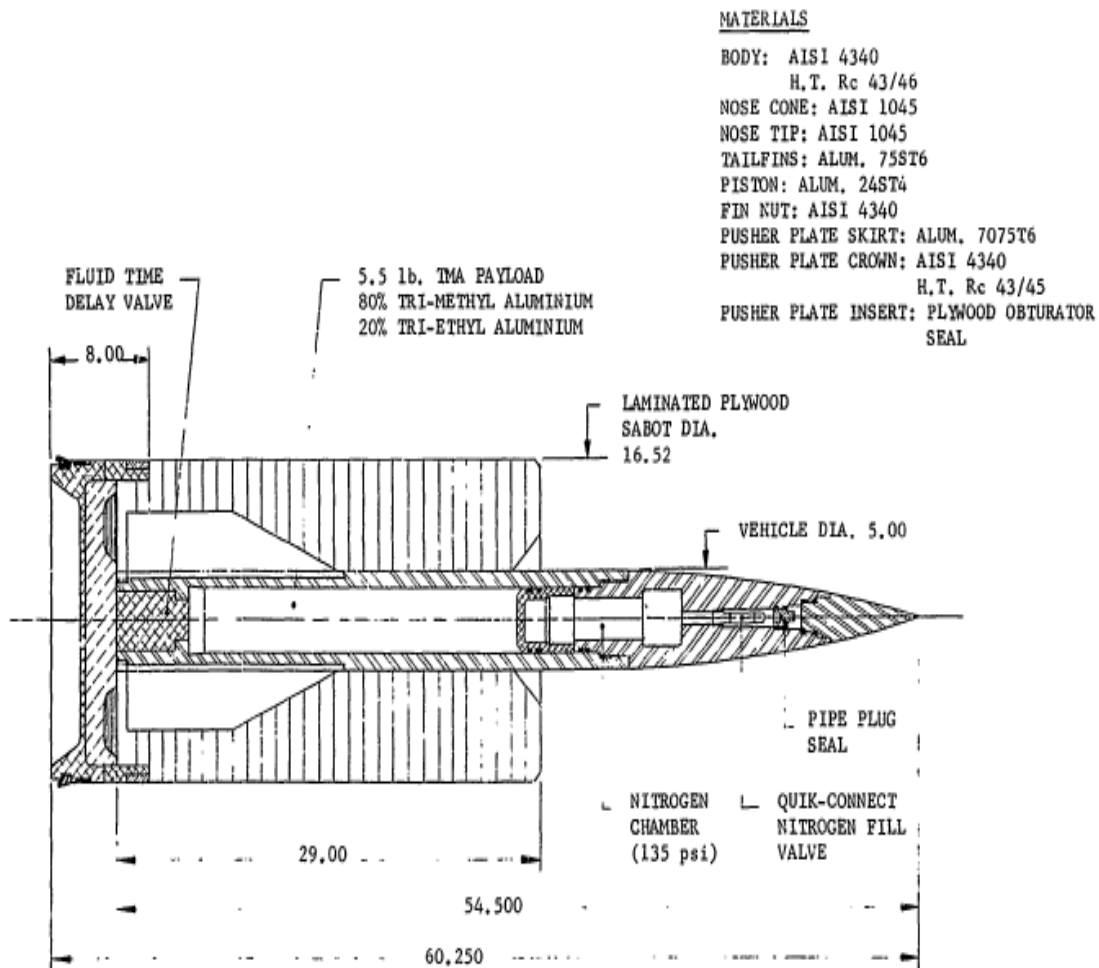


Figure 6.1 Drawing of the Martlet 2C (Mod 2) [11]

The primary justification for the HARP program was to study upper atmospheric wind patterns. The time delay valve in the projectile was set to open after the projectile left the lower sensible atmosphere and then leak a trail of luminescent material that could be photographed from observation posts and used to estimate wind speeds and patterns. Once outside of the sensible atmosphere, the loss of mass has only a negligible effect on

trajectory assuming that the luminescent material is not released with sufficient velocity to produce a noticeable propulsion effect. As the fluid payload did not release until the upper atmosphere where drag forces are negligible, the motion of the projectile can be assumed to be a point mass trajectory. The Martlet 2C (Mod 2) was developed based upon the initial designs of the German V-3 projectiles with a finned sabot approach that ensured that projectile was aerodynamically stable within the atmosphere.

The Martlet 2C (Mod 2) had multiple failures initially most likely due to structural damage received during the high acceleration profile in the barrel. Over time, the modifications to the gun and propellant lowered the acceleration profile to the point that the Martlet 2C (Mod 2) became the most successful projectile utilized as part of the HARP program.

B. HARP Trajectory Data Collected

Apparently due to the combined support of the Canadian and United States military, the HARP program was funded to the point that multiple data collection techniques were available. The data available to analyze the trajectories included radars, cameras, muzzle probes, and optical observations.

Two radars are mentioned in the HARP technical reports, a MPS-19 and M-33. The technical reports mention the Trinidad radar which is assumed to be located on nearby island of Trinidad and is most likely the M-33. The MPS-19 radar was located at the gun site itself on Barbados. Altitude and range data is provided in table format in the HARP report [11,12].

The muzzle velocity as the projectile leaving the barrel is a critical piece of data

for the trajectory evaluation. Three methods were used in the HARP program to evaluate muzzle velocity. Electronic probes were installed at the end of the barrel to measure the velocity of the bullet immediately prior to leaving the barrel. Two probes were installed on each side of the barrel and the average velocity calculated between the two was utilized if a good signal could be obtained from both. In the event of one probe set malfunction, the velocity was calculated using only one probe set.

Smear cameras were also utilized to try to obtain accurate muzzle velocities. The cameras were pointed and focused several feet from the end of the barrel and triggered to open their shutter when the projectile was in the picture and close the shutter after a fixed time. The resulting “smear” caused by the projectile as it moved across the photograph could be measured to estimate the distance moved over the exposure time. This method in particular was apparently prone to poor readings and was eventually discarded. There is also the mention of a Fastax camera system which is assumed to be an early attempt at high speed photography.

Finally, the muzzle velocity was estimated from radar data. The earliest radar data that is included in the tables is at 4 seconds after launch with the majority starting at 10 seconds. The altitude and range at this time was used to estimate the initial velocity.

All Martlet rounds used in this study were fired at an elevation of 85 degrees relative to the horizon. No specifics are given on how the barrel evaluation was measured but it is assumed that it was measured accurately. The gun barrel shown in Figures 6.2 & 6.3 is approximately 40 meters long with the extension that was added to the original gun barrel. The length of the barrel increases the likelihood of barrel “whip” creating uncertainty in the exact initial velocity vector direction.

The azimuth of the Barbados gun is fixed at 109 degrees from True North as shown in Figure 6.4.



Figure 6.2 16 inch Barbados HARP Gun [50]

(image used with permission)



Figure 6.3 16 inch Barbados HARP Gun (Present Day)



Figure 6.4 Barbados Gun Site, Gun Bearing Measured Relative to Airstrip [51]

(image used with permission)

C. Martlet 2C (Mod 2) Apogee Comparison for the Barbados Gun

The drag coefficient, cross-sectional area, and projectile mass are needed for the ballistic constant for use of the Modified Kepler equation. Data taken from a HARP report containing detailed trajectory information of multiple rounds fired from the Barbados gun can be used to evaluate the aerodynamic properties of the Martlet 2C (Mod 2).

The mass is readily available as the weight of each projectile was measure prior to launch. The drag coefficient and other aero coefficients of the Martlet 2C (Mod 2) were found in a report from the HARP program [52].

Using the firing data from 23 Martlet 2C (Mod 2) projectiles, the apogee of each round can be calculated using the three term ECI Modified Kepler solution. The apogee will occur at the first minima of the inverse radius. This can be calculated by the first derivative of the solution of the Modified Kepler equation.

$$\frac{du}{d\theta} = c_1 \cos(\theta) - c_2 \sin(\theta) - \tau c_4 e^{-\tau\theta} - 2\tau c_5 e^{-2\tau\theta} = 0. \quad (6.1)$$

The radar data shows that apogee happens well over 100 km where the effects of the atmosphere have disappeared. Thus, equation (6.1) can be simplified to:

$$c_1 \cos(\theta) - c_2 \sin(\theta) = 0, \quad (6.2)$$

$$\frac{c_1}{c_2} = \tan(\theta), \quad (6.3)$$

$$\theta_{\text{apogee}} = \tan^{-1} \left(\frac{c_1}{c_2} \right). \quad (6.4)$$

Apogee can be predicted for each HARP projectile by the full solution of the Modified Kepler equation with three terms:

$$a_{\text{apogee}} = [c_1 \sin(\theta_{\text{apogee}}) + c_2 \cos(\theta_{\text{apogee}}) + c_3 + c_4 e^{-\tau\theta_{\text{apogee}}} +$$

$$c_5 e^{-2\tau\theta_{\text{apogee}}}]^{-1} - 6378 \text{ km}, \quad (6.5)$$

with:

$$c_1 = \frac{-\tan\phi}{r_0} - \frac{2\beta c_3 \cos\mu \tau}{1+\tau^2} \left(\frac{V_{\text{rel}}}{V}\right)^2 + \frac{4\tau\beta^2 c_3 \cos^2\mu}{1+(2\tau)^2} \left(\frac{V_{\text{rel}}}{V}\right)^4, \quad (6.6)$$

$$c_2 = \frac{1}{r_0} - c_3 + \frac{2\beta c_3 \cos\mu}{1+\tau^2} \left(\frac{V_{\text{rel}}}{V}\right)^2 - \frac{2\beta^2 c_3 \cos^2\mu}{1+(2\tau)^2} \left(\frac{V_{\text{rel}}}{V}\right)^4, \quad (6.7)$$

$$c_3 = \frac{m^2 MG}{L_\infty^2}, \quad (6.8)$$

$$c_4 = \frac{-2\beta c_3 \cos\mu}{1+\tau^2} \left(\frac{V_{\text{rel}}}{V}\right)^2, \quad (6.9)$$

$$c_5 = \frac{2\beta^2 c_3 \cos^2\mu}{1+(2\tau)^2} \left(\frac{V_{\text{rel}}}{V}\right)^4, \quad (6.10)$$

and,

$$\beta = \frac{C_{D0} \rho_0 A}{2 \text{ km} \sin\phi}, \quad (6.11)$$

$$\tau = k r_0 \tan\phi, \quad (6.12)$$

$$L_0 = |V| r_0 \cos\phi, \quad (6.13)$$

$$L_\infty = L_0 e^{-\beta \cos\mu}, \quad (6.14)$$

$$\vec{V} = \vec{V}_{\text{rel}} + \vec{\omega} \times \vec{r}_0 + \vec{V}_{\text{tangent}}. \quad (6.15)$$

The Latitude of the HARP gun on Barbados is 13°4'38" (13.0772 degrees) taken from a survey of the gun site. Assuming the perfectly spherical Earth, this results in the Earth rotation correction of:

$$\vec{\omega} \times \vec{r}_0 = \frac{2\pi}{86400 \text{ sec}} 6378 \text{ km} \cos 13.0772^\circ = 0.4518 \frac{\text{km}}{\text{sec}}. \quad (6.16)$$

The direction the Barbados gun is pointed is not contained in any of the reports reviewed but is needed for the accurate evaluation of the trajectory. The bearing of fire can be measured from Figure 5.4 as 109 'True' by measurement relative to the runway in

the picture. Note that the airport runway is visible in the picture and that the approaching runway number “27” refers to the magnetic heading for approaching aircraft, 270 ‘Magnetic’. The angle of the runway to the horizontal was measured as 15.5 degrees which is equivalent to the declination at this location ($15^{\circ} 22'$) at the year the picture was taken (2012) given by the National Oceanic and Atmospheric Administration’s National Geophysical Data Center for the island of Barbados.

The difference between the predicted apogee and the measured or evaluated apogee for each round is used to create an apogee error and is shown in Figure 6.5. The error in the apogee is within 0.4 km of the center of the data with a standard deviation of 2.25 km. The data used to calculate each data point in Figure 6.5 is given in Appendix D.

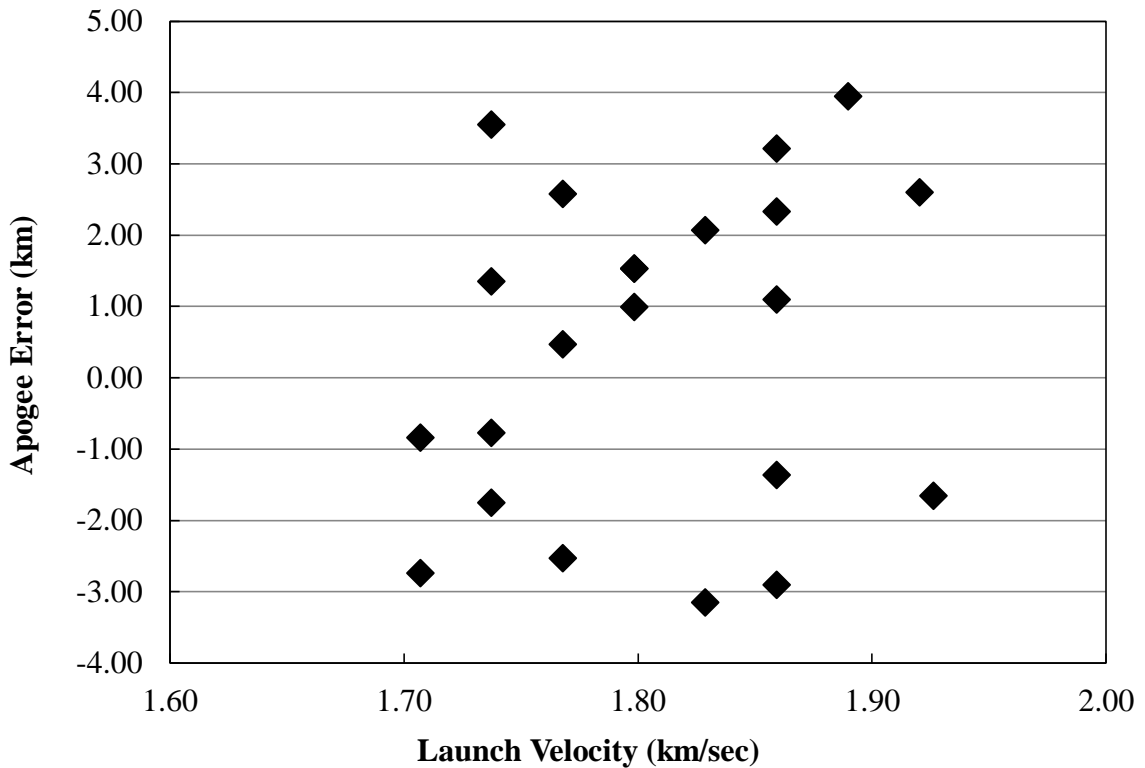


Figure 6.5 Apogee Error between Corrected Modified Kepler Solution and Measured Apogee Data for Barbados 16'' HARP Gun Martlet 2C (Mod 2) Rounds.

The exact method that the apogee is measured by (optical observations, radar data, or simulation curve fits) is not given in the reports. It must therefore be assumed that the apogee given for each round uses the most accurate data from the various means available.

No atmospheric data (temperature, pressure, humidity, surface wind speed and direction) was included in the reports. The atmospheric density used for the Modified Kepler solution was the nominal value used in the US Standard Atmosphere (1.225 kg/m^3). This is a good approximation for the island of Barbados as the temperate location ensures an average temperature of approximately 80 degrees Fahrenheit during the day and 70 degrees Fahrenheit at night year round.

D. Martlet 2C (Mod 2) Apogee Comparison for the Yuma Gun

Apogee data is also given for projectiles fired from the Yuma, Arizona 16" HARP gun report [4]. The Yuma gun was equivalent in all aspects to the Barbados gun with the exception of the azimuth, latitude, and atmospheric properties at launch. The Yuma gun also fired the Martlet 2C (Mod 2) projectiles and utilized equivalent muzzle velocities.

The Yuma gun was mounted at a latitude of $32^{\circ}52'33''$ N at a bearing of 078T as given in the report. The majority of the firings happened in the evening hours where the illuminate trails would be most visible. The atmosphere at the Yuma site is considerably drier and colder during the evenings when the gun was fired. An surface density of 1.14 kg/m^3 was used for the Yuma site based upon based upon the average evening temperature and density calculated from the National Oceanic and Atmospheric

Administration's National Climate Data Center for the year 1966 at the Yuma airport [53]. 22 Martlet 2C (Mod 2) rounds fired from the Yuma gun for which apogee data was given can be used to validate the ECI Modified Kepler solutions at a different bearing and latitude. The drag properties derived from the Barbados data was used to calculate the apogee for the Yuma rounds. The results of the comparison are shown in Figure 6.6 with the data presented in Appendix D. The error for the Yuma data is 0.44 km from the center of the data with a standard deviation of 2.65 km.

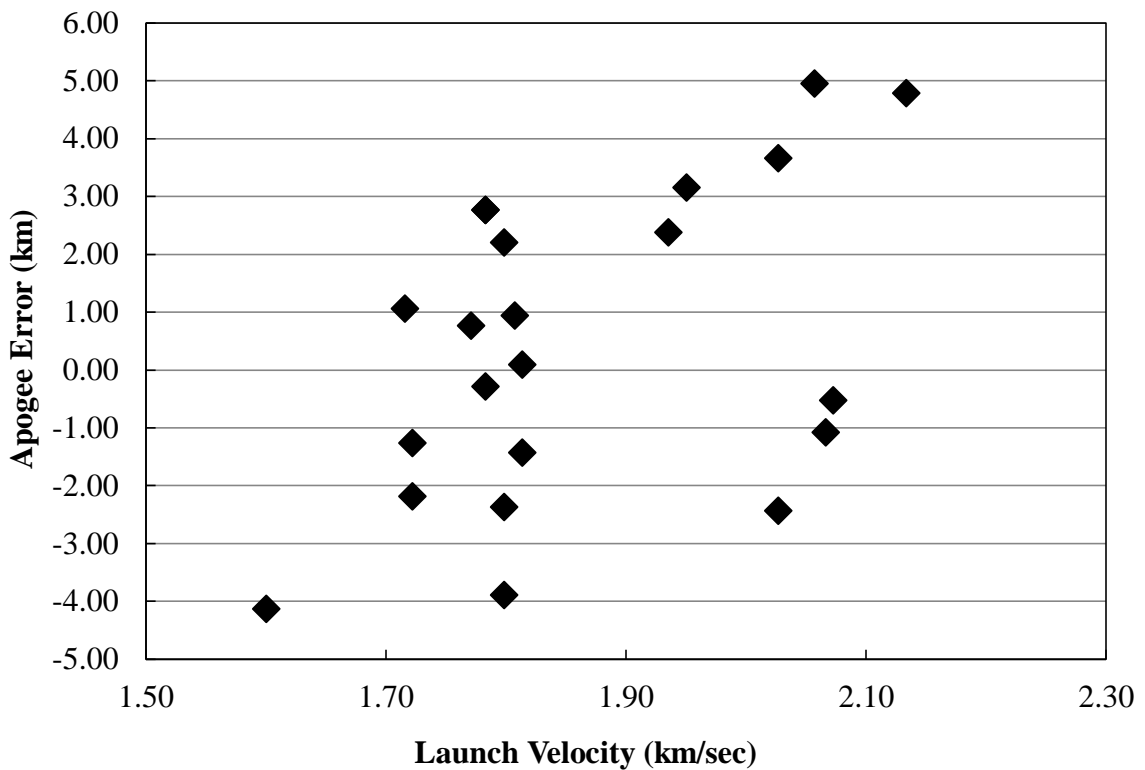


Figure 6.6 Apogee Error between Corrected Modified Kepler Solution and Measured Apogee Data for Yuma 16'' HARP Gun Martlet 2C (Mod 2) Rounds

E. Martlet 2C (Mod 2) Trajectory Comparisons

The Barbados report also includes tables of range and altitude radar data as the projectile were tracked in flight. The radar data from can be compared to the analytical

results of the ECI Modified Kepler solution. The comparison for several trajectories is shown in the figures below. Note that the range displayed is the relative range between the original launch location and the current position of the projectile as is measured by the radar.

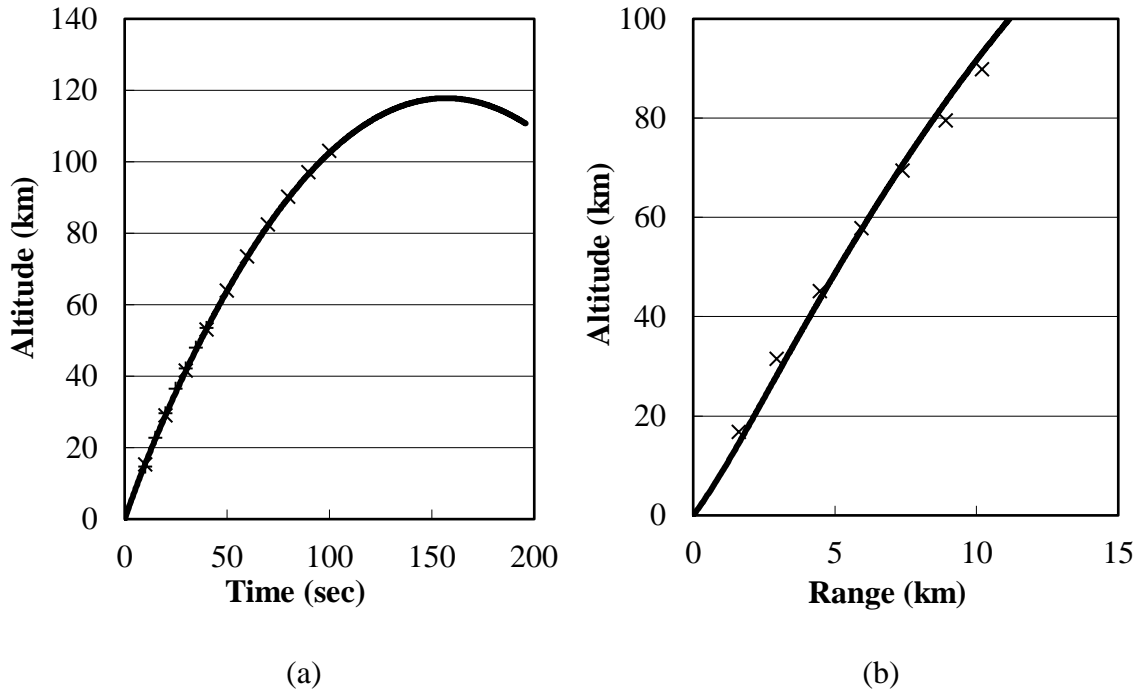


Figure 6.7 Radar Data and ECI Modified Kepler Solution for Round 206 from Barbados Gun

Round 206 is a good example of the radar data compared to the ECI Modified Kepler Solution. The Altitude as a function of time is captured relatively accurately but the altitude as a function of range shows some error. It is not known what orientation the radar was set up or what error ranges was measured on each direction. It is possible that the radar was pointed down the axis of the trajectory and thus the distance along the trajectory would be relatively accurate while the range would be a combination of

distance along trajectory and angular displacement from the original direction. Radars usually have lower accuracy when measuring angular measurements and this may explain the range errors.

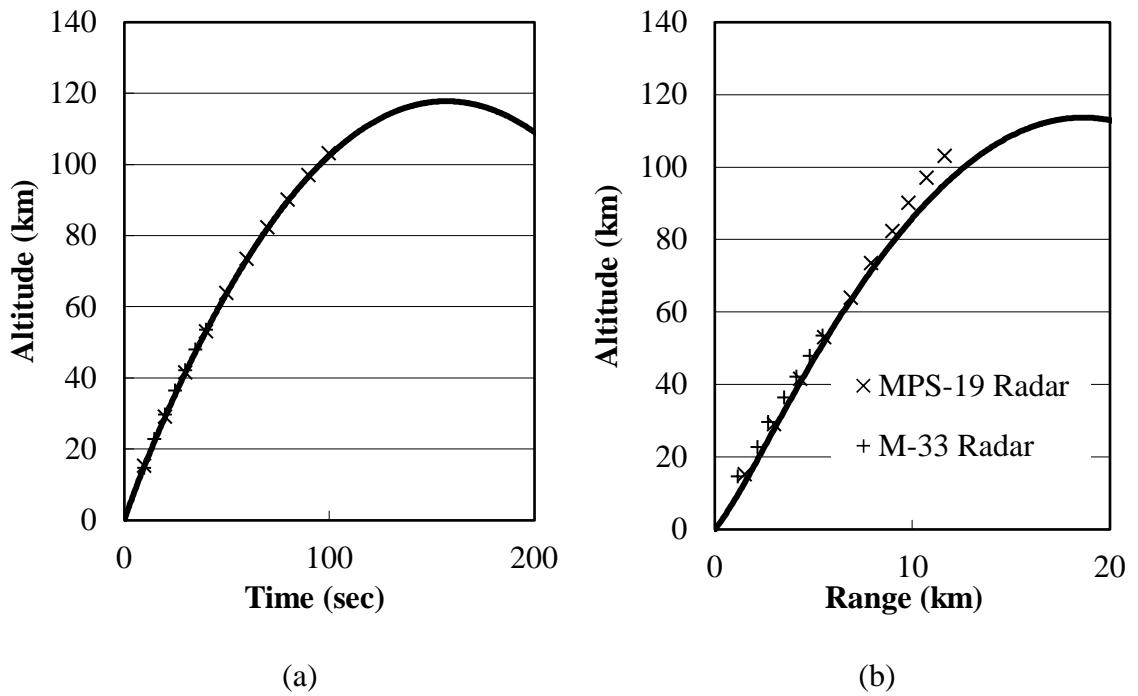


Figure 6.8 Radar Data and ECI Modified Kepler Solution for Round 188 from Barbados Gun

Round 188 is another example of a typical set of trajectory data collected. Again the altitude as a function of time is well captured while the altitude as a function of range is slightly distorted. Notice that both radars were used for this test and the trajectory data is in agreement. The M-33 radar appears to have lost the track at an altitude above 50 km.

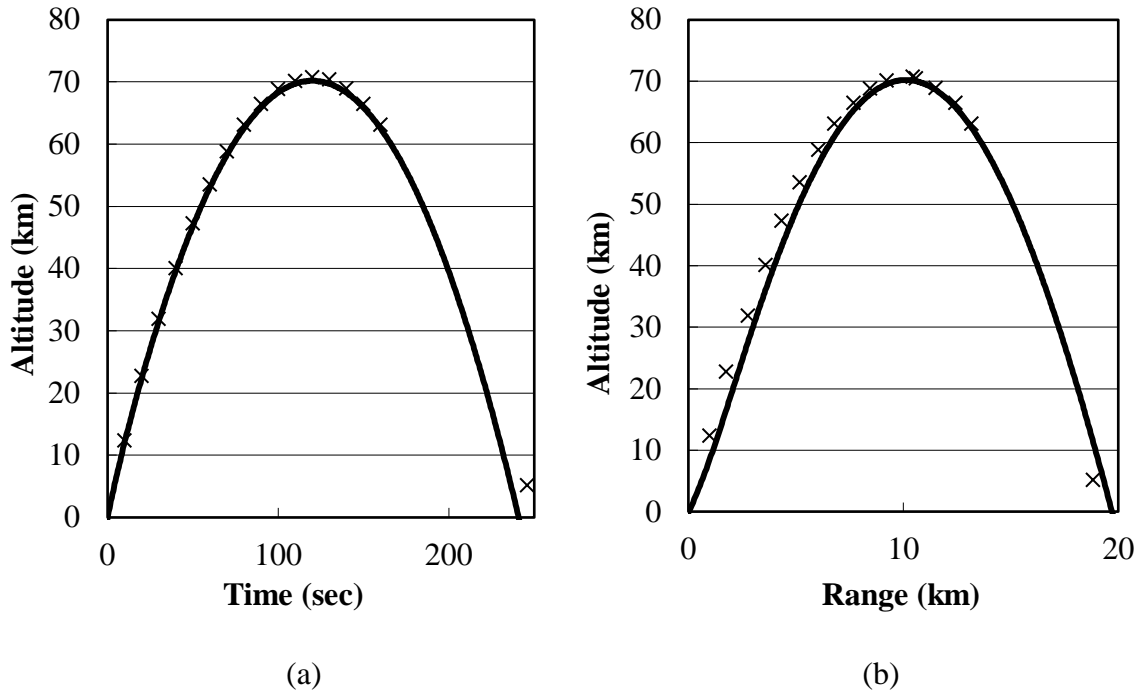


Figure 6.9 Radar Data and ECI Modified Kepler Solution for Round 227 from Barbados Gun

Round 227 is one of the few trajectories in which the projectile was tracked past apogee. The projectile was then reacquired just before impact with the water. As expected from the ECI Modified Kepler comparison with the numerical simulation, the ECI Modified Kepler solution diverges from the radar data when the projectile reenters the thick atmosphere at lower altitudes. Note that the altitude with time is still accurate until reentry but that the altitude as a function of range shows error that is a combination of the error in the ECI Modified Kepler solution and the error in the radar measurements.

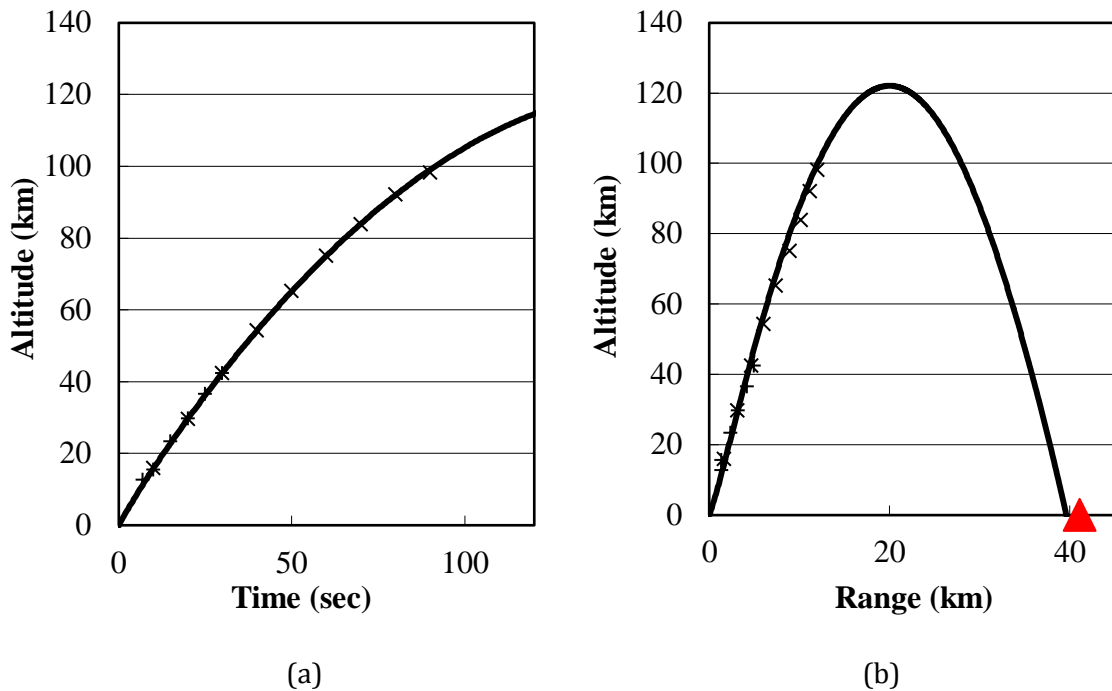


Figure 6.10 Radar Data and ECI Modified Kepler Solution for Round 181 from Barbados Gun

Round 181 is unique in that the splash of the projectile was observed. There were multiple observers that attempted to observe and triangulate the location of the round impact with the water with very little success. An observer was looking at just the right spot in the ocean when round 181 hit and was able to observe the spot. The triangulated range was 41.1 km.

As can be seen, this observation agrees with the ECI Modified Kepler results relatively well and verifies the range data without radar data. The ECI Modified Kepler solution predicts a range of 39.6 km resulting in an error of 1.5 km, or 3.6% of the range.

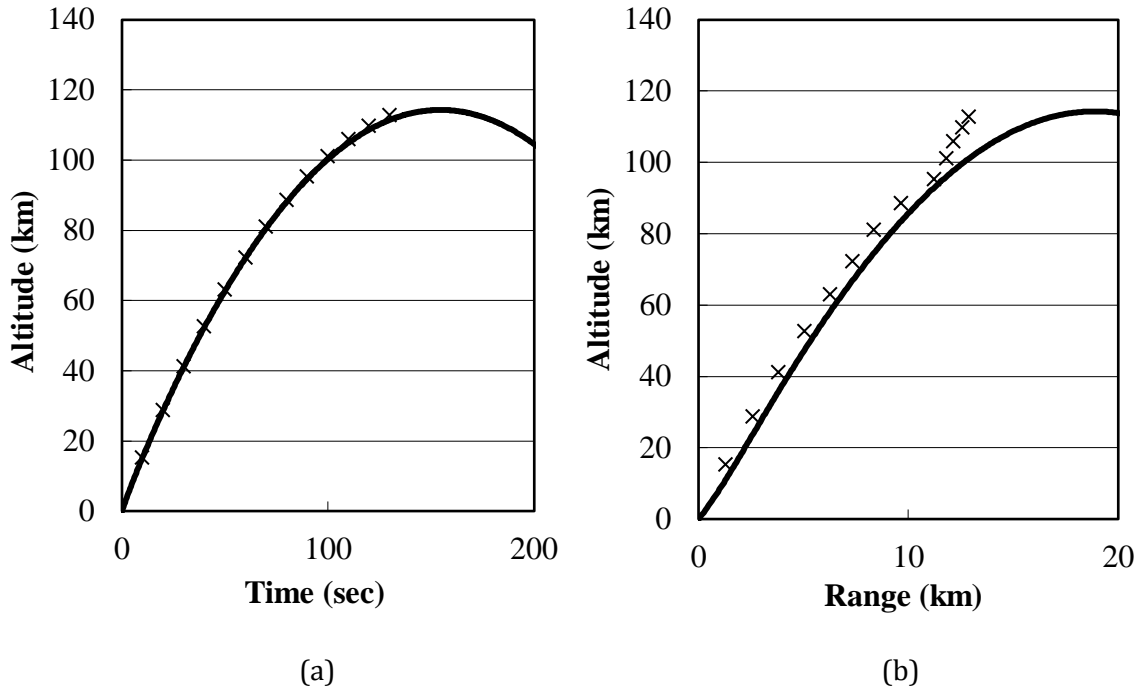


Figure 6.11 Radar Data and ECI Modified Kepler Solution for Round 221 from Barbados Gun

Round 221 is an example of a trajectory that significantly departs from the radar data. Again the altitude as a function of time is accurately captured but the radar data appears to show a course change when the projectile reaches 100 km. This may be due to a failure in the release of the tracking fluid that created a thrust effect and changed the trajectory.

No radar data was found from the Yuma gun but the close correlation of the apogee data between the Yuma gun and Barbados gun suggest that the trajectory data would fit the ECI Modified Kepler solution as well.

The HARP data proves remarkably good at verifying the Modified Kepler equation and its solution. Without any error estimates from the HARP data, it cannot be known if the ECI Modified Kepler solution is within the 0.5 km accuracy estimated by

comparison with the numerical simulation, but the data shows a good agreement in all dimensions.

CHAPTER 7

CONCLUSIONS AND FUTURE RESEARCH

The Modified Kepler approach appears to give good estimates of the position of an aerodynamically stable projectile launched with an initial speed and elevation that it leaves the lower atmosphere. The analytic nature of the solution results in a much quicker evaluation of trajectory than with any possible numerical solution. The primary purpose of this work was to enable hypersonic projectiles for ballistic missile defense. The steps to utilize the Modified Kepler solution for firing solution equitation are relatively straightforward.

A. Use of the Modified Kepler Solution to Intercept Ballistic Missiles

The first step in calculating a potential firing solution for a ballistic missile will be to estimate the future position of the target. If the missile has burned out and is outside of the atmosphere the future position is a simple solution of the standard Kepler solution with the error being in the uncertainty of the initial position and velocity vectors.

If the missile is still boosting then the future position must be estimated by a real-time numerical simulation or by the development of fly-out tables for the type of targets that are expected. The major error in this method is in the assumption of the behavior of

the missile while it is still maneuvering which vanishes upon the observation of the missile after burnout.

The Modified Kepler solution cannot be manipulated to isolate the elevation and bearing which means that the firing solution cannot be solved directly. The suggested approach would be to run a non-linear solver to iterate the Modified Kepler solution until a firing solution was found. This may require solving the equation of motion dozens or even hundreds of times. This would be compared to solving the non-linear numerical simulation equations of motion several hundreds of thousands or millions of times to converge to a solution. Based upon the comparison of computational effort (FLOPS) for each of the methods used to calculate space gun trajectories, it is suspected that all possible intercepts could be found using the Modified Kepler approach in less time than it would take to solve for one intercept trajectory using an iterative 3DOF numerical solution using equivalent computational power.

If a firing solution with a greater accuracy than is available with the Modified Kepler solution is needed and time is available, the results of the Modified Kepler solution may be used as an input to a high fidelity numerical simulation that could verify the accuracy of the solution and possibly iterate a few times to increase the accuracy of the solution.

The final step would be to numerically integrate the angular momentum to determine the time of flight to the intercept point. If the time to intercept is greater than the time available, then the opportunity is lost and the next intercept point is evaluated.

The accuracy of the firing solution is an initial guess at the divert capability that the projectile will need to perform direct intercept. For a debris field, the accuracy of the

firing solution is an estimate of the debris field size needed to ensure that the missile flies through it and the probability of the missile hitting a particle.

The use of fly-out tables or look-up tables of potential positions of the projectile and missile based upon numerical simulations is also a possible method to develop intercept solutions. This method divides the volume of above the surface of the Earth into discrete volumes and then runs multiple numerical simulation until the trajectory is centered in the discrete volume. The firing solution into this space is then recorded in the fly-out table and the time of flight. The fly-out table for the target and projectile is then searched to find potential intercepts. The limit on this method is the size of the discrete volume. If the discrete volume is sufficiently large, then the number of simulations required to develop the tables is reasonable and the size of the tables is also reasonable. As the size of the discrete volume is decreased to increase accuracy, the number of simulations and size of the tables increase to an unreasonable size.

The combination of an analytic solution to the motion of the missile combined with the Modified Kepler solution for the motion of the projectile is expected to be the fastest and most accurate method of calculating firing solutions. This combination is valid now for missiles that have burned out and follow a standard Kepler motion. For boost phase intercept calculations, the development of an analytic solution to missile while still boosting and past burnout is still pending development.

B. Other Sources of Uncertainty

There are numerous other sources of uncertainty in a practical fire control system. These other factors can be roughly divided into gun control and environmental effects.

The accuracy in which the gun can be pointed will become important for these long trajectories, possible down to the milli-radian or lower. The accuracy of the muzzle velocity will also become critically important to accurately predict the motion. The latitude of the gun on the surface of the Earth must also be known with a sufficient accuracy. Finally the timing of fire will need to be very accurately controlled to ensure an intercept is possible.

The variation in atmospheric density will also need to be taken into account. The loss of angular momentum due to precipitation would be expected to dramatically change the predicted motion of the projectile as well.

All of these sources of potential errors will need to be studied to predict the impact on the accuracy of any firing solution. These uncertainties may end up being much larger than the uncertainties contained in the simplification assumptions made to make the Modified Kepler equation solvable.

Finally, the projectile itself will need to be aerodynamically stable and have a low MKS beta (drag to weight) value. The lower the MKS beta value, the more accurately the projectile matches the assumptions used to derive the MKS. From the various projectiles used in this study, a MKS beta value of less than 0.25 is needed for reasonably accurate MKS trajectories.

C. Ground Support Fire

Although the purpose of this study was to evaluate the trajectory of hypersonic projectiles for ballistic missile defense, it would be foolish not to take the opportunity to evaluate the relevance of the work for ground to ground fire support. The first concern is

the minor mismatch of predicted angular momentum with reality that causes the error of the projectile to grow over the trajectory. A set of empirical correction factors may be developed that provides a slight improvement of the prediction or a look-up table approach may be used to correct for this mismatch to improve the overall accuracy of the system.

The second area of concern is the error associated with reentry. In this case, the total position error is slightly misleading. The error associated with hitting a ground target 0.5 seconds late is unimportant but at 2 km/sec may result in a 1 km miss relative to a ballistic missile. For the Modified Kepler solution to be utilized for ground support fire, more work on accurately predicting the asymptotic angular momentum and decay of angular momentum during reentry would be recommended.

D. Closing

The next few years is expected to be very exciting for space gun research. For the first time in over 50 years the possibility of collecting trajectory data from a real system is possible. The data from the US Navy Railgun will make it possible to further validate and improve the Modified Kepler approach. The formalization of a fire control system to intercept ballistic missiles and thus help eliminate this threat is one step closer. It is my sincere hope that we can take unfinished technology of the Nazi war machine (the V3) to make obsolete one of the greatest evils produced by the same regime (the V2 and all subsequent ballistic missiles).

APPENDICES

APPENDIX A

3DOF Numerical Simulation of Hypersonic Projectiles

The numerical simulation was written in Visual Basic for Applications as a Microsoft Excel Macro.

```
Private Sub CommandButton1_Click()
'This simulation calculates the trajectory of a railgun projectile
'By: John Stutz, P.E., Missile Defense Agency
'created 10/11/2010

Dim GM As Double
GM = 398600.4418 'Mass of earth times gravitational constant km^3/s^2
Dim RE As Double
RE = 6378 'Radius of earth km
Dim Xbullet(2), Ybullet(2), Zbullet(2) As Double
Dim Xo, Yo, Zo As Double
Dim Rbullet, Thetabullet, Phibullet As Double
Dim Xgrav, Ygrav, Zgrav As Double
Dim VX(2), Vr(2) As Double
Dim Pi As Double
Pi = 3.14159265358979
Dim dt As Double
dt = Worksheets("Main Page").Cells(4, 2).Value
Dim Jacobian(2, 2) As Double
Dim earthspin As Double 'angular rate of earth rotation
earthspin = 0 '0.0000727221 'radians/second
Dim time As Double
Dim q, w As Double
Dim dens, t, p, a As Double
Dim Xdrag, Ydrag, Zdrag As Double
Dim drag As Double
Dim bulletMa As Double
Dim Cd As Double
Dim k As Integer
Dim dtheta As Double
Dim theta As Double
Dim L(2) As Double
Dim dL As Double
Dim flag As Double
L(1) = Worksheets("Main Page").Cells(19, 2).Value
'XXXXXXXXXXXXXXXXXXXXXXXXXXXXXXXXXXXXXXXXXXXXXXXXXXXXXXXXXXXXXXXXXXXX
time = dt * 3
flag = 0
k = 0
Worksheets("Main Page").range("d2:i10000").ClearContents

Xbullet(0) = RE * Math.Cos(Worksheets("Main Page").Cells(6, 2).Value *
Pi / 180) * Math.Cos(Worksheets("Main Page").Cells(7, 2).Value * Pi /
180)
Ybullet(0) = RE * Math.Cos(Worksheets("Main Page").Cells(6, 2).Value *
Pi / 180) * Math.Sin(Worksheets("Main Page").Cells(7, 2).Value * Pi /
```

```

180)
Zbullet(0) = RE * Math.Sin(Worksheets("Main Page").Cells(6, 2).Value *
Pi / 180)
Xo = Xbullet(0)
Yo = Ybullet(0)
Zo = Zbullet(0)

'Calculate R, theta, phi
Rbullet = RE
Thetabullet = Worksheets("Main Page").Cells(7, 2).Value * Pi / 180
Phibullet = Worksheets("Main Page").Cells(6, 2).Value * Pi / 180

Vr(0) = Worksheets("Main Page").Cells(11, 2).Value *
Math.Sin(Worksheets("Main Page").Cells(9, 2).Value * Pi / 180)
Vr(1) = Worksheets("Main Page").Cells(11, 2).Value *
Math.Cos(Worksheets("Main Page").Cells(9, 2).Value * Pi / 180) *
Math.Sin(Worksheets("Main Page").Cells(10, 2).Value * Pi / 180) +
earthspin * RE
Vr(2) = Worksheets("Main Page").Cells(11, 2).Value *
Math.Cos(Worksheets("Main Page").Cells(9, 2).Value * Pi / 180) *
Math.Cos(Worksheets("Main Page").Cells(10, 2).Value * Pi / 180)

'Jacobian constants to convert polar vectors to cartesian
Jacobian(0, 0) = Math.Cos(Phibullet) * Math.Cos(Thetabullet)
Jacobian(0, 1) = Math.Cos(Phibullet) * Math.Sin(Thetabullet)
Jacobian(0, 2) = Math.Sin(Phibullet)
Jacobian(1, 0) = -Math.Sin(Thetabullet)
Jacobian(1, 1) = Math.Cos(Thetabullet)
Jacobian(1, 2) = 0
Jacobian(2, 0) = -Math.Sin(Phibullet) * Math.Cos(Thetabullet)
Jacobian(2, 1) = -Math.Sin(Phibullet) * Math.Sin(Thetabullet)
Jacobian(2, 2) = Math.Cos(Phibullet)

'Convert Velocity vector into cartesian
For i = 0 To 2
VX(i) = 0
Next i
For i = 0 To 2
    For j = 0 To 2
        VX(i) = VX(i) + Vr(j) * Jacobian(j, i)
    Next j
Next i

Xbullet(1) = Xbullet(0) + VX(0) * dt
Ybullet(1) = Ybullet(0) + VX(1) * dt
Zbullet(1) = Zbullet(0) + VX(2) * dt

'XXXXXXXXXXXXXXXXXXXXXXXXXXXXXXXXXXXXXXXXXXXXXXXXXXXXXXXXXXXXXXXXXXXX
10 'This bookmark is the start of the iteration to solution

'Calculate a normal vector pointing toward the origin (center of
earth)
Xgrav = -Xbullet(1) / Math.Sqrt(Xbullet(1) ^ 2 + Ybullet(1) ^ 2 +
Zbullet(1) ^ 2)
Ygrav = -Ybullet(1) / Math.Sqrt(Xbullet(1) ^ 2 + Ybullet(1) ^ 2 +
Zbullet(1) ^ 2)

```

```

Zgrav = -Zbullet(1) / Math.Sqrt(Xbullet(1) ^ 2 + Ybullet(1) ^ 2 +
Zbullet(1) ^ 2)

'Calculate density for drag calculations of bullet
Rbullet = Math.Sqrt(Xbullet(1) ^ 2 + Ybullet(1) ^ 2 + Zbullet(1) ^ 2)
a = Rbullet - RE
t = 141.89 + 0.00299 * a * 1000
p = 2.488 * (t / 216.6) ^ -11.388
If a < 25 Then
t = -56.46 + 273.1
p = 22.65 * Math.Exp(1.73 - 0.000157 * a * 1000)
End If
If a < 11 Then
t = 288.14 - 0.00649 * a * 1000
p = 101.29 * (t / 288.08) ^ 5.256
End If
dens = p / (0.2869 * (t))

'Calculate bullet velocity relative to motion of air spinning with
earth
VX(0) = (Xbullet(1) - Xbullet(0)) / dt - Ybullet(1) * earthspin
VX(1) = (Ybullet(1) - Ybullet(0)) / dt + Xbullet(1) * earthspin
VX(2) = (Zbullet(1) - Zbullet(0)) / dt

'Calculate bullet Mach number and drag coefficient
If t > 0 Then
bulletMa = Math.Sqrt(VX(0) ^ 2 + VX(1) ^ 2 + VX(2) ^ 2) * 1000 /
Math.Sqrt(1.4 * 287 * t)
Cd = 0.077 * Exp(-0.38 * bulletMa) + 0.014
Else
Cd = 0
End If

'Calculate drag on projectile
drag = 0.5 * dens * Cd * Worksheets("Main Page").Cells(13, 2).Value
* (VX(0) ^ 2 + VX(1) ^ 2 + VX(2) ^ 2) * 1000 ^ 2
Xdrag = drag * VX(0) / Math.Sqrt(VX(0) ^ 2 + VX(1) ^ 2 + VX(2) ^ 2)
Ydrag = drag * VX(1) / Math.Sqrt(VX(0) ^ 2 + VX(1) ^ 2 + VX(2) ^ 2)
Zdrag = drag * VX(2) / Math.Sqrt(VX(0) ^ 2 + VX(1) ^ 2 + VX(2) ^ 2)

'Calculate position of bullet
Xbullet(2) = 2 * Xbullet(1) - Xbullet(0) + ((GM * Xgrav * dt ^ 2) /
(Rbullet ^ 2)) - Xdrag * dt ^ 2 / (Worksheets("Main Page").Cells(14,
2).Value * 1000)
Ybullet(2) = 2 * Ybullet(1) - Ybullet(0) + ((GM * Ygrav * dt ^ 2) /
(Rbullet ^ 2)) - Ydrag * dt ^ 2 / (Worksheets("Main Page").Cells(14,
2).Value * 1000)
Zbullet(2) = 2 * Zbullet(1) - Zbullet(0) + ((GM * Zgrav * dt ^ 2) /
(Rbullet ^ 2)) - Zdrag * dt ^ 2 / (Worksheets("Main Page").Cells(14,
2).Value * 1000)
Rbullet = Math.Sqrt(Xbullet(2) ^ 2 + Ybullet(2) ^ 2 + Zbullet(2) ^ 2)

```

```

    'Calculate the Angular Momentum and Rate of Angular Momentum of the
    Bullet
    dtheta = (Xbullet(2) * Xbullet(1) + Ybullet(2) * Ybullet(1) +
    Zbullet(2) * Zbullet(1))
    dtheta = dtheta / Math.Sqrt(Xbullet(2) ^ 2 + Ybullet(2) ^ 2 +
    Zbullet(2) ^ 2)
    dtheta = dtheta / Math.Sqrt(Xbullet(1) ^ 2 + Ybullet(1) ^ 2 +
    Zbullet(1) ^ 2)
    dtheta = WorksheetFunction.Acos(dtheta)
    L(2) = (Xbullet(2) ^ 2 + Ybullet(2) ^ 2 + Zbullet(2) ^ 2) * dtheta
    / dt
    dL = (L(2) - L(1)) / dtheta
    L(1) = L(2)
    theta = (Xbullet(2) * Xo + Ybullet(2) * Yo + Zbullet(2) * Zo)
    theta = theta / Math.Sqrt(Xbullet(2) ^ 2 + Ybullet(2) ^ 2 +
    Zbullet(2) ^ 2)
    theta = theta / Math.Sqrt(Xo ^ 2 + Yo ^ 2 + Zo ^ 2)
    theta = WorksheetFunction.Acos(theta)

'Display data
'this section reduces the amount of output to display on chart
If (time > (k * 0.5)) Then
    Worksheets("Main Page").Cells(k + 2, 4).Value = time
    Worksheets("Main Page").Cells(k + 2, 5).Value = Rbullet - RE
    q = 0
    q = RE * Math.Cos(Worksheets("Main Page").Cells(6, 2).Value * Pi /
    180) * Math.Cos((Worksheets("Main Page").Cells(7, 2).Value * Pi / 180))
    * Xbullet(2) ' earthspin * time
    q = q + RE * Math.Cos(Worksheets("Main Page").Cells(6, 2).Value *
    Pi / 180) * Math.Sin((Worksheets("Main Page").Cells(7, 2).Value * Pi /
    180)) * Ybullet(2) '+ earthspin * time
    q = q + RE * Math.Sin(Worksheets("Main Page").Cells(6, 2).Value *
    Pi / 180) * Zbullet(2)
    q = q / (Rbullet * RE)
    q = WorksheetFunction.Acos(q)
    'q = (RE * Math.Cos(Worksheets("Main Page").Cells(6, 2).Value * Pi
    / 180) * Math.Cos((Worksheets("Main Page").Cells(7, 2).Value * Pi /
    180)) - Xbullet(2)) ^ 2
    'q = q + (RE * Math.Cos(Worksheets("Main Page").Cells(6, 2).Value *
    Pi / 180) * Math.Sin((Worksheets("Main Page").Cells(7, 2).Value * Pi /
    180)) - Ybullet(2)) ^ 2
    'q = q + (RE * Math.Sin(Worksheets("Main Page").Cells(6, 2).Value *
    Pi / 180) - Zbullet(2)) ^ 2
    'q = Math.Sqrt(q - (Rbullet - RE) ^ 2)
    'q = q / RE
    Worksheets("Main Page").Cells(k + 2, 6).Value = q
    Worksheets("Main Page").Cells(k + 2, 7).Value = Math.Sqrt(VX(0) ^ 2
    + VX(1) ^ 2 + VX(2) ^ 2)
    Worksheets("Main Page").Cells(k + 2, 8).Value = Math.Sqrt(Xbullet(1)
    ^ 2 + Ybullet(1) ^ 2 + Zbullet(1) ^ 2)
    Worksheets("Main Page").Cells(k + 2, 9).Value = L(2)

```

```

    k = k + 1
End If

'Update old values for numerics
  For i = 0 To 1
    Xbullet(i) = Xbullet(i + 1)
    Ybullet(i) = Ybullet(i + 1)
    Zbullet(i) = Zbullet(i + 1)
  Next i

time = time + dt 'update sim time
time = WorksheetFunction.Round(time, 4)
If Rbullet > RE Then
GoTo 10
End If
'XXXXXXXXXXXXXXXXXXXXXXXXXXXXXXXXXXXXXXXXXXXXXXXXXXXXXXXXXXXXXXXXXXXX
20 'Use this bookmark to jump out early

End Sub

```

APPENDIX B

6DOF Numerical Simulation of Hypersonic Projectiles

The numerical simulation was written in MATLAB by Dr. Nathan Slegers.

```
clc
clear all
global mass rho GM Ix Iy Iz d cx0 cx2 cypa cna clp cmq cldd dx dxmag
mass = 15.66; % mass [kg] 4.894
GM = 398600.4418; % gravitational acceleration km^2/s^2
d=0.0395; % diameter of the projectile (M)
Ix = (15.66/5.029)*(0.0395/0.0256)^2*0.00033;
Iy = (15.66/5.029)*(0.0395/0.0256)^2*0.24021;
Iz = Iy; % [Kg*m^2];
%
% M829 AeroTables Mach numbers and corresponding coefficients
%
M_Table = [0.00,1.00,1.50,2.00,2.50,3.00,4.00,5.00,8.00];
CX0_TAB = [-0.60,-1.00,-1.35,-1.22,-1.04,-0.91,-0.69,-0.543,-0.449];
CX2_TAB = [-8.35,-11.53,-17.21,-16.29,-15.73,-13.91,-12.18,-10.41,-
9.08];
CNA_TAB = [17.94,22.37,21.09,19.97,18.77,17.63,15.36,13.15,9.92];
CYP_TAB = [0.0,0.0,0.0,0.0,0.0,0.0,0.0,0.0,0.0];
CMQ_TAB = [-7288,-8697,-9064,-8000,-7523,-7047,-6091,-5129,-4224];
CLP_TAB = [-21.46,-27.47,-25.0,-23.6,-22.3,-20.2,-16.1,-13.4,-11.4];
CLDD_TAB = [0.084,0.084,0.076,0.072,0.068,0.062,0.049,0.041,0.035];
SLDEL = [-0.2615,-0.2615,-0.2615,-0.2615,-0.2314,-0.2000,-0.1661,-
0.1512,-0.1507];
SLMAG = [0.0,0.0,0.0,0.0,0.0,0.0,0.0,0.0,0.0];
Coeff_Table = [CX0_TAB' CX2_TAB' CNA_TAB' CYP_TAB' CMQ_TAB' CLP_TAB'
CLDD_TAB' SLDEL' SLMAG'];
%
% initial state conditions
% x y z phi theta psi u v w p q r
state = [0.0; 0.0; 0.0; 0.0; 0.872665; 0.0; 2022; 0.0; 0.0; 10.0; 0.0;
0.0];
%
time(1)=0.0; % time at i=1
ti=0; % initial time
tf=270; % final time
h=0.0005; % time step in seconds

b=1;
%
% RK4 Integration
%
for i=1:(tf-ti)/h;
% Compute Density and Speed of Sound Meters
Vtot(i) = sqrt(state(7,i)^2+state(8,i)^2+state(9,i)^2);
if (state(3,i) < -10769.00)
rho = 0.37454745*exp(0.00015682*(state(3,i) +10769.0));
a = 295.92987;
else
rho = 1.2258100*(1+0.00002257* state(3,i) )^4.256;
```



```

        a = 14.9390*sqrt(518.4+0.01170* state(3,i) );
    end
    %rho=0;
    Mach(i) = Vtot(i)/a; % Mach Number
    %
    aeros = interp1(M_Table,Coeff_Table,Mach(i));
    cx0 = aeros(1);
    cx2 = aeros(2);
    cna = aeros(3);
    cypa= aeros(4);
    cmq = aeros(5);
    clp = aeros(6);
    cldd= aeros(7);
    dx = aeros(8);
    dxmag= aeros(9);
    %
    k1=h*PROJ6DOF_M829_DERV(time(i),state(:,i));
    k2=h*PROJ6DOF_M829_DERV(time(i)+0.5*h,state(:,i)+0.5*k1);
    k3=h*PROJ6DOF_M829_DERV(time(i)+0.5*h,state(:,i)+0.5*k2);
    k4=h*PROJ6DOF_M829_DERV(time(i)+h,state(:,i)+k3);
    s=(k1+2*k2+2*k3+k4)/6;
    state(:,i+1)=state(:,i)+ s;
    %

    if (time(i)>(0.5*b))
        output(b,1)=time(i);
        output(b,2)=state(1,i);
        output(b,3)=state(2,i);
        output(b,4)=state(3,i);
        output(b,5)=Vtot(i);

output(b,6)=sqrt(state(8,i)^2+state(9,i)^2)*180/(state(7,i)*pi);
        b=b+1;
    end

    i=i+1;
    time(i) = time(i-1) + h;

end

function dstate= PROJ6DOF_M829_DERV(time,state)
global mass rho GM Ix Iy Iz d cx0 cx2 cypa cna clp cmq cldd dx dxmag

x=state(1,1);
y=state(2,1);
z=state(3,1);
phi=state(4,1);
theta=state(5,1);
psi=state(6,1);
u=state(7,1);
v=state(8,1);
w=state(9,1);
p=state(10,1);

```

```

q=state(11,1);
r=state(12,1);
%
c_theta = cos(theta);
s_theta = sin(theta);
c_phi = cos(phi);
t_theta= tan(theta);
s_phi = sin(phi);
c_psi = cos(psi);
s_psi = sin(psi);
t_theta= tan(theta);
thetacorrect=theta+atan(sqrt(x^2+y^2)/(6378000-z));
%
%TIB a transformation matrix from the Inertia reference frame I to the
body
%frame B
TIB=[c_theta*c_psi          c_theta*s_psi          -
s_theta;
s_phi*s_theta*c_psi-c_phi*s_psi  s_phi*s_theta*s_psi+c_phi*c_psi
s_phi*c_theta;
c_phi*s_theta*c_psi+s_phi*s_psi  c_phi*s_theta*s_psi-s_phi*c_psi
c_phi*c_theta];

TIB2=[cos(thetacorrect)*c_psi
cos(thetacorrect)*s_psi          -sin(thetacorrect);
s_phi*sin(thetacorrect)*c_psi-c_phi*s_psi
s_phi*sin(thetacorrect)*s_psi+c_phi*c_psi  s_phi*cos(thetacorrect);
c_phi*sin(thetacorrect)*c_psi+s_phi*s_psi
c_phi*sin(thetacorrect)*s_psi-s_phi*c_psi  c_phi*cos(thetacorrect)];
% Kinematic equation matrix
K=[1  s_phi*t_theta          c_phi*t_theta;
0  c_phi          -s_phi;
0  s_phi/c_theta          c_phi/c_theta];
% Weight
%Weight = (mass*GM*1000/((6378-z/1000)^2+(x/1000)^2))*TIB2*[0; 0; 1];
Weight = (mass*GM*1000/((6378-
z/1000)^2+(x/1000)^2))*TIB*(1/sqrt(x^2+y^2+(6378000-z)^2))*[-x; -y; -
z+6378000]);
%Weight = mass*9.81*TIB*[0; 0; 1];
% Angular velocity skew symmetric matrix
SW = [0 -r q; r 0 -p; -q p 0];
% Inertia and Inverse
Inertia =[Ix 0 0; 0 Iy 0; 0 0 Iz];
IntInv =[1/Ix 0 0; 0 1/Iy 0; 0 0 1/Iz];

%

V = (u^2+v^2+w^2)^0.5;          % body velocity
qa = 0.125*pi*rho*V^2*d^2;
% Forces
FSA = qa*(cx0 + cx2*(v^2+w^2)/V^2); -cna*v/V; -cna*w/V];
FMAG = 0.0625*rho*pi*d^3*p*cypa*[0.0; w; -v];
FA = FSA+FMAG;
%Moments
%Steady Moments
MSA = qa*cna*dx*[0.0; w/V; -v/V];

```

```

%Unsteady Moments
MUA = qa*d*[cldd+(p*clp*d)/(2*V); (q*cmq*d)/(2*V); (r*cmq*d)/(2*V)];
%Magnus Moments
MMAG = 0.0625*rho*pi*d^3*p*cypa*dxmag*[0.0; v; w];
% Total moment
MA= MSA + MUA + MMAG;
% Kinematic equations and dynamic equations
PositionKIN=TIB'*[u; v; w];
RoatationKIN=K*[p; q; r];
TranslationDYN =(1/mass)*(FA+Weight)-SW*[u; v; w];
RotatitionDYN =IntInv*(MA-SW*Inertia*[p; q; r]);
% Output
dstate=[PositionKIN; RoatationKIN ; TranslationDYN; RotatitionDYN];

```

APPENDIX C

Taylor-Maccoll Solution of Drag Coefficient

The Taylor-Maccoll method was written in Visual Basic for Applications as a Microsoft Excel Macro.

```
Private Sub CommandButton1_Click()
'This code solves the famous Taylor-Maccoll equations for conical
supersonic flow over a right cone.
'by: John Stutz, P.E.
'16 June 2011

Dim i As Integer
i = 7
Dim Vr(2), Vt, M1, M2, Vmax, M1n As Double
Dim p1, p2, ps, Ms, pt As Double
p1 = Worksheets("Sheet1").Cells(4, 9).Value
Dim Gamma As Double
Gamma = Worksheets("Sheet1").Cells(4, 7).Value
Dim T1, a1, T2, a2, Ts, a3, Tt As Double
Dim Shockang As Double
Dim dtheta, theta As Double
dtheta = Worksheets("Sheet1").Cells(2, 9).Value * 3.14159 / 180
T1 = (Worksheets("Sheet1").Cells(2, 7).Value - 32) * (5 / 9) + 273
Dim alpha, beta As Double
'cells(row, collum)
Shockang = 70 * 3.14159 / 180

10 'Mach Number itteration- outer most loop
'look up Mach number for this itteration
M1 = Worksheets("Sheet1").Cells(i, 1).Value
'calculate the free stream speed of sound
a1 = Math.Sqrt(Gamma * 287 * T1)
'calculate the RSS velocity behind shock
Vmax = Math.Sqrt(2 * ((a1 ^ 2) / (Gamma - 1)) + (M1 * a1) ^ 2 / 2))

20 'Shock Angle itteration- middle loop
'calculate the velocity of the radial component behind shock
Vr(0) = M1 * a1 * Math.Cos(Shockang)
'calculate Mach number normal to shock
M1n = M1 * Math.Sin(Shockang)
'calculate the Mach number normal to shock behnind shock
M2 = Math.Sqrt((1 + ((Gamma - 1) * (M1n ^ 2) / 2)) / (Gamma * (M1n ^ 2)
- ((Gamma - 1) / 2)))
'calculate the air temp behind the shock
T2 = T1 * (1 + (2 * Gamma * ((M1n ^ 2) - 1) / (Gamma + 1))) * ((2 +
(Gamma - 1) * (M1n ^ 2)) / ((Gamma + 1) * (M1n ^ 2)))
'calculat the local speed of sound behind the shock
a2 = Math.Sqrt(287 * Gamma * T2)
'calculate the pressure behind the shock
p2 = p1 * (1 + 2 * Gamma * (M1n ^ 2 - 1) / (Gamma + 1))
'calculate the velocity of the normal component behind the shock
Vt = -M2 * a2
```

```

'calculate the total temperature
Tt = T2 * (1 + (Gamma - 1) * (Math.Sqrt(Vt ^ 2 + Vr(0) ^ 2) / a2) ^ 2 /
2)
'calculate the total pressure
pt = p2 * (Tt / T2) ^ (Gamma / (Gamma - 1))
'set angle for next iteration loop
theta = Shockang - dtheta

30 'Taylor Maccoll iteration- inner loop
'these are algebra terms to simplify the code per line
alpha = ((Gamma - 1) / 2) * ((Vmax ^ 2) - (Vr(0) ^ 2) - (Vt ^ 2))
beta = (Vr(0) * (Vt ^ 2) - alpha * (2 * Vr(0) + (Vt / Math.Tan(theta))))
/ (alpha - (Vt ^ 2))
'calculate the radial velocity at the next ray angle
Vr(1) = Vr(0) - Vt * dtheta + beta * (dtheta ^ 2)
'calculate the new normal velocity at the next ray angle
Vt = (Vr(0) - Vr(1)) / dtheta
'substitute new value for old value
Vr(0) = Vr(1)
'check to see if we are at the cone surface-close inner loop
If Vt < 0 Then
theta = theta - dtheta
GoTo 30
End If

'calculate surface speed of sound
a3 = Math.Sqrt(((Vmax ^ 2 - Vr(1) ^ 2) / 2) * (Gamma - 1))
'calculate surface mach number
Ms = Vr(1) / a3
'calculate surface pressure
ps = pt / (1 + (Gamma - 1) * Ms ^ 2 / 2) ^ (Gamma / (Gamma - 1))
If Shockang = 70 * 3.14159 / 180 Then
Worksheets("Sheet1").Cells(i, 2).Clear
Worksheets("Sheet1").Cells(i, 3).Clear
Worksheets("Sheet1").Cells(i, 4).Clear
Worksheets("Sheet1").Cells(i, 5).Clear
Worksheets("Sheet1").Cells(i, 6).Clear
Else
Worksheets("Sheet1").Cells(i, 2).Value = Vr(1)
Worksheets("Sheet1").Cells(i, 3).Value = Vt
Worksheets("Sheet1").Cells(i, 4).Value = Shockang * 180 / 3.14159
Worksheets("Sheet1").Cells(i, 5).Value = ps
Worksheets("Sheet1").Cells(i, 6).Value = 2000 * (ps - p1 *
Worksheets("Sheet1").Cells(4, 12).Value) / (Vmax ^ 2 *
Worksheets("Sheet1").Cells(2, 12).Value)
End If
'check to see if cone angle is correct-close middle loop
If (theta * 180 / 3.14159) - Worksheets("Sheet1").Cells(2, 4).Value > 0
Then
Shockang = Shockang - dtheta
GoTo 20
End If
If i < 28 Then
i = i + 1
GoTo 10
End If
End Sub

```

APPENDIX D

Tabulated Data and Calculations for Barbados 16" HARP Gun Apogee Data Fit

round #	apogee (km)	mass (kg)	Vo (km/s)	Mach	mu	V tangent	corrected elevation	corrected Velocity	Corrected Azimuth	Beta	Li (km ² /s)
181	122	83.2356	1.80	5.24	13.78	0.08	71.44	1.89	95.09	0.18	3837.40
188	119	83.2356	1.77	5.15	14.01	0.08	71.21	1.86	95.03	0.18	3821.02
189	131	83.0088	1.86	5.42	13.36	0.08	71.86	1.95	95.22	0.18	3870.16
190	117	83.4624	1.77	5.15	14.01	0.08	71.21	1.86	95.03	0.18	3821.02
191	132	83.2356	1.86	5.42	13.36	0.08	71.86	1.95	95.22	0.18	3870.16
192	140	83.2356	1.92	5.60	12.95	0.08	72.26	2.01	95.35	0.18	3902.94
194	122	83.2356	1.80	5.24	13.78	0.08	71.44	1.89	95.09	0.18	3837.40
195	130	83.4624	1.86	5.42	13.36	0.08	71.86	1.95	95.22	0.18	3870.15
196	116	83.2356	1.74	5.06	14.24	0.08	70.98	1.83	94.96	0.18	3804.65
198	128	84.3696	1.86	5.42	13.36	0.08	71.86	1.95	95.22	0.18	3870.14
199	137	83.2356	1.89	5.51	13.15	0.08	72.07	1.98	95.29	0.18	3886.54
206	137	83.916	1.93	5.61	12.92	0.08	72.30	2.01	95.36	0.18	3906.21
209	114	83.4624	1.77	5.15	14.01	0.08	71.21	1.86	95.03	0.18	3821.02
210	122	84.3696	1.80	5.24	13.78	0.08	71.44	1.89	95.09	0.18	3837.38
211	127	83.916	1.83	5.33	13.57	0.08	71.65	1.92	95.16	0.18	3853.76
212	122	84.3696	1.83	5.33	13.57	0.08	71.65	1.92	95.16	0.18	3853.76
213	109	77.5656	1.74	5.06	14.24	0.09	70.98	1.83	94.96	0.20	3804.74
214	106	83.6892	1.71	4.98	14.48	0.08	70.75	1.80	94.90	0.18	3788.28
223	114	83.6892	1.74	5.06	14.24	0.08	70.98	1.83	94.96	0.18	3804.65
224	111	83.916	1.74	5.06	14.24	0.08	70.98	1.83	94.96	0.18	3804.64
235	108	83.916	1.71	4.98	14.48	0.08	70.75	1.80	94.90	0.18	3788.28
205	126	83.4624	1.86	5.42	13.36	0.08	71.86	1.95	95.22	0.18	3870.15
181	122	83.2356	1.80	5.24	13.78	0.08	71.44	1.89	95.09	0.18	3837.40

APPENDIX E

Tabulated Data and Calculations for Yuma 16" HARP Gun Apogee Data Fit

round #	Error	apogee (km)	mass (kg)	Vo (km/s)	Mach #	mu (degrees)	Beta	V tangent	corrected elevation	corrected Velocity	Corrected Azimuth	Li (km ² /s)	delta apogee
4	0.94	126.49	83.916	1.81	5.36	11.91	0.16	0.07	73.17	1.88	86.62	3473.46	0.94
5	0.76	121.31	83.916	1.77	5.25	12.14	0.16	0.07	72.94	1.85	86.67	3453.35	0.76
8	1.05	114.30	83.916	1.72	5.09	12.51	0.16	0.07	72.57	1.79	86.74	3423.18	1.05
9	2.76	124.97	83.916	1.78	5.29	12.06	0.16	0.07	73.02	1.86	86.65	3460.05	2.76
10	-4.13	94.49	83.916	1.60	4.75	13.37	0.16	0.07	71.72	1.68	86.91	3359.53	-4.13
11	-1.43	124.97	83.916	1.81	5.38	11.87	0.16	0.07	73.21	1.89	86.61	3476.81	-1.43
12	-0.53	164.59	83.916	2.07	6.15	10.44	0.16	0.07	74.63	2.14	86.28	3619.35	-0.53
14	2.20	126.49	83.916	1.80	5.33	11.96	0.16	0.07	73.12	1.87	86.63	3468.43	2.20
15	-1.08	163.07	83.916	2.07	6.13	10.47	0.16	0.07	74.60	2.14	86.29	3615.99	-1.08
18	-3.90	120.40	83.916	1.80	5.33	11.96	0.16	0.07	73.12	1.87	86.63	3468.43	-3.90
20	0.09	126.49	83.916	1.81	5.38	11.87	0.16	0.07	73.21	1.89	86.61	3476.81	0.09
22	-2.37	121.92	83.916	1.80	5.33	11.96	0.16	0.07	73.12	1.87	86.63	3468.43	-2.37
23	2.76	124.97	83.916	1.78	5.29	12.06	0.16	0.07	73.02	1.86	86.65	3460.05	2.76
24	-2.44	155.45	83.916	2.03	6.01	10.67	0.16	0.07	74.41	2.10	86.33	3594.18	-2.44
25	3.14	149.35	83.916	1.95	5.79	11.07	0.16	0.07	74.01	2.02	86.43	3552.26	3.14
26	3.66	161.54	83.916	2.03	6.01	10.67	0.16	0.07	74.41	2.10	86.33	3594.18	3.66
27	-0.29	121.92	83.916	1.78	5.29	12.06	0.16	0.07	73.02	1.86	86.65	3460.05	-0.29
28	4.78	179.83	83.916	2.13	6.33	10.15	0.16	0.07	74.92	2.20	86.20	3652.90	4.78
30	2.37	146.30	83.916	1.94	5.74	11.15	0.16	0.07	73.93	2.01	86.45	3543.87	2.37
31	-2.19	111.86	83.916	1.72	5.11	12.47	0.16	0.07	72.61	1.80	86.74	3426.53	-2.19
32	-1.27	112.78	83.916	1.72	5.11	12.47	0.16	0.07	72.61	1.80	86.74	3426.53	-1.27
33	4.95	167.64	83.916	2.06	6.10	10.52	0.16	0.07	74.56	2.13	86.30	3610.96	4.95

REFERENCES

- [1] Epler, W., Fagot, J., "Upper Atmosphere Winds from Gun Launched Vertical Probes," Space Research Instruments, Inc., DA-01-009-AMC-169(X), Atlanta, GA, August 1968.
- [2] Murphy, C., Bull, G., "HARP 5-Inch and 16-Inch Guns at Yuma Proving Ground, Arizona," Ballistics Research Laboratories, AD-654123, Aberdeen Proving Ground, Maryland, February 1967.
- [3] Bozic, O., Giese, P., "Aerothermodynamic Aspects of Railgun-Assisted Launches of Projectiles With Sub and Low-Earth-Orbit Payloads," *IEEE Transactions on Magnetics*, Vol. 43, No. 1, January 2007, pp. 474-479.
- [4] Lehmann, P., "Overview of the Electric Launch Activities at the French-German Research Institute of Saint-Louis (ISL)," *IEEE Transactions on Magnetics*, Vol. 39, No. 1, January 2003, pp. 24-28.
- [5] Han, J., Pan, Y., He, J., "Study of Employing Railguns in Close-in Weapons Systems," *IEEE Transactions on Magnetics*, Vol. 45, No. 1, January 2009, pp. 641-644.
- [6] Elwell, J., Duchesne, L., Rizzo, V., McNab, I., "Airborne Electromagnetic Railgun Launched Interceptor for Midcourse/Decent and Boost Phase Missile Defense," AIAA Missile Sciences Conference Paper, The Charles Draper Laboratory, Cambridge, MA, November 2008.
- [7] Ballistic Missile Trajectory Overview (background image), www.STRAFOR.com, Aug 2012.
- [8] Neshor, O., Klipstein, P., "High Performance IR detectors at SCD present and future," *Opto-Electronics Review*, Vol. 14, No. 1, 2006, pp. 59-68.
- [9] Lowry, H., Nicholson, R., Simpson, R., Mead, K., Crider, D., Fedde, M., "Test and Evaluation of Space and Airborne Imaging Sensor Platforms," *Journal of Spacecraft and Rockets*, vol. 48, No. 6, November-December 2011, pp. 999-1011.
- [10] Blanchard, R., Wilmoth, R., Glass, C., Merski, N., Berry, S., Bozung, T., Tietjen, A, Wendt, J., Dawson, D., "Infrared Sensing Aeroheating Flight Experiment: STS-96 Flight Results," *Journal of Spacecraft and Rockets*, vol. 38, No. 4, July-August 2001, pp. 465-472.
- [11] Ford, R., *Germany's Secret Weapons in World War II*, MBI Publishing, Osceola, WI, 2000.

- [12] Wade, M., “V-3,” *Encyclopedia Astronautica* , <http://www.astronautix.com/lvs/v3.htm>, Aug 2012.
- [13] “Overachiever,” *Air and Space Smithsonian*, February-March 1992, pp. 52.
- [14] Brownlee, R., *Learning to Contain Underground Nuclear Explosions*, <http://nuclearweaponarchive.org/Usa/Tests/Brownlee.html>, Aug 2012.
- [15] Schematic Diagram of a Railgun, <http://en.wikipedia.org/wiki/Railgun>, Aug 2012.
- [16] Voelkel, J., *The Composition of Kepler’s Astromnia Nova*, Princeton University Press, 2001.
- [17] Caspar, M., *Kepler*, Abelard-Schuman Limited, London, 1959, pp. 192.
- [18] Newton, I., *Philosophiæ Naturalis Principia Mathematica*, Macmillan and Co., 1863.
- [19] Logsdon, T., *Orbital Mechanics: Theory and Applications*, Wiley, New York, 1998.
- [20] Prussing, J., Conway, B., *Orbital Mechanics*, Oxford, New York, 1993.
- [21] Gevelhoff, H., Manz, B., “Probability of Hit of a Satellite by Ballistic Projectiles,” Directorate of Aerospace Studies, DAS-TR-90-2, Kirkland AFB, New Mexico, August 1990.
- [22] Ahn, J., roh, W., “Noniterative instantaneous Impact Point Prediction Algorithm for Launch Operations,” *Journal of Guidance, Control, and Dynamics*, Vol. 35, No. 2, 2012, pp. 645-648.
- [23] Humi, M, Carter, T., “Nearly Circular Equatorial Orbits About an Oblate Body with Atmosphere,” *Journal of Guidance, Control, and Dynamics*, Vol. 32, No. 4, 2009, pp. 1287-1294.
- [24] Brouwer, D., and Hori, G., “Theoretical Evaluation of Atmospheric Drag Effects in the Motion of an Artificial Satellite,” *Astronomical Journal*, Vol. 66, No. 5, 1961, pp. 193–225.
- [25] King-Hele, D., *Satellite Orbits in an Atmosphere*, Blackie, London, 1987.
- [26] Melton, R. G., “Time-Explicit Representation of Relative Motion Between Elliptical Orbits,” *Journal of Guidance, Control, and Dynamics*, Vol. 23, No. 4, 2000, pp. 604–610.

- [27] Liu, J. J. F., “Advances in Orbit Theory for an Artificial Satellite with Drag,” *Journal of the Astronautical Sciences*, Vol. 31, No. 2, 1983, pp. 165–188.
- [28] Humi, M., and Carter, T., “Models of Motion in a Central-Force Field with Quadratic Drag,” *Celestial Mechanics and Dynamical Astronomy*, Vol. 84, No. 3, 2002, pp. 245–262.
- [29] Carter, T., and Humi, M., “Clohessy-Wiltshire Equations Modified to Include Quadratic Drag,” *Journal of Guidance, Control, and Dynamics*, Vol. 25, No. 6, 2002, pp. 1058–1063.
- [30] Humi, M., and Carter, T., “Closed-Form Solutions for Near-Circular Arcs with Quadratic Drag,” *Journal of Guidance, Control, and Dynamics*, Vol. 30, No. 1, 2007, pp. 248–251.
- [31] Humi, M., and Carter, T., “Two-Body Problem with High Tangential Speeds and Quadratic Drag,” *Journal of Guidance, Control, and Dynamics*, Vol. 30, No. 1, 2007, pp. 248–251.
- [32] Carter, T., and Humi, M., “Two-Body Problem with Drag and High Tangential Speeds,” *Journal of Guidance, Control, and Dynamics*, Vol. 31, No. 3, 2008, pp. 641–646.
- [33] Kechichian, J. A., “Motion in General Elliptic Orbit with Respect to a Dragging and Precessing Coordinate Frame,” *Journal of the Astronautical Sciences*, Vol. 46, No. 1, 1998, pp. 25–45.
- [34] Schweighart, S. A., and Sedwick, R. J., “Cross-Track Motion of Satellite Formations in the Presence of J_2 Disturbances,” *Journal of Guidance, Control, and Dynamics*, Vol. 28, No. 4, 2005, pp. 824–826.
- [35] Nayfeh, A., *Introduction to Perturbation Techniques*, Wiley, New York, NY, 1981.
- [36] Holmes, M. H., *Introduction to Perturbation Methods*, Springer-Verlag, New York, NY, 1995.
- [37] Han, J., Pan, Y., He, J., “Study of Employing Railguns in Close-in Weapon System,” *IEEE Transactions on Magnetics*, Vol. 45, No. 1, 2009, pp. 641–644.

- [38] Shi, Y., Pottsepp, L., "Asymptotic Expansion of a Hypervelocity Atmospheric Entry Problem," *AIAA Journal*, Vol. 7, No. 2, 1969, pp. 353-355.
- [39] Shi, Y., Pottsepp, L., Eckstein, M. C., "A Matched Asymptotic Solution for Skipped Entry into Planetary Atmosphere," *AIAA Journal*, Vol. 9, No. 4, 1971, pp. 736-738.
- [40] Carlson, N. A., "An Analytic Guidance Technique for Planetary and Lunar Approach Trajectories," *AIAA Paper*, No. 75-15, 1972.
- [41] Deakin, M., Troup, G., "Approximate Trajectories for Projectile Motion with Air Resistance," *American Journal of Physics*, Vol. 66, No. 1, 1998, pp. 34-37.
- [42] Hayen, J., "Projectile Motion in a Resistant Medium Part II: Approximate Solution and Estimates," *International Journal of Non-Linear Mechanics*, Vol. 38, 2003, pp. 371-380.
- [43] McCoy, R., *Modern Exterior Ballistics*, Schiffer, Attlen, PA, 1999, pp. 221-244.
- [44] Hahn, P., Frederick, R., Slegers, N., "Predictive Guidance of a Projectile for Hit-to-Kill Interception," *IEEE Transactions on Control Systems Technology*, Vol. 17, No. 4, 2009, pp. 745-755.
- [45] Hainz, L. Costello, M., "Modified Projectile Linear Theory for Rapid Trajectory Prediction," *Journal of Guidance, Control, and Dynamics*, Vol. 28, No. 5, 2005, pp. 1006-1013.
- [46] Slegers, N., "Predictive Control of a Munitions Using Low-Speed Linear Theory," *Journal of Guidance, Control, and Dynamics*, Vol. 31, No. 3, 2008, pp. 768-775.
- [47] U.S. Standard Atmosphere, 1976, U.S. Government Printing Office, Washington, D.C., 1976.
- [48] Ayyub, B., McCuen, R., *Numerical Methods for Engineers*, Prentice Hall, 1996.
- [49] Anderson, J. D., "Conical Flow," *Modern Compressible Flow with Historical Perspective*, 3rd ed., McGraw Hill, New York, 2003, pp. 366-372.
- [50] Graf, R., "A Brief History of the HARP Project," *Encyclopedia Astronautica*, <http://www.astronautix.com/articles/abroject.htm>, Aug 2012.

[51] Satellite imagery of Barbados Gun Site, www.maps.google.com, Aug 2012.

[52] Eyre, F., "Outline Aerodynamics and Performance of the Martlet 2C," Space Research Institute, SRI-H-TN-1, McGill university, Montreal, November 1964.

[53] National Oceanic and Atmospheric Administration National Climatic Data Center, <http://www.ncdc.noaa.gov>, Aug 2012